PROSTAGLANDIN E_2 RECEPTOR 3 (EP_3) CONTRIBUTES TO POLYURIA, GLOMERULAR HYPERFILTRATION, AND RENAL INJURY IN DIABETES

Ramzi Hassouneh

This thesis is submitted as a partial fulfillment of the M.Sc. program in Cellular and Molecular Medicine.

May 2015

University of Ottawa

Ottawa, Ontario

ABSTRACT

Cyclooxygenases (COXs) and their main renal product, prostaglandin E_2 (PGE_2), regulate many physiological renal functions and are involved in the pathogenesis of diabetic kidney disease. The PGE_2 receptor EP_3 has been repeatedly shown to be upregulated during diabetes. Physiologically, EP_3 is best recognized to act as a diuretic by antagonizing arginine-vasopressin (AVP)-mediated water reabsorption. Incidentally, the first renal manifestation of diabetes is polyuria, which may trigger a cascade of events leading to DN. We hypothesize that EP_3 contributes to polyuria and kidney dysfunction during diabetes. We injected $EP_3^{-/-}$ mice with streptozotocin (STZ) and evaluated their renal function 12-weeks post injection. $EP_3^{-/-}$ STZ mice exhibit attenuated polyuria while exhibiting increased urine osmolality suggesting enhanced water reabsorption. Western blots reveal that $EP_3^{-/-}$ STZ mice have increased expression of aquaporin-1 and aquaporin-2 as well as reduced urinary AVP excretion compared to STZ mice. However, salt transporters were equivalently increased in STZ and $EP_3^{-/-}$ STZ mice. In vitro microperfusion shows that EP_3 completely abrogates AVP-mediated water reabsorption in STZ cortical collecting ducts. Furthermore, $EP_3^{-/-}$ STZ mice showed blunted renal COX-2 expression as well as reduced renal hypertrophy, glomerular hyperfiltration, and albuminuria. Taken together, the data suggests that EP_3 contributes to polyuria during diabetes by inhibiting expression of aquaporins. Additionally, EP_3 seems to contribute to renal COX-2 induction during diabetes. The lack of an increase in renal COX-2 protein levels in $EP_3^{-/-}$ STZ mice may be protective by preventing further renal damage.

TABLE OF CONTENTS

LIST OF TABLES

LIST OF FIGURES

LIST OF ABBREVIATIONS

AC	Adenylate cyclase
ACE	Angiotensin-converting enzyme
AQP	Aquaporin
AT	Angiotensin
AVP	Arginine-vasopressin
cAMP	Cyclic adenosine monophosphate
CCD	Cortical collecting duct
COX	Cyclooxgenase
COXIB	Cyclooxygenase-2 inhibitor
CTGF	Connective tissue growth factor
DEPC	Diethylpyrocarbonate
DM	Diabetes mellitus
DMEM	Dulbecco's modified Eagle's medium
DMSO	Dimethyl sulfoxide
DN	Diabetic nephropathy
DNA	Deoxyribonucleic acid
ELISA	Enzyme-linked immunosorbent assay
ENaC	Epithelial sodium channel
EP	E-prostanoid
ESRD	End-stage renal disease
FBS	Fetal bovine serum
FITC	Fluorescein isothiocyanate
GAPDH	Glyceraldyehyde-3phosphate dehydrogenase
GFR	Glomerular filtration rate
GLP	Glucagon-like peptide
GLUT	Glucose transporter
IMCD	Inner-medullary collecting duct
IP	Intra-peritoneal
IV	Intra-venous
Jv	Net fluid reabsorption
MAPK	Mitogen-activated protein kinase
mRNA	Messenger ribonucleic acid
NF-κB	Nuclear factor kappa-light-chain enhancer of activated B cells
NKA	Sodium potassium ATPase
NKCC2	Sodium potassium chloride co-transporter 2
NSAID	Non-steroidal anti-inflammatory drug
PAS	Periodic-acid Schiff
PBS	Phosphate buffered saline
PCR	Polymerase chain reaction
PG	Prostaglandin
PKC	Protein kinase C

PKD	Polycystic kidney disease
PLA2	Phospholipase A_2
PLC	Phospholipase C
PT	Proximal tubule
qPCR	Quantitative polymerase chain reaction
RAAS	Renin-angiotensin-aldosterone system
RIPA	Radioimmunoprecipitation assay
ROS	Reactive oxygen species
SLP	Sulprotone
SSRE	Shear stress responsive element
STZ	Streptozotocin
TAL	Thick ascending limb
TBS-T	Tris buffered saline-Tween 20
TGF	Tubuloglomerular feedback
TGF-β	Transforming growth factor beta
WT	Wild-type

ACKNOWLEDMENTS

I am in debt to my colleagues and friends who have lent me their continuous support and made this thesis possible. I would like to thank my supervisor Dr. Richard L. Hébert for his constant encouragement and support. I also am grateful to him for giving me the opportunity to complete my master's degree in his laboratory. I can confidently say that this experience not only fulfilled my desire for scientific investigation but also helped me improve as a person by becoming a better communicator, mentor, and leader. I also would like to thank Dr. Rania Nasrallah who I consider as my second supervisor. She was instrumental in helping me cultivate my laboratory skills and techniques. With her incredible patience and guidance, I was able to integrate easily into my new environment. Her unmatched commitment for perfection in her work aspired me to be as productive as possible and allowed me to achieve a lot during my graduate training. I would also like to thank all the members of the Kidney Research Centre for making these last two years so pleasant and enjoyable.

I appreciate all the guidance and support provided by my thesis advisory committee members and thesis evaluators, Dr. Chris Kennedy, Dr. Mario Tiberi, and Dr. Dylan Burger. I would like to thank them for their time and patience in reading my reports and providing me with helpful suggestions.

Finally, I would not have been able to complete my master's without the everlasting support and encouragement from my family and friends.

1. INTRODUCTION

1.1 The Kidneys

The kidneys are a pair of organs located in the back of the abdomen of invertebrates responsible for several key functions (1, 2). The kidneys participate in the maintenance of a relatively constant extracellular environment that is necessary for the organism to function normally (1, 2). This is achieved by excretion of waste products of metabolism (e.g. urea, creatinine, and uric acid), conservation of water and electrolytes, and maintenance of acid-base balance (1, 2). The kidneys also secrete hormones that participate in the regulation of systemic and renal hemodynamics (e.g. renin, angiotensin II, and prostaglandins), red blood cell production (i.e. erythropoietin), and mineral metabolism (i.e. calcitriol) (1, 2). Lastly, the kidneys participate in the catabolism of peptide hormones and the synthesis of glucose (i.e. gluconeogenesis) under fasting conditions (1, 2).

Each kidney contains up to a million functioning units called nephrons. A nephron consists of a filtering unit of tiny blood vessels contained in a capsule called a glomerulus attached to a tubule (1, 2). The normal glomerular filtration rate (GFR) in humans averages between 90 and 120 ml/ min/ 1.73 m^2 (1, 2). This represents a daily volume of about 170 liters, which is more than 10 times that of extracellular fluid volume and approximately 60 times that of plasma volume (1, 2). Therefore, an individual's survival requires that virtually all of the filtered solutes and water be returned to the systemic circulation by tubular reabsorption. Figure 1 shows the organization of the

nephron and lists the contributions of the different nephron segments to the reabsorption of filtered solutes and fluid (1, 2).

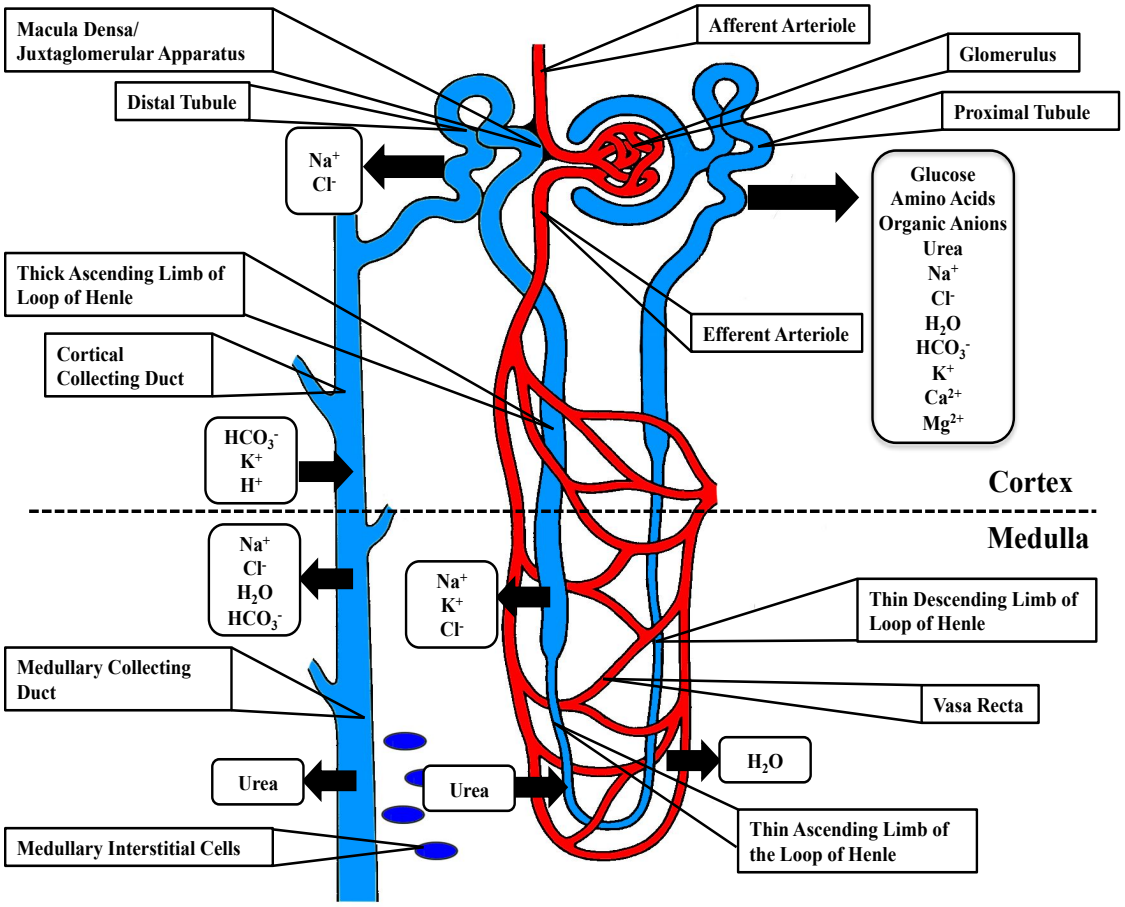

Figure 1. Structure and function, with respect to solute reabsorption and secretion, of the different nephron segments. The proximal tubule reabsorbs filtered glucose, amino acids, organic anions, Na^+, Cl^-, H_2O, HCO_3^-, K^+, Ca^{2+}, and Mg^{2+}. The thin descending limb of the loop of Henle reabsorbs H_2O only, while the thin ascending limb of the Loop of Henle secretes urea and reabsorbs Na^+ and Cl^-. The thick ascending limb of the loop of Henle reabsorbs Na^+, K^+, and Cl^-. The distal tubule reabsorbs Na^+ and Cl^-. The cortical and medullary collecting ducts reabsorb Na^+, Cl^-, H_2O, and HCO_3^- and secretes HCO_3^-, K^+, and H^+. Finally, the medullary collecting duct reabsorbs urea.

1.2 Diabetic Nephropathy

Diabetes, correctly termed, diabetes mellitus (DM) is a major epidemic of this century. There are approximately 200 million people with diabetes mellitus worldwide, and this number is projected to increase to 366 million by 2030 (3). Diabetes is a syndrome of impaired carbohydrates, fat, and protein metabolism caused by either lack of insulin (type 1 diabetes) or decreased sensitivity of the tissues to insulin (type 2 diabetes) (4). Diabetes is associated with a number of complications including diabetic kidney disease or diabetic nephropathy (DN) (4). Up to one third of individuals with type 1 diabetes eventually develop nephropathy, after approximately 20 years of diabetes (4). Among those with type 2 diabetes, the risk of nephropathy is less clear and depends on many factors including ethnicity, duration of DM, blood glucose levels, blood pressure, and diet (4). According to the US Renal Data System, DN was the primary diagnosis in 45% of patients starting renal replacement therapy (5).

Clinically, DN is typically defined by albuminuria – that is, a urinary albumin excretion rate of 300mg/24 hours – or albuminuria alongside abnormal renal function as represented by an abnormal serum creatinine or GFR (6). However, some patients may present with progressive deterioration of renal function due to diabetes without developing significant proteinuria (6). The late stages of DN are characterized by a progressive increase in proteinuria and decline in GFR, hypertension, and a high risk of cardiovascular morbidity and mortality (6). If left untreated, this can result in one or more fatal outcomes (e.g. uremia, hyperkalemia, metabolic acidosis) due to the lack of filtration (6).

The pathophysiology of DN is complex especially due to the diversity of cell populations present within the kidney and the various physiological roles of this organ. The early stage of DN is characterized by glomerular hyperfiltration mainly due to dilation of the afferent arterioles (4, 6, 7). The resultant increased intra-glomerular pressure alters the synthesis and turnover of mesangial matrix, leading to albuminuria alongside tubular dysfunction (4, 6, 7). Following this initial period of growth, begins a gradual decline in renal function associated with the development of glomerular and tubulointerstitial fibrosis, and finally apoptotic loss of glomerular and tubular cells (4, 6, 7).

Altered renal hemodynamics is an early characteristic feature of diabetes in humans as well as animal models (4, 6-8). It is widely held that glomerular capillary hypertension in diabetes is the major hemodynamic alteration that contributes to progressive glomerular injury (4, 6, 7). The increase in glomerular blood flow occurs alongside an increase in glomerular capillary pressure, which is caused by afferent arteriolar dilation with vasoconstriction of the efferent arteriole (4, 6, 7). An imbalance of a variety of vasoactive and growth factors including the renin-angiotensin-aldosterone system (RAAS), insulin-like growth factor-1, endothelin, nitric oxide, and prostaglandins have been implicated in diabetic hyperfiltration (4, 6, 7). The two prevailing theories to account for the hemodynamic changes in the glomerular alterations are (1) a primary alteration in vascular function or (2) a primary alteration in tubular function (4, 6-8). The vascular theory suggests that vascular smooth muscle cells, mesangial cells, and endothelial cells are primarily responding to a combination of high-glucose concentrations, local autacoids, and systemic signals to alter the normal autoregulatory

response (4, 6, 7). The tubular theory suggests that tubuloglomerular feedback (TGF), a mechanism the kidney uses to regulate GFR in response to various stimuli, as the initiating factor for the hemodynamic changes in DN (8). If the perfusion to the juxtaglomerular apparatus in the kidney's macula densa region decreases, then the juxtaglomerular cells release the enzyme renin (1, 2). Renin cleaves angiotensinogen released from the liver converting it into angiotensin I. Angiotensin I is then converted to angiotensin II by angiotensin-converting enzyme (ACE), which is thought to be found mainly in lung capillaries (1, 2). Angiotensin II binds to angiotensin II type-1 (AT1) receptors on the efferent arteriole causing it to constrict, ultimately bringing GFR to an appropriate level (1, 2). Physiologically, a large sodium chloride concentration sensed at the macula densa is indicative of an elevated GFR, while low sodium chloride concentration indicates a depressed GFR (1, 2). In diabetes, hypertrophy of tubules stimulates increased uptake of sodium in the proximal tubule and in the medullary thick ascending limb and this may limit sodium chloride delivery to the macula densa, thus stimulating tubuloglomerular feedback and promoting constriction of the efferent arteriole (8). Regardless of the cause of hemodynamic alterations in diabetes, progressive renal injury eventually ensues (4, 6-8).

DN not only causes renal intraglomerular hypertension but also systemic hypertension (4, 6, 7). In turn, systemic hypertension is also an important pathogenic factor in the progression of DN (4, 6, 7). The kidney plays a key role in the physiological long-term regulation of blood pressure mediated by the process of pressure natriuresis whereby sodium excreted in the urine lowers blood volume because osmotic forces make water follow sodium out of the body's circulation and into the urine (1, 2). The RAAS is

the most significant physiological regulator of blood pressure (1, 2). Angiotensin II and aldosterone have both systemic and renal mechanisms of action to regulate blood pressure by modifying vascular tone and sodium and water balance (1, 2). First line therapies for DN target the RAAS through the use of ACE inhibitors and AT1 receptor antagonists (4).

As a consequence of hyperfiltration and the diabetic milieu, the kidney filters increased amounts of glucose, which is free to trigger a number of pathological pathways (4, 6, 7). Renal cells do not require insulin for glucose uptake causing them to be particularly susceptible to greater loads of intracellular glucose (4, 6, 7). Excess unused glucose enters the polyol pathway resulting in abnormalities of cellular function, including activating protein kinase C (PKC) and mitogen-activated protein kinase (MAPK), myo-inositol depletion, and reactive oxygen species (ROS) generation (4, 6, 7). The polyol pathway may also produce metabolites capable of non-enzymatically glycating intracellular proteins (4, 6, 7). Progressive tissue damage is closely related to the deposition of glycated proteins (4, 6, 7). Tight glycemic control does not always prevent further injury and evolution to end-stage renal disease (ESRD) suggesting that many other factors are involved (4, 6, 7). The sustained responses to glucose are likely mediated by activation of other factors including transforming growth factor beta (TGF-β) (4, 6, 7). TGF-β is central to the pro-fibrotic response during diabetes contributing to cytoskeletal reorganization, matrix changes, and scarring (4, 6, 7).

The early diabetic kidney undergoes significant hypertrophy (4, 6, 7). Hypertrophy is seen within the glomeruli, which is accompanied by mesangial expansion and thickening of the glomerular basement membrane (4, 6, 7). However, the tubules,

which constitute greater than 90% of the kidney mass, account for the greatest change in growth in diabetes (4, 6, 7). In addition to tubular cell enlargement, dilatation and increased fluid content of tubules, mainly collecting ducts, contribute substantially to the maintenance of kidney size in DN with advanced chronic renal failure (4, 6, 7).

The earliest renal manifestation in untreated or poorly controlled diabetes in addition to glucose in the urine (i.e. glucosuria) is excess urine production or polyuria as well as a reduced urine concentrating ability (9). This is reflected in the origin of the term diabetes, which derives from the Ancient Greek verb 'διαβαινω' (to pass through) (9). The diagnosis of diabetes for many centuries was based on observing the urine volume or flow rate (9). The differential diagnosis was determined by utilizing the taste buds whereby urine was classified as mellitus from the Latin word for honey or insipidus from the Latin word tasteless (9). The extent of polyuria in diabetes is mostly defined by glucose concentration-dependent osmotic forces (9). However even with strict glycemic control, diabetics can develop polyuria particularly when exposed to strenuous conditions such as temperature extremes or lack of access to hydration (9). Polyuria changes the rheology of tubular flow and increases flow rate, particularly in the collecting ducts where flow rates are physiologically low (10, 11). This causes pressure-induced activation of tubular epithelial cells that respond with the upregulation of pro-inflammatory mediators and pro-fibrogenic cytokines (12-15). Molecules thought to be pathogenic in diabetic tubulointerstitial nephropathy including: TGF-β, connective tissue growth factor (CTGF), and alpha smooth muscle actin (α-SMA), are preferentially or exclusively expressed in dilated segments of the distal nephron (12-15).

In addition to distal nephron dilation and elevated luminal pressure, tubular cells are exposed to shear stress due to polyuria (9). Tubular cells exposed to shear stress at the apical membrane prompt significant re-arrangement of the actin cytoskeleton (16, 17). Additionally, during diabetes tubular microvillar height is significantly reduced possibly in response to flow induced shear stress. Increased tubular shear stress is correlated to increased transcription factor binding to the shear stress response element (SSRE) (16, 17). The sequence of SSRE is found in pro-inflammatory transcription factors such as NF-κB (nuclear factor kappa-light-chain-enhancer of activated B cells) (18). Furthermore, increased shear stress specifically in collecting ducts raises nitric oxide and activates several nitric oxide synthase isoforms which are responsible for the regulation of sodium and water excretion possibly further exacerbating polyuria and its associated damage (19).

1.3 Mouse Models of Diabetic Nephropathy

The major disadvantage of animal models of DN is the absence of renal failure presumably due to the inadequate duration of hyperglycemia (20-22). Animal models typically do not progress to advanced renal disease which is characterized by a loss of glomerular filtration, overt proteinuria, and advanced structural lesions such as glomerular and tubular basement membrane thickening, tubulointerstitial fibrosis, and arteriolar hyalinosis (20-22). On the other hand, several of the short-term consequences of diabetes and DN, including polyuria, kidney hypertrophy, glomerular hyperfiltration, moderately increased albuminuria, and some of the characteristic histopathologic and

biochemical changes, can be detected in animal models (20-22). One can argue that since diabetic nephropathy is characterized by a long clinically silent period without signs or symptoms of disease, animal models are sufficient to develop improved methods of detecting early mediators of renal injury and potential new therapeutic targets that prevent progression to ESRD.

The most widely utilized animal models of diabetes involve the low-dose injection of the pancreatic beta cell toxin streptozotocin (STZ) (20-22). STZ is a glucosamine-nitrosourea compound making it toxic to cells by causing damage to DNA. DNA damage induces activation of poly ADP-ribosylation, which is likely more important for diabetes induction than DNA damage itself (20-22). STZ is similar enough to glucose to be transported into the cell by glucose transporter 2 (GLUT2), but is not recognized by the other glucose transporters (20-22). This explains its specific toxicity to pancreatic beta cells, since these cells have relatively high levels of GLUT2 (20-22). Given the resistance of mice to single doses of STZ and the presence of GLUT2 in a variety of other tissues, multiple low-dose STZ injections cause repetitive low-grade beta cell damage while mitigating nonspecific cytotoxicity (20-22). It is important to note that similar to DN in humans, the genetic disposition of the animal plays a large role in determining its susceptibility to developing DN (20-22). Unfortunately, the most widely used inbred mouse strain, C57BL/6, is highly resistant to the development of DN as defined by the Animal Models of Diabetic Complications Consortium criteria (20-22). Nevertheless, this mouse model (C57BL/6 strain with STZ) does develop the early renal diabetic changes described above (20-22).

1.4 Renal Prostaglandins

A group of lipid compounds derived enzymatically from fatty acids, called prostaglandins (PG), play an essential role in maintaining homeostatic renal function and are suggested to be involved in the pathophysiology of kidney disease (23-25). The kidney is a major source of prostaglandin synthesis (23-25). As shown in Figure 2, PGs are synthesized through a cascade of events starting with the release of arachidonic acid from phospholipids by phospholipase A_2 (PLA_2) (23-25). Arachidonic acid enters the cyclooxygenase pathway where it is converted to prostaglandin H_2 by one of two cyclooxygenases (COX) (23-25). COX-1 is constitutively expressed in the glomerulus, proximal tubule, collecting duct, and medullary interstitial cells and is responsible for housekeeping functions (23-25). On the other hand, COX-2 is rapidly induced by stress stimuli (e.g. diabetes) in the glomerulus, proximal tubule, thick ascending limb, macula densa, collecting duct, and medullary interstitial cells (23-25). However, studies have shown that COX-2 is involved in certain renal housekeeping functions including kidney development (26). The COX isoforms contain two enzymatic active sites (23-25). The first site facilitates the oxygenation of arachidonic acid to produce PGG_2, an unstable intermediate (23-25). The second site possesses a peroxidase activity that allows the conversion of PGG_2 into PGH_2, a more stable intermediate (23-25). The COX isoforms can be inhibited by non-steroidal anti-inflammatory drugs (NSAIDs), such as ibuprofen and acetylsalicylic acid (23-25). Finally prostaglandin H_2 is converted to prostaglandin E_2, prostaglandin $F_{2\alpha}$, prostaglandin D_2, prostacyclin, or thromboxane by PGE, PGF, PGD, PGI, or TXA synthase, respectively (23-25).

The most abundant prostaglandin in the kidney is PGE_2 (23-25). All renal cell types can synthesize PGE_2, but the highest production is seen in the glomeruli and collecting ducts (23-25). Following its synthesis, PGE_2 can exit the cell by passive diffusion or via a prostaglandin transporter to act on resident and neighboring cells (23-25). PGE_2 can mediate a variety of renal processes by activating specific cell surface G-protein coupled receptors, namely EP_1, EP_2, EP_3, and EP_4 (23-25). Figure 2 illustrates the COX cascade leading to PGE_2 synthesis and its multiple signaling pathways in the kidney (23-25). The diverse effects of PGE_2 derive from the different cells in which these receptors are expressed as well as the diverse signaling pathways that mediate their effects. Binding of PGE_2 to EP_1 activates $G_{\alpha q}$ protein and increases intracellular Ca^{2+} through phospholipase C (PLC) (23-25). The highest levels of EP_1 are observed in the collecting duct, but EP_1 is also detected in glomerular mesangial cells, podocytes, and proximal tubule cells (23-25). The EP_2 receptor stimulates adenylate cyclase via G_s and is mainly found in vascular and interstitial compartments of the kidney (23-25). Renal EP_3 is highly expressed in the thick ascending limb and most abundant in the cortical and medullary collecting duct (23-25). EP_3 is unique among other EP receptors because it has several splice variants that couple to different signaling pathways (23-25). Three different EP_3 signaling pathways have been detected in the kidney: inhibition of adenylate cyclase (AC) via a pertussis toxin sensitive G_i-protein, increasing intracellular calcium via G_{aq}, and activation of Rho kinase via the G_{12}/G_{13} protein pathway (23-25). EP_4 is highly abundant in the afferent arteriole; however, it has also been detected in almost all renal cell types (23-25). The EP_4 receptor stimulates adenylate cyclase increasing cyclic AMP

(cAMP) via G_s, similar to EP_2, but it can also activate phosphoinositide 3-kinase (23-25). Additionally, EP_4 stimulates AMP-activated protein kinase in mouse podocytes (23-25).

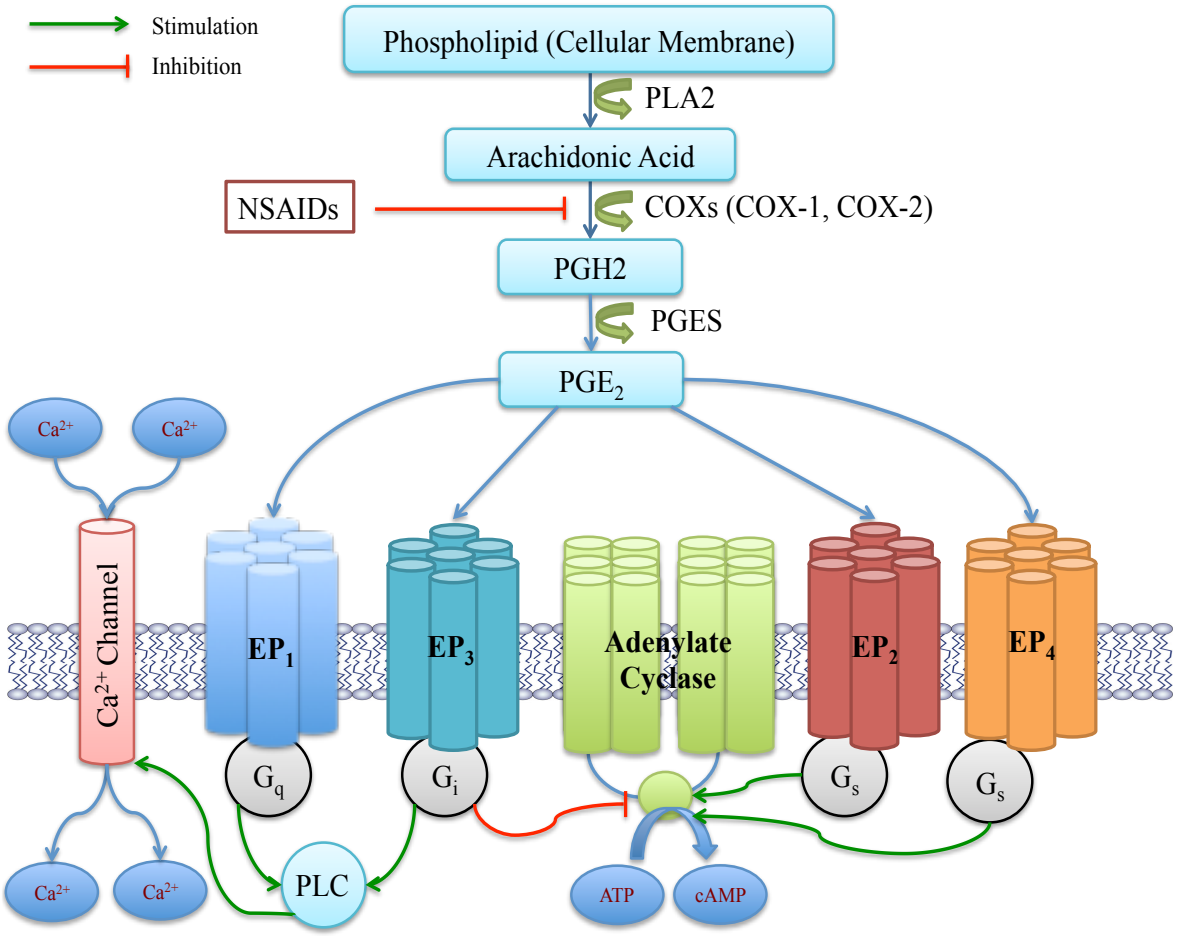

Figure 2. Prostaglandin E_2 synthesis and signaling pathways. Arachidonic acid is released by PLA_2 from membrane phospholipids and converted into PGH_2 by cyclooxygenases (COX-1/COX-2). COX activity is inhibited by NSAIDs. PGE_2 is produced by PGE synthase (PGES) and signals by binding to its G protein-coupled receptors: $EP_{1–4}$. Activation of EP_1 (coupled to G_q) increases intracellular Ca^{2+} via PLC. Activation of EP_3 (coupled to G_i) increases intracellular Ca^{2+} via PLC and/or inhibits cAMP production via adenylate cyclase (AC). Activation of EP_2 or EP_4 (both coupled to G_s) stimulates cAMP production via AC.

1.5 PGE_2 and Diabetes

Renal COX expression and the urinary excretion of PGE_2 and its metabolite are consistently reported to be increased in both rodent and human diabetes (27-32). Additionally, the expression of all four renal EP receptors is altered (32). Although slight differences were observed in the magnitude of change of EP receptor mRNA depending on the diabetic animal model, overall regional alterations were similar (32). In the renal cortex, EP_1, EP_2, and EP_3 are increased while EP_4 is decreased. In the renal medulla, EP_1 and EP_3 are increased (32). Additionally, PGE_2 and COX2 are upregulated in the pancreatic islets during diabetes alongside increases in EP_3 (33).

1.3 PGE_2 and Vascular Hemodynamics

As previously mentioned, dysregulation of glomerular hemodynamics is a key mechanism underlying the pathogenesis of DN. PGE_2 is an important regulator of renal vascular tone and hemodynamics (23-25). In the rat afferent arteriole, PGE_2 elicits a vasodilatory effect via EP_4-cAMP (34). The same effect was observed in rat preglomerular microvessels (36). The contribution of EP_4 to the vasodilatory response of the tubuloglomerular feedback mechanism was confirmed by using specific EP_4 antagonists (37). Similarly, EP_2 receptors cause vaodilation of mouse afferent arterioles and buffer vasoconstrictor effects via EP_1 and EP_3 (38). However, baseline renal hemodynamics was unchanged in mice lacking EP_2 receptors but mice lacking EP_3

receptors had increased renal blood flow and decreased resistance (39). PGE_2 has been shown to constrict the afferent arteriole at supra-physiological concentrations through EP_3 (40). This vasoconstrictive action of PGE_2 via EP_3 has been shown to be more pronounced in the interlobular arteries preceding the afferent arteriole (41). Furthermore, EP_3 agonism decreased perfusion of the cortex and medulla in rats (42). Combining the EP_3 agonist with a RAAS blocker confirmed that the vasoconstrictive effect in the rat cortex is mediated by EP_3 independently of RAAS activation (42). Additionally, EP_1 receptors may contribute to the vasoconstrictor effects of angiotensin II as mice lacking EP_1 are protected from diabetic hyperfiltration (43). Altogether, the overall effect of PGE_2 may be vasodilatory or vasoconstrictive dependent on several factors including relative expression of EP receptors, the presence of other hormonal signals and the cell context. PGE_2 can indirectly increase GFR via EP_4 by stimulating macula densa renin release to increase angiotensin II, which constricts the efferent arteriole (44, 45). NSAID use can reduce GFR suggesting that the overwhelming effect of PGE_2 is to vasodilate the afferent arteriole and/or vasoconstrict the efferent (9, 44, 45). Additionally, NSAID use in individuals with existing renal disease, when GFR is already low, further exacerbates the decline in renal function (9). However, COX-2 inhibition in normofiltering diabetics was seen to increase GFR (9). Recent studies have shown that activation of EP_3 reverses the effect of COX inhibitors on COX-2 expression in the mouse thick ascending limb, revealing that EP_3 may also indirectly modulate GFR by regulating renin release and tubuloglomerular feedback (46).

DN can contribute to the development of systemic hypertension, while systemic hypertension can contribute to the development of DN. An important modulator of

systemic blood pressure control is PGE_2, where EP receptors have functionally antagonistic actions (47). Activation of EP_2 and EP_4 generally lowers blood pressure whereas activation of EP_1 and EP_3 receptors generally raises blood pressure (47). Systemic infusion of PGE_2 was found to cause a reduction in mean arterial pressure by activating the EP_2 receptor (48). On the other hand, intra-cerebroventricular infusion of PGE_2 was found to cause a rise in mean arterial pressure by activation of the EP_3 receptor (49).

1.7 PGE_2 and Renal Water and Salt Transport

A feature of DN is disturbances in salt and water balance with increased diuresis and natriuresis in early DN (6, 7). These mechanisms contribute to increased fluid flow in the tubular lumen, which can damage the kidneys (9). Physiologically, the body responds to acute volume depletion by stimulating the production of the antidiuretic hormone, arginine-vasopressin (AVP), within the hypothalamic paraventricular and supraoptic neurons (1, 2). AVP is then processed, stored, and secreted into the venous flow by the posterior pituitary to interact with renal V_2 receptors located in the principal cells of the collecting duct to promote aquaporin 2 (AQP2) dependent water reabsorption (1, 2). AVP and angiotensin II also increase the body's thirst response to restore any depleted fluid volume (1, 2). Diabetes typically induces AVP production presumably due to the volume contraction caused by the polyuria; however, inconsistent increases and decreases in the expression of AQP2 are reported suggesting that the physiological pathway is dysfunctional in diabetes (50-57).

Renal PGE_2 antagonizes the action of AVP since NSAIDs transiently enhance urine concentration and promote water retention (58). In the cortical collecting duct (CCD), PGE_2 and the EP_1/EP_3 agonist, sulprostone, decreases cAMP and water permeability through both pertussis toxin (G-protein inhibitor) and staurosporine (protein kinase C inhibitor) sensitive mechanisms (59-62). Therefore, it can be hypothesized that EP_3 inhibits AQP2 membrane targeting through binding to Gi and EP_1 acts through protein kinase C to increase AQP2 endocytosis (59-62). Inner medullary collecting ducts (IMCD) show decreased AVP induced water permeability in response to PGE_2 and AQP2 membrane targeting is abolished in response to EP_3 stimulation (63-66). Through several experimental setups, the effect in the IMCD seems to occur at a post-cAMP level, which is opposite to what occurs in the CCD (63-66). However, the differences in the segments could be due to species differences, alterations in EP receptor profile, or different EP_3 splice variants (59, 67, 68). Additionally, EP_1 is highly expressed in the IMCD, in contrast to EP_3 which has the opposite expression profile, suggesting that the IMCD effects are through EP_1 (68). PGE_2 also increases the production of hyaluronan in medullary interstitial cells (69). Hyaluronan is capable of binding to large amounts of water causing resistance to water flow (70). EP_2 is located in the medullary interstitial cells and it is coupled to Gs similar to hyaluronan synthases implicating this receptor in diuresis (71).

Transport of sodium ions out of the lumen of the CCD is strongly and rapidly upregulated by AVP and it depends on the apical entry of sodium ions through the epithelial sodium channel (ENaC) followed by the pumping of sodium into the basolateral side by Na^+/K^+-ATPase (1, 2). ENaC is a heterotrimeric complex made up of

alpha, beta, and gamma subunits (1, 2). AVP can increase the abundance of all three subunits. RAAS can also affect ENaC activity, whereby angiotensin II stimulates the secretion of the mineralocorticoid, aldosterone, from the adrenal cortex, which can then increase the abundance of the alpha subunit of ENaC (αENaC) (1, 2). Thus, the overall regulation of the electrogenic transport in the CCD is synergistically dependent on both AVP and aldosterone (1, 2). Specific activation of EP_1 receptor during RAAS activation has been shown to antagonize the action of aldosterone on αENaC expression in the renal medulla (72). It is not inconceivable that EP_3 can antagonize the AVP mediated abundance of ENaC similar to AQP2 however this has not been tested.

Similar to ENaC, AVP and aldosterone can stimulate the activity of the sodium-potassium-chloride cotransporter 2 (NKCC2) found in the cells of the thick ascending limb of the of Henle (1, 2). NKCC2 maintains electroneutrality by moving two positively charged solutes (sodium and potassium) alongside two parts of a negative charged solute (chloride) (1, 2). Studies have shown that EP_3 reduces countercurrent multiplication by decreasing solute transport in the medullary thick ascending limb (73-75). Through coupling to G_i, EP_3 regulates AVP-induced increases in cAMP and thereby prevents recycling of NKCC2 (73-75). Furthermore, Nusing et al demonstrated that $EP_1^{-/-}$, $EP_3^{-/-}$, and $EP_4^{-/-}$ mice exhibit blunted responses to chronic infusion of the NKCC2 inhibitor, furosemide (44). The furosemide-induced diuresis was most significantly blunted in $EP_4^{-/-}$ mice, suggesting that it predominates over other EP receptors in this response (44).

1.8 PGE_2 and Glucose Metabolism

PGE_2 in particular has long been known as a physiological inhibitor of insulin secretion, acting via autocrine or paracrine mechanisms (76-77). Recently, EP_3 is being suggested as an emerging target for type 2 DM therapeutics (33). Antagonizing EP_3 has been shown to significantly improve the insulin secretory response of diabetic mouse and human islets (33). EP_3 opposes the action of the glucagon-like peptide 1 (GLP-1) receptor, a Gs-coupled receptor, and inhibits glucose-stimulated insulin secretion (33). EP_3 also plays a critical role in systemic metabolic regulation (78). Mice lacking EP_3 develop obesity, insulin resistance, glucose intolerance, and eat considerably more than wild-type controls (78). EP_3 knockout mice showed altered nocturnal activity and feeding behavior. This can be explained in part by elevated leptin and insulin levels (78).

1.9 Rationale

Despite the many advances made in DN research, to this day therapy is limited, and the development of chronic kidney disease is still on the rise. PGE_2 and its EP receptors are interesting targets for therapeutic measures since they are heavily implicated in many mechanisms of the pathogenesis of DN. Of all the EP receptors, the role of EP_3 in the diabetic milieu is not well understood. Renal EP_3 is considerably increased in both the cortex and medulla while other EP receptor subtypes are either unchanged or modestly increased (32). Additionally, EP_3 is implicated in many early changes of diabetes,

including glucose metabolism, polyuria, glomerular hyperfiltration, and blood pressure regulation. The ability of EP_3 to inhibit insulin secretion and affect eating habits may contribute to diabetic complications (33, 78). The role of EP_3 in glomerular hemodynamics is less clear. Studies show that EP_3 acts as a vasoconstrictor in the interlobular arteries and the afferent arteriole, thereby suggesting that it may reduce glomerular hyperfiltration in diabetes (34). However, EP_3 also was found to reverse the renal effect of COX-2 inhibitors, which are known to reduce GFR (46). This finding suggests that EP_3 may facilitate increases in GFR by potentiating COX-2 activity. Regardless of its effect, this warrants further exploration. Importantly EP_3 is implicated in urine production. Fleming et al showed that basal osmolality was similar in $EP_3^{-/-}$ and wild-type mice (79). However, after inhibition of endogenous PGE_2 production by indomethacin, urine osmolality increased significantly in wild-type mice but not in $EP_3^{-/-}$ mice (79). Furthermore, Zhang et al documented that genetic deletion of the purinergic receptor, P_2Y_2, offers significant resistance to the development of Li-induced polyuria due to altered PGE_2 signaling mediated by a marked decrease in EP_3 in the renal medulla (80). These findings suggest that PGE_2 acts through EP_3 to modulate urine production, but only in pathophysiological states such as diabetes (80). Lastly, EP_3 is suggested to act as a vasoconstrictor in systemic vessels therefore contributing to increased blood pressure (47). Increased blood pressure is an important pathogenic mechanisms in DN. Considering all this evidence, we postulate that renal EP_3 receptors contribute to disturbances in glucose metabolism, glomerular hyperfiltration, polyuria, and increased blood pressure during diabetes. An essential tool in achieving our goal is the EP_3 knockout mouse, which allows the examination of the effects of PGE_2/EP_3 receptors in

the diabetic kidney. This work should reveal the benefit of targeting renal EP_3 receptors as a therapeutic measure for diabetic kidney disease.

1.10 Hypothesis

We hypothesize that PGE_2 contributes to the development of DN via renal EP_3 receptors: (1) by promoting polyuria and (2) by contributing to kidney growth and exacerbating the decline in kidney function.

1.11 Objectives

1. To characterize the phenotype of global EP_3 deletion in C57BL/6 mice.
2. To characterize the phenotype of global EP_3 deletion in STZ diabetic C57BL/6 mice.
3. To characterize the role of EP_3 in altering water and salt transport in STZ diabetic C57BL/6 mice, M1 cortical collecting duct cells, and in vitro microperfused tubules.

2. MATERIALS AND METHODS

2.1 Animals

All procedures were approved by the Animal Care and Veterinary Service at the University of Ottawa. Baseline experiments were performed on 8-week-old male $EP_3^{-/-}$ mice (global deletion on a pure C57BL/6 background) and on wild-type (WT) mice (C57BL/6, Charles River, Wilmington, MA). Heterozygous $EP_3^{+/-}$ mice were generously donated by Dr. Richard M. Breyer (Vanderbilt University, Nashville, TN) (81). These mice were generated using Cre-LoxP technology. The contiguous γ C-terminal coding region on exon 2 of the EP_3 gene was flanked by LoxP sites. These animals were crossed with C57BL/6 Ella Cre mice, to generate a global deletion of all EP_3 splice variants. The resulting heterozygote progeny were backcrossed to C57BL/6 to select for the loss of the Ella Cre allele (81). Two female $EP_3^{+/-}$ were mated with one male $EP_3^{+/-}$ when they reached sexual maturity (6 to 8 weeks old). $EP_3^{-/-}$ pups were identified by genotyping as described below. Two female $EP_3^{-/-}$ were mated with one male $EP_3^{-/-}$ when they reached sexual maturity (6 to 8 weeks old). Litters were genotyped for two generations to confirm that all progeny are $EP_3^{-/-}$.

2.2 Genotyping

Male mice were genotyped after weaning for approximately four weeks. The REDExtract-N-Amp Polymerase Chain Reaction (PCR) ReadyMix Kit (Sigma-Aldrich,

St. Louis, MO) was used to extract DNA from freshly snipped ear tissue as per manufacturers guidelines. PCR was then used to determine the genotype of extracted DNA. Wild type master mix (16 µl per reaction) was prepared as follows: 2 µl diethylpyroarbonate (DEPC) -treated water, 10 µl Sigma REDExtract-N-Amp PCR reaction mix, 2 µl wild type EP_3 sense primers (sequence: gct gtc tcc agt tgc tct a) (10.5 µM) and 2 µl wild type EP_3 anti-sense primers (sequence: tgc ctc agt cca taa ggg tta ggg) (10.5 µM). The null master mix (16 µl per reaction) was prepared as follows: 2 µl DEPC-treated water, 10 µl Sigma REDExtract-N-Amp PCR reaction mix, 2 µl EP_3 null sense primers (sequence: tgg cac aga aag gat tat cta) (10.5 µM) and 2 µl EP_3 null anti-sense primers (sequence: aac gct tgt caa atg ttc at) (10.5 µM). Two separate reactions were run with wild-type and null primers (81). Each reaction contained 16 µl of master mix and 4 µl of DNA sample.

The PCR tubes were placed in a thermal cycler and the following program was run:

Table 1. PCR thermal cycler settings for genotyping protocol

	Taq polymerase Activation	**PCR**			**Extend**	**Store**
	HOLD	Cycle (40 cycles)			HOLD	HOLD
		Denature	Anneal	Extend		
Time	3 min	15 sec	15 sec	30 sec	10 min	∞
Temperature	94°C	95°C	58°C	72°C	72°C	4°C

A 1% agarose gel (Thermo Fisher Scientific, Waltham, MA) was used to analyze the reactions. The polymerized gel was transferred into a horizontal electrophoresis system and was submerged in 1X tris-acetate buffer. DNA ladder (300 µl) was prepared as follows: 50 µl 100bp DNA Ladder (1 µg/µl) (Thermo Fisher Scientific), 50 µl 6X DNA loading buffer (10 ml total: 3 ml glycerol, 25 mg bromophenol blue, and 7 ml water), and 200 µl deionized water. DNA ladder (10 µl) was loaded into the first well while the DNA samples were loaded into the remaining wells. Electrophoresis was run at 100 V for 30 minutes. Once the run was complete, the gel was viewed in an AlphaImager system (ProteinSimple, San Jose, CA) for analysis. Expected band sizes are 152 bp for wild type and 721 bp for EP_3 null (81).

2.3 Glucose Tolerance Test

A glucose-tolerance test was performed at the onset of the light cycle (6:00 am) (78). Eight-week-old baseline mice were weighed and fasted for 16 hours before the glucose-tolerance test. Access to drinking water was allowed during this period. On the day of the test, baseline glucose levels and body weight were determined before challenge with a glucose load of 1.5 mg of glucose per gram of body weight (D-glucose, anhydrous; Sigma-Aldrich) dissolved in sterile distilled water (0.75 g of D-glucose, anhydrous in 10 ml of sterile water). The conscious mouse was restrained in a 50 ml Falcon tube and the hind leg was immobilized in the extended position and the fur was shaved to reveal the saphenous vein. Using a 27-gauge needle, the saphenous vein was punctured and a small drop (~ 5 µl) of blood was placed on the glucometer test strip and a blood glucose meter

(both from Home Diagnostics, Fort Lauderdale, FL). After a 5 seconds developing time, the baseline blood glucose value was recorded (in mM), and the mouse was returned to his original cage. After the baseline glucose measurement, the mouse was injected intra-peritoneal (i.p) with the glucose solution by using a 1-ml syringe and a 27-gauge needle. The time of the injection was noted, and 15, 30, 60, and 120 minutes post-injection blood glucose measurements were performed again. After the end of the study, mice were returned, and food and water was provided *ad libitum*.

2.4 Insulin Tolerance Test

The effects of insulin injection were assessed in non-fasted male mice (78). Similar to the glucose tolerance test described above, blood was withdrawn from the saphenous vein without anesthesia before administration of human insulin (1 unit/kg, i.p.; Sigma-Aldrich). Samples were collected 15, 30, 60, and 120 minutes after the insulin challenge. Blood glucose levels were determined using a blood glucose meter (Home Diagnostics).

2.5 Blood Pressure Measurement

Systolic blood pressure was measured via tail-cuff plethysmography (BP 2000, Visitech systems, Apex, NC). Mice were trained for at least three days. Following the training period, daily blood pressure was measured at the same time each day for at least five days. During the measurement period, 5 preliminary readings were performed followed by 10 actual readings. Blood pressure readings for each day were retained only if at least

4 out of 10 successful readings were obtained and the standard deviations for the readings are within 20 mm Hg. At least five days of readings were averaged to obtain final values.

2.6 Metabolic Cages and Urine Analysis

Daily urine output as well as daily food and water intake was monitored using specially designed metabolic cages (Techniplast, West Chester, PA). Mice were placed in metabolic cages with free access to water and food for 24 hours to assimilate before performing actual measurements. Following the assimilation period, food and water receptacles were refilled and the starting amounts were recorded and mice were left in their cages for another 24 hours. Following 24 hours, urine volume was recorded and collected and the remaining amounts of food and water were recorded. Urine samples were spun at 9,600 G for ten minutes to separate food, feces, or debris from the urine. Urine was then transferred into new microcentrifuge tubes and the pellet was discarded. Approximately 150 µl of urine was sent to IDEXX laboratories (Markham, ON) for urine biochemistry analysis. Urine albumin was quantified using a Mouse Albumin ELISA Kit (Bethyl, Montgomery, TX) as per manufacturer's guidelines. Urine samples from WT mice were diluted 1:1,000 while urine samples from diabetic mice were diluted 1:500. The kit employs a sandwich enzyme-linked immunosorbent assay (ELISA) using goat anti-mouse albumin antibody. Concentration of samples is determined by comparing their absorbance (at 450nm) to that of a mouse reference serum. Daily urine albumin excretion was determined by correcting for 24-hour urine output. Urine AVP was quantified using the Arg^8-Vasopressin ELISA Kit (Enzo Life Sciences, Farmingdale, NY) as per

manufacturer's guidelines. Urine samples from WT mice were diluted 1:6 while urine samples from diabetic mice were not diluted. The kit employs a competitive ELSIA using a rabbit polyclonal antibody to vasopressin and the concentration of unknown samples is determined by comparing their absorbance (at 450nm) to that of an Arg^8-vasopressin standard. Daily urine AVP excretion was determined by correcting for 24-hour urine output.

2.7 Estimation of Glomerular Filtration Rate

Glomerular filtration rate was estimated by fluorescein isothiocyanate (FITC)-inulin (Sigma-Aldrich) plasma clearance (82). 5% FITC-inulin was prepared in 0.9% NaCl. To remove residual FITC not bound to inulin, the solution was filled into a 1000 Daltons cut-off dialysis membrane (Spectra/Pro 6, Spectrum Laboratories Inc., Rancho Dominguez, CA). The dialysis membrane filled with FITC-inulin was stirred suspended in 0.9% NaCl for 24 hrs at room temperature. Prior to use, the dialyzed solution was sterilized by filtration through a 0.22 μm filter (Sigma-Aldrich). The conscious mouse was restrained in a 50 ml Falcon tube and the tail vein was dilated by submerging the tail in warm water for approximately 1 minute. 5% FITC-inulin (3.74 μl/ g body weight) was injected in the tail vein. The inner thigh was shaved and wiped with 75% ethanol, revealing the saphenous vein. Approximately 20 μl blood was collected in a heparinized capillary tube (Thermo Fisher Scientific) by puncture of the vein using a sterile 23-gauge syringe needle. On average, this yields 10 μl of plasma following centrifugation (1,500 G, 10 min). Blood was sampled via the saphenous vein at 3, 7, 10, 15, 35, 55, and 75 minutes

post injection of FITC-inulin. A two-compartment clearance model was employed for the calculation of GFR. At any given time (tx), the plasma concentration of the tracer (Y) equals Ae – αtBe – βtx + Plateau. The parameters of the above equation were calculated using a non-linear regression curve fitting program (GraphPad Prism, GraphPad Software, Inc., San Diego, CA). GFR was calculated using the equation: GFR = I/ (A/α + B/β), where I is the amount of FITC-inulin delivered by the i.v. injection, A (Span 1) and B (Span 2) are the y-intercept values of the two decay rates, and α and β are the decay constants for the distribution and elimination phases, respectively.

2.8 Blood Collection

Blood was collected from conscious mice equaling approximately 10% of their total blood volume as per the ACVS guidelines. The conscious mouse was restrained in a 50 ml Falcon tube and the hind leg was immobilized in the extended position and the fur was shaved to reveal the saphenous vein. Using a 27-gauge needle, the saphenous vein was punctured and blood was collected in heparinized microcentrifuge tubes (BD, Franklin Lakes, NJ). Samples were centrifuged at 9,600 G for 10 minutes. Plasma was collected and stored at -80°C for future analysis. Approximately 150 µl of plasma was sent to IDEXX laboratories for plasma biochemistry analysis.

2.9 Kidney Collection

Each mouse was placed in a CO_2/O_2 chamber until completely unconscious and motionless, and then decapitated. The abdominal cavity was opened and the intestines and surrounding fat and connective tissue were removed to free the kidneys from the animal. Excess fat and vasculature was carefully cut from the renal pelvis. The renal capsule was carefully peeled from top end of kidney. The kidneys were weighed and stored in cold PBS for dissection. Renal medulla and cortex were carefully dissected under a dissecting light microscope and consequently snap frozen in liquid nitrogen. Tissue samples were stored at -80°C for later analysis.

2.10 Microdissection of Nephron Segments

Mice were sacrificed as described above and the kidneys were quickly removed, and 1 to 2 mm coronal slices were placed in chilled dissection dishes for freehand dissection of proximal tubules, thick ascending limbs, and cortical collecting ducts, distinguished from other segments based on various properties: diameter difference, cell heterogeneity, and translucency. The tubules were placed on ice for mRNA isolation as described in section 2.11.

2.11 Micro-Sized RNA Isolation

RNA was isolated from the freshly microdissected nephron segments using the RNAqueous-Micro Total RNA Isolation Kit (Thermo Fisher Scientific) which employs a guanidinium-based lysis/denaturant and glass fiber filter separation technology. The samples were then treated with the optional DNase I (provided with kit) as per manufacturers guidelines to remove trace amounts of contaminating genomic DNA.

2.12 Quantitative PCR using TaqMan-based detection

Quantitative PCR (qPCR) was performed to determine the levels of EP receptors in the microdissected nephron segments. Samples were prepared using the TaqMan One-step RT-PCR Master Mix Reagents (Thermo Fisher Scientific). The sequences of the probes and primers are shown below (32):

Table 2. Primer and TaqMan probe sequences for mouse EP receptors.

Target	Size	Primer sequences	Probes sequences
EP_1	336 bp	Sense: ccaaagctaggccaaaccatt	tgggctcaaggg
		Anti-sense: ccctaggcacactgagtttgaga	ttcaagggcata
EP_2	401 bp	Sense: tgctccttgcctttcacaatc	ttgcctacatggatga
		Anti-sense: gagctcggaggtcccacttt	aacctcttccctaaa
EP_3	437 bp	Sense: gctggccatgttgcttgtg	cgcgcagcta
		Anti-sense: ggaaagacttttgcgtttgct	tagacgccgg
EP_4	423 bp	Sense: tgtacgcgggcttcagttc	ttcctcatcctc
		Anti-sense: cgcacaccagcacattgc	gccaccgtgct

The ABI Prism 7000 sequence detection system (Thermo Fisher Scientific) was used to perform the sample analysis. The amplification conditions consisted of: 30 minutes at 48°C (RT step), 10 minutes at 95°C (AmpliTaq Gold activation), and 40 cycles of 15 seconds at 95°C and 1 minute at 60°C (PCR). Expression of each receptor was normalized to GAPDH mRNA levels, detected with the TaqMan Rodent GAPDH control reagent kit (Thermo Fisher Scientific). A standard curve was produced for absolute quantification. The RNA standard curve included 8 points derived from WT renal cortex: 150 ng, 75 ng, 37.5 ng, 18.75 ng, 9.38 ng, 4.69 ng, 2.35 ng, and 0 ng (water blank).

2.13 Streptozotocin Induced Diabetes

Type 1 diabetes was induced by injecting 8-week-old mice with low-dose streptozotocin (STZ) (Sigma-Aldrich) (83). Mice were fasted for 4-6 hours prior to injections to lower blood glucose which may compete with STZ for GLUT2. Sodium citrate solution (100mM, pH 4.5) (Thermo Fisher Scientific) was prepared and sterilized by filtration through a 0.22 μm filter (Sigma-Aldrich) to serve as the vehicle for STZ. Mice were weighed and baseline blood glucose was determined by a blood glucose meter (Home Diagnostics). A solution of 5mg/ml STZ (Sigma-Aldrich) was prepared in sodium citrate immediately prior to injection. Mice were injected i.p. with 50 mg/ kg body weight of STZ or vehicle only. This protocol was repeated for five consecutive days. Blood glucose levels were measured four weeks post injection to confirm hyperglycemia (i.e. $\geq$ 15 mmol/ l).

2.14 Trizol RNA Isolation

TRIzol Reagent (Thermo Fisher Scientific) was used to isolate RNA from renal cortex and medulla. Snap-frozen tissue (10-15 mg renal medulla and 50-100 mg renal cortex) was homogenized using a COE CapMixer (GC America, Alsip, IL) set to 10 seconds and 1,800 G. The homogenate was then dissolved in 1 ml TRIzol Reagent and RNA was isolated as per manufacturers guidelines. RNA was suspended in 20 μl diethylpyrocarbonate (DEPC)-treated water and treated with 0.3 U/μg DNAse I (Thermo

Fisher Scientific). RNA concentration was determined by measuring absorbance at 260 nm.

2.15 Quantitaitve PCR using SYBR Green-based detection

The RNA derived from renal cortex and medulla was reverse-transcribed into cDNA using the High-Capacity cDNA Reverse Transcription Kit (Thermo Fisher Scientific) as per manufacturer's guidelines. mRNA expression of EP receptors was quantified using SYBR Advantage qPCR Premix (ClonTech, Mountain View, CA) as per manufacturer's guidelines. The sequences of primers and probes are as described earlier (Section 2.12). The ABI Prism 7000 sequence detection system was used to perform the sample analysis. The amplification conditions consisted of: denaturing at 94°C for 240 seconds, followed by 35 cycles of denaturing at 94°C for 15 seconds; annealing at 60°C for 30 seconds; extension at 72°C for 30 seconds, then 72°C for 10 min; and finally, cooldown to 4°C. Expression of each receptor was normalized to GAPDH mRNA levels, detected with the TaqMan Rodent GAPDH control reagent kit (Thermo Fisher Scientific). Gene expression levels were determined using the $\Delta\Delta C_T$ method (84).

2.16 Western Blots

Following collection of kidneys from mice, total protein isolation was performed. Snap-frozen tissue was homogenized using a COE CapMixer (GC America, Alsip, IL) set to 10 seconds. The homogenate was then suspended in modified radioimmunoprecipitation

assay (RIPA) protein lysis buffer (1% Nonidet P-40, 1% sodium deoxycholate, 0.1% sodium dodecyl sulfate (SDS w/v), 4.5mM NaCl, 2.5mM Tris base (pH 7.4), 8μM EDTA, 0.2mM sodium phosphate (pH 7.2), 0.5mM phenylmethanesulfonyl fluoride (PMSF), 1:100 protease inhibitor cocktail (Sigma, St.Louis), 1mM sodium pyrophosphate, 10mM sodium fluoride and 100μM sodium orthovanadate). The protein lysate was then centrifuged at 9,600 G for 10 minutes at 4°C, and the supernatant was transferred to a clean Eppendorf tube.

Protein quantification was performed using Bradford reagent (Bio-Rad, Hercules, CA). Samples were combined with Laemmli loading buffer and heated at 70°C for 15 minutes to denature the proteins. Samples were then loaded into a polyacrylamide gel (10-15% resolving gel with a 4% stacking gel) and electrophoresed at 150V for approximately 60 minutes. Following separation, the proteins were transferred onto a nitrocellulose membrane (GE healthcare, Piscataway, NJ) at 100V for 60 minutes. Membranes were blocked in 5-10% milk/TBS-T (137mM NaCl, 20mM Tris base, 0.1% Tween 20) for 60 minutes and incubated overnight with a primary antibody (Table 3). Three washes of 15 minutes in TBS-T were performed the next day and the appropriate secondary antibody (in 5-10 % milk/TBS-T) was applied to the membranes for 90 minutes. Finally, the membranes were washed three times in TBS-T for 90 minutes. The protein bands of interest were viewed on the AlphaImager System (ProteinSimple) or on BioMax autoradiography film (Carestream, Rochester, NY) following a 5-minute incubation with SuperSignal West Pico Chemiluminescent reagents (Thermo Fisher Scientific). β-actin protein expression was used as a loading control. Densitometric analysis was performed using ImageJ (NIH, Bethesda, MD). A list of antibodies with

their respective dilutions and secondary antibody is provided in the table below. All the secondary antibodies were obtained from Promega (Madison, WI):

Table 3. Primary and secondary antibody dilutions and blocking solution composition.

Primary Antibody		Secondary Antibody	
Name	Dilution	Name	Dilution
β-actin (Sigma)	1:10,000, 5% milk	Anti-mouse IgG HRP	1:4,000
AQP2 (Cell Signaling)	1:1,000, 10% milk	Anti-rabbit IgG HRP	1:2,000
AQP1 (Pierce)	1:1000, 10% milk	Anti-mouse IgG HRP	1:2,000
Na^+/K^+-ATPase α-1 (Pierce)	1:10,000, 5% milk	Anti-mouse IgG HRP	1:4,000
α-ENaC (Pierce)	1:1,000, 10% milk	Anti-rabbit IgG HRP	1:2,000
NKCC2 (Abcam)	1:1,000, 10% milk	Anti-rabbit IgG HRP	1:2,000
COX-1 (Cayman)	1:200, 10% milk	Anti-rabbit IgG HRP	1:2,000
COX-2 (Cayman)	1:200, 10% milk	Anti-rabbit IgG HRP	1:2,000

2.17 Histology and Immunofluorescene

At sacrifice, kidneys were excised, dissected, and immediately fixed in 4% paraformaldehyde. Paraffin-embedded kidney sections (3 μm) were obtained and stained with periodic-acid Schiff (PAS) reagent. All sectioning, paraffin embedding, and PAS-staining were performed by the University of Ottawa's pathology department. Kidney sections were viewed under light-microscopy at 20X magnification (Axioskop 2 Imager A1, Zeiss, Germany). Representative glomerular areas (20-25 glomeruli/mouse) and collecting duct luminal areas (40-50 collecting ducts/mouse) for each group were

analyzed in a blinded manner. ImageJ (NIH) software was used to quantify aforementioned areas.

Renal AQP1 (Thermo Fisher Scientific) immunofluorescence was performed on paraffin-embedded sections mounted on glass slides. Sections were deparaffinized in mixed xylene (Thermo Fisher Scientific) and rehydrated through a gradient of ethanol and distilled water. Sections were washed three times in PBS, boiled for 20 minutes in 0.1 M Na-Citrate buffer (pH 6.0) for antigen unmasking. Sections were blocked in PBS containing 10% donkey serum/ 1% BSA for 1 hour and incubated with mouse anti-AQP1 (1:500) overnight at 4°C. Slides were washed and treated with a FITC-labeled donkey anti-mouse secondary antibody (1:1000; Molecular Probes, Burlington, ON) for 1 hour. Sections were covered with fluorescent mounting medium (Vector laboratories, Burlington, ON) and coverslips. Slides were visualized under fluorescence microscopy whereby representative medullary profiles from each group were obtained in a blinded manner.

2.18 Cell Culture

In vitro experiments were conducted on the M-1 CCD cell line (ATCC, Manassas, VA; #CRL-2038). M-1 cells are commonly used as a model of the CCD and display many important morphological and physiological characteristics of this segment. This immortalized cell line was derived from a mouse transgenic for the early region of Simian Virus 40, Tg(SV40E)Bri/7 (85). These cells exhibit a significant transepithelial

solute gradient, an amiloride-sensitive Na^+ transport system, expression of epithelial Na^+ channel (ENaC) and expression of specific CCD antigens (85).

The cells were cultured in Dulbecco's modified Eagle's medium and Ham's F-12 nutrient medium (DMEM:F12 1:1, Gibco, Carlsbad, CA) containing 7.5mM glucose, 2.5mM L-glutamine, 15mM HEPES, 0.5mM sodium pyruvate and 1.2g/L sodium bicarbonate, pH 7.4. The media was supplemented with 5% fetal bovine serum (FBS) and 1% penicillin/streptomycin (Gibco). The cells were grown at 37°C and 5% CO_2.

To determine the effects of arginine-vasopressin (AVP; Sigma-Aldrich), high salt, and/or sulprostone (SLP; Sigma-Aldrich), the cell culture media was replaced with fresh serum-free media containing 10^{-8} M AVP, 10^{-7} M SLP, and/or high salt (240mM NaCl) 24 hours before the cells reached confluence.

2.19 In Vitro Microperfusion

Note: Joe Zimpelmann performed the freehand dissections and perfusions. I prepared the mice, solutions, and analyzed the data.

Male WT or $EP_3^{-/-}$ mice 12 weeks post STZ or vehicle injection were sacrificed as described previously (Section 2.9). The kidneys were quickly removed, and 1 to 2 mm coronal slices were placed in chilled dissection dishes for freehand dissection of cortical collecting duct (CCD), distinguished from other segments based on various properties: diameter difference, cell heterogeneity, transluscency (86). The microdissected CCD was

then transferred to a chamber for in vitro perfusions and measurement of net fluid reabsorption (Jv).

Microdissected cortical collecting ducts were transferred to a thermostatically controlled chamber of 1 cm^3 volume and cannulated using concentric micropipettes. Bath solution was continuously exchanged at 0.5 ml/min by infusion pump (Harvard Apparatus, Holliston, MA) and was maintained at 37^oC. The dissecting solution consisted of 137mM NaCl, 1mM $MgCl_2$, 0.8mM MgSO4, 5mM KCl, 0.25mM $CaCl_2$, 10mM Tris HCl, 0.33mM Na_2HPO_4, 2mM glutamine, 0.44mM KH_2PO_4, and 2mM L-lactate. The perfusate composition was 40mM NaCl, 2mM calcium lactate, 5.5mM glucose, 23mM $NaHCO_3$, 0.2mM sodium citrate, 0.8mM K_2HPO_4, and 0.24 $MgSO_4$. The composition of bath medium was 118mM NaCl, 2mM calcium lactate, 5.5mM glucose, 23mM $NaHCO_3$, 1mM sodium citrate, 4mM K_2HPO_4, and 1.2mM $MgSO_4$. Bovine serum albumin (5%, Sigma, St. Louis, MO) was also added prior to dissections. The perfusate, which contained ^{3}H-inulin (75 μCi/ml) as a volume marker was collected into a constriction pipette of known volume (between 90 and 130 nl) and counted for ^{3}H-inulin (New England Nuclear, Boston, MA). The perfusion rate was maintained between 12-20 nl/min by adjusting the hydrostatic pressure. In control studies, 30 min of equilibration were allowed and then, three collections were made for calculation of basal Jv in $nl \cdot mm^{-1} \cdot min^{-1}$. Tubules with a negative basal Jv were discarded. Then 10^{-8} M AVP (Sigma) was added to the bath and five timed collections were made to determine net volume reabsorption (Jv). Following the five collections, 10^{-7} M SLP was added and an additional five collections were made to determine Jv. In the experimental period the 3 highest collections of 5 were used to calculate mean Jv as the difference between the perfusion rate V_o and the

collection rate V_L, both in nl/min, normalized to tubule length (L, in mm): $Jv = (V_o - V_o)/L$, where $V_o = V_L (C_L/C_o)$, where C_L and C_o are perfusate and collected fluid concentrations in cpm/nl, respectively.

2.20 Statistics

Graphpad Prism (version 4) was used to analyze and present the data. Values are expressed as means ± standard error of the mean (SEM). Statistical analysis for multiple comparisons was done using one-way ANOVA followed by a Tukey post-test. A p-value < 0.05 with $n \geq 3$ was considered statistically significant assuming a normal distribution.

3. RESULTS

3.1 Confirmation of $EP_3^{-/-}$ Genotype

Heterozygous $EP_3^{+/-}$ C57BL/6 mice generously donated by Dr. Richard M. Breyer (Vanderbilt University, Nashville, TN) were intercrossed to generate homozygous null animals. Following the weaning of pups, DNA was extracted from freshly snipped ear tissue and the genotype was determined. Figure 3 shows a representative agarose gel of DNA viewed under UV light, whereby figure 3A shows the wild-type bands (152 bp) and figure 3B shows the mutant bands (721 bp). Samples 1 and 3 are $EP_3^{-/-}$ due to the presence of a mutant band and the absence of a WT band while sample 2 is $EP_3^{+/-}$ since both bands are present.

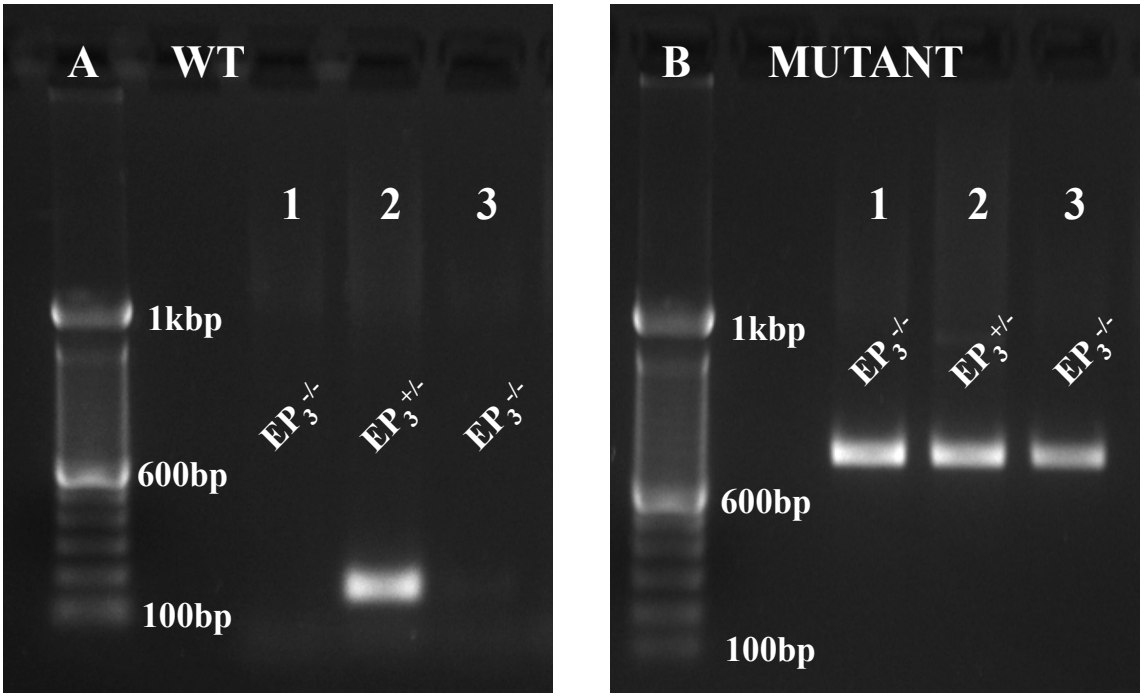

Figure 3. Representative agarose gel of DNA viewed under UV light showing (A) wild-type (WT) and (B) mutant EP_3 bands. The WT EP_3 band is 152 bp while the mutant EP_3 band is 721 bp. Samples 1 and 3 are derived from $EP_3^{-/-}$ mice while sample 2 is derived from an $EP_3^{+/-}$ mouse. Agarose gel (1%) was run in a horizontal electrophoresis system at 100V for 1 hour. A 1 kbp DNA ladder was loaded into the first lane.

3.2 $EP_3^{-/-}$ Mice Exhibit Increased Body Weight, Impaired Glucose Tolerance, and Increased Blood Pressure

Previous studies have reported that $EP_3^{-/-}$ mice develop an obese phenotype under a normal fat died fed *ad libitum* (78). Therefore, we examined the metabolic characteristics of $EP_3^{-/-}$ mice at 8-weeks of age. $EP_3^{-/-}$ mice show significantly increased body weight compared to wild-type mice (WT: 23.2 ± 0.4 g vs. $EP_3^{-/-}$: 25.9 ± 0.4 g; n = 25 per group; $p < 0.01$ using unpaired t-test). Non-fasting blood glucose concentrations were comparable between both groups (WT: 9.20 ± 0.5 mM vs. $EP_3^{-/-}$: 9.60 ± 0.5 mM; n = 25 per group). The mice were then fasted for 16 hours before performing a glucose tolerance test. The mice were challenged with a 1.5 mg of glucose per gram of body weight. Blood glucose concentrations were similarly elevated after 15 min in $EP_3^{-/-}$ and WT mice, but blood glucose concentrations reached higher levels in $EP_3^{-/-}$ mice after 30 min and remained higher until 120 min post-injection (Figure 4A). Non-fasted mice were then injected with 1 unit of human insulin per kg of body weight to assess their insulin tolerance. No significant difference was observed between the groups in blood glucose concentrations up to 120 min post-injection (Figure 4B).

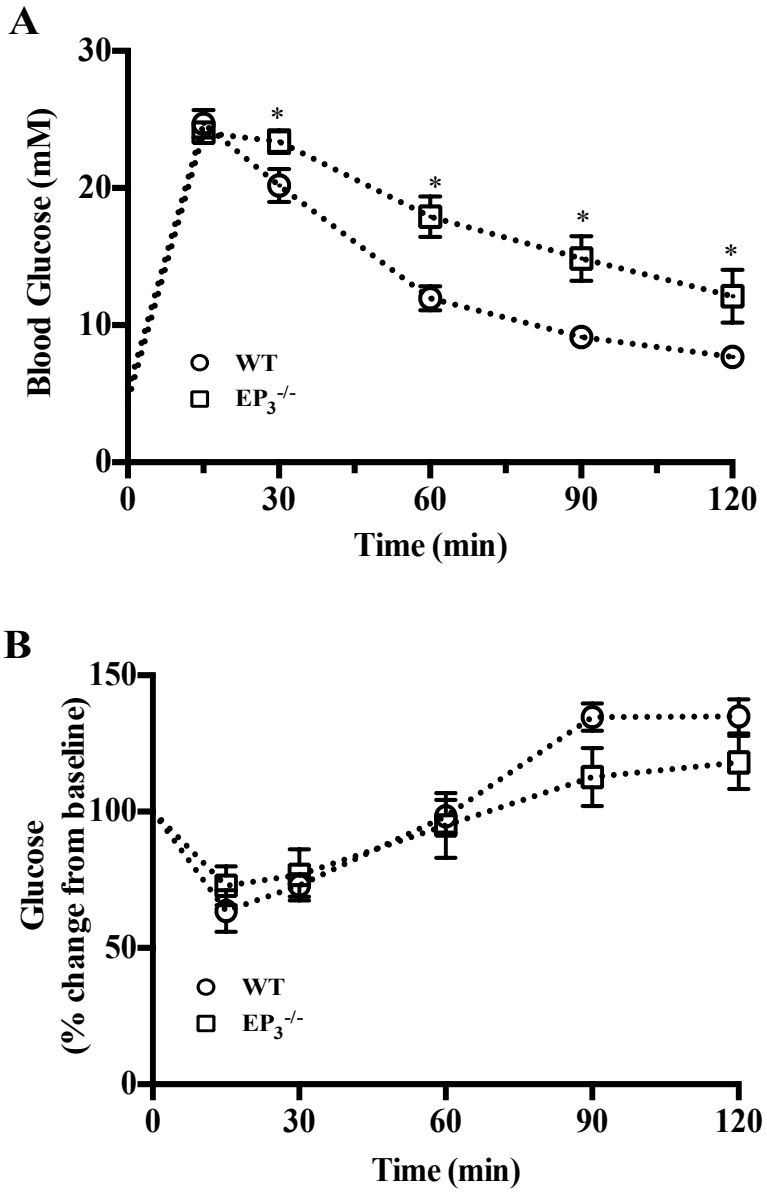

Figure 4. $EP_3^{-/-}$ mice exhibit impaired glucose tolerance but normal insulin tolerance. (A) Glucose tolerance test presented as blood glucose concentration following glucose challenge. (B) Percentage of change from baseline on the ability of insulin to acutely stimulate glucose clearance by performing an acute insulin challenge. N = 10 per group; *P < 0.05 vs. WT using an unpaired t-test.

PGE_2 has been shown to act as a systemic vasoconstrictor through EP_3, therefore we assessed blood pressure in these mice (47). By tail-cuff plethysmography, $EP_3^{-/-}$ mice show increased systolic blood pressure compared to WT mice (WT: 101 ± 2 mmHg vs. $EP_3^{-/-}$: 118 ± 2 mmHg; n = 25 per group; $p < 0.01$ using unpaired t-test).

3.3 Altered EP mRNA Profile in $EP_3^{-/-}$ Mice

EP_3 deletion may change the renal PGE_2/EP signaling pathway. Consequently, we isolated proximal tubules (PT), thick ascending limbs (TAL), and cortical collecting ducts (CCD) from a subset of 8-week old $EP_3^{-/-}$ and WT mice and analyzed EP_1, EP_2, and EP_4 mRNA expression. $EP_3^{-/-}$ and WT mice express comparable levels of EP_1, EP_2, and EP_4 mRNA in the PT and CCD (Figures 5A-5C). However, EP mRNA was markedly altered in the TAL, where $EP_3^{-/-}$ mice exhibit a 3-fold increase in EP_4 mRNA while EP_2 mRNA decreased by 3-fold (Figures 5A-5C). Additionally, EP_1 mRNA was numerically decreased by approximately 50% in the TAL in $EP_3^{-/-}$ mice but this effect did not reach statistical significance (Figures 5A-5C).

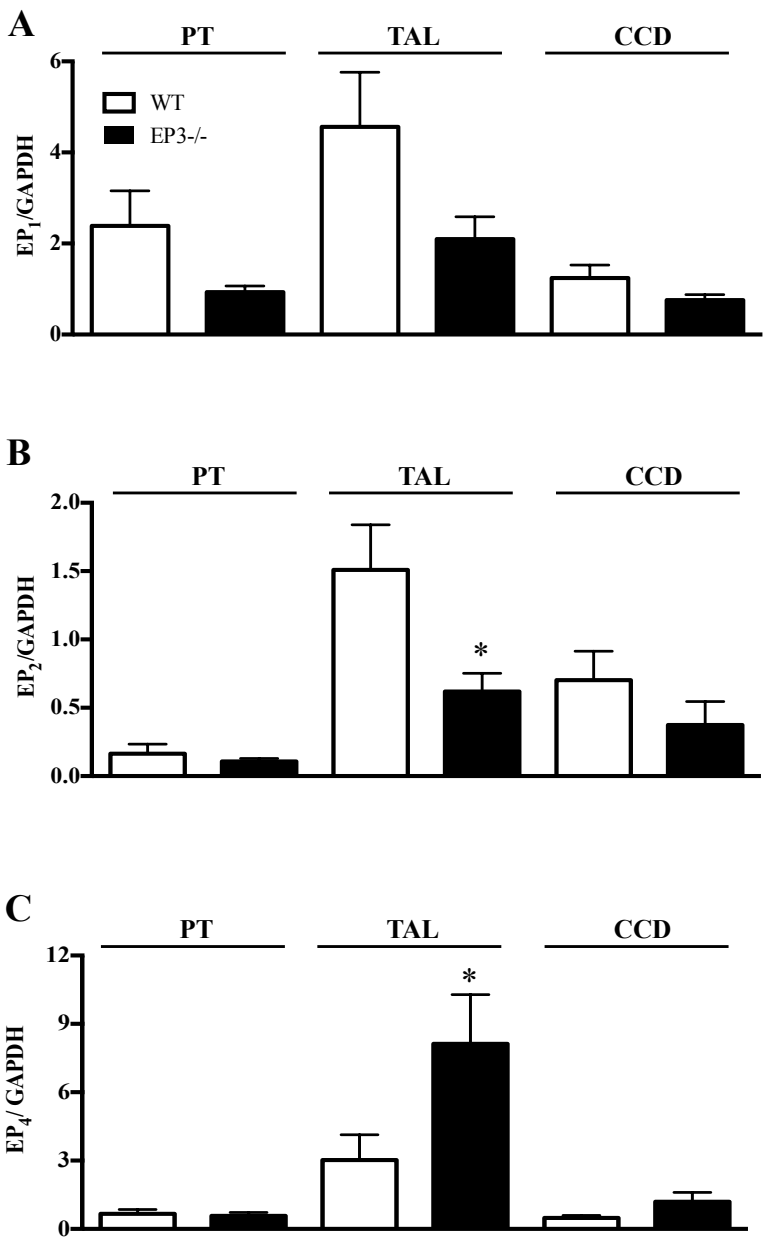

Figure 5. (A) EP_1, (B) EP_2, and (C) EP_4 mRNA expression in proximal tubule (PT), thick ascending limb (TAL), and cortical collecting duct (CCD) isolated from $EP_3^{-/-}$ (black bars) and WT (white bars) mice. N = 5 per group. *P < 0.05 versus WT using one-way ANOVA with a Tukey post-test.

3.4 Hyperglycemia and Renal Hypertrophy are Unchanged in $EP_3^{-/-}$ STZ Mice

We hypothesized that the PGE_2/EP_3 axis is detrimental in the diabetic kidney, therefore we injected 8-week old WT and $EP_3^{-/-}$ mice with STZ or vehicle (sodium citrate) and analyzed their physiological parameters 12-weeks post injection. At 12-weeks post STZ injection, STZ and $EP_3^{-/-}$ STZ mice show a 3-fold elevation in blood glucose concentration and a massive increase in urine glucose concentration compared to the non-diabetic mice (Table 4). Additionally, STZ and $EP_3^{-/-}$ STZ mice show an approximately 20% increase in kidney weight corrected for body weight when compared to non-diabetic mice (Table 4). Additionally, STZ and $EP_3^{-/-}$ STZ mice show an approximate 30% reduction in body weights compared to the non-diabetic mice (Table 4). $EP_3^{-/-}$ STZ mice show a numerically increased body weight compared to STZ mice; however, this is likely due to their greater baseline body weight prior to STZ injection (Table 4). An upward trend in systolic blood pressure was observed in the STZ and $EP_3^{-/-}$ STZ mice, but this did not reach statistical significance (Table 4). Additionally, $EP_3^{-/-}$ mice continue to exhibit a numerically elevated systolic blood pressure (BP) compared to WT mice (Table 4). No change in heart weight was observed between all four groups (Table 4).

Table 4. Physiological parameters of diabetic and non-diabetic $EP_3^{-/-}$ and WT mice. KW = kidney weight, BW = body weight, BP = blood pressure. N = 5 – 10 per group. $^{*}P < 0.05$ vs. WT and $^{\dagger}P < 0.05$ vs. $EP_3^{-/-}$ using a one-way ANOVA and a Tukey post-test.

	WT	**$EP_3^{-/-}$**	**STZ**	**$EP_3^{-/-}$ STZ**
Plasma Glucose (mM)	9.0 ± 1.0	7.8 ± 1.0	27.5 ± 4.0*	26.9 ± 4.0†
Urine Glucose (mM)	2.7 ± 0.2	2.1 ± 0.2	135.0 ± 0.1*	136.0 ± 0.1†
Body Weight (g)	30.2 ± 1	34.5 ± 1	23.6 ± 0.3*	26.9 ± 0.7†
Kidney Weight (mg)	169 ± 10	187 ± 10	204 ± 10*	208 ± 4
KW/ BW (mg/g)	5.8 ± 0.2	5.2 ± 0.2	8.1 ± 0.2*	7.6 ± 0.4†
Tibia Length (mm)	17.6 ± 0.2	17.4 ± 0.1	17.3 ± 0.05	17.3 ± 0.2
KW/TL (mg/m)	9.6 ± 0.5	10.8 ± 0.4	11.8 ± 0.5*	11.0 ± 0.3
Heart Weight (mg)	154 ± 5	157 ± 5	145 ± 10	138 ± 5
HW/ BW (mg/g)	5.3 ± 0.3	4.4 ± 0.2	5.7 ± 0.4	5.0 ± 0.2
Systolic BP (mmHg)	103 ± 1	110 ± 2	109 ± 3	116 ± 4

3.5 Glomerular Enlargement is Unchanged in $EP_3^{-/-}$ STZ Mice

Persistent hyperglycemia can lead to glomerular enlargement as well as increased mesangial matrix deposition (6, 7). Both diabetic groups show a modest but significant increase of 25% in glomerular area (Figures 6A, 6B). Mesangial area was numerically increased in the STZ mice however it did not reach statistical significance (Figures 6A-6C).

A

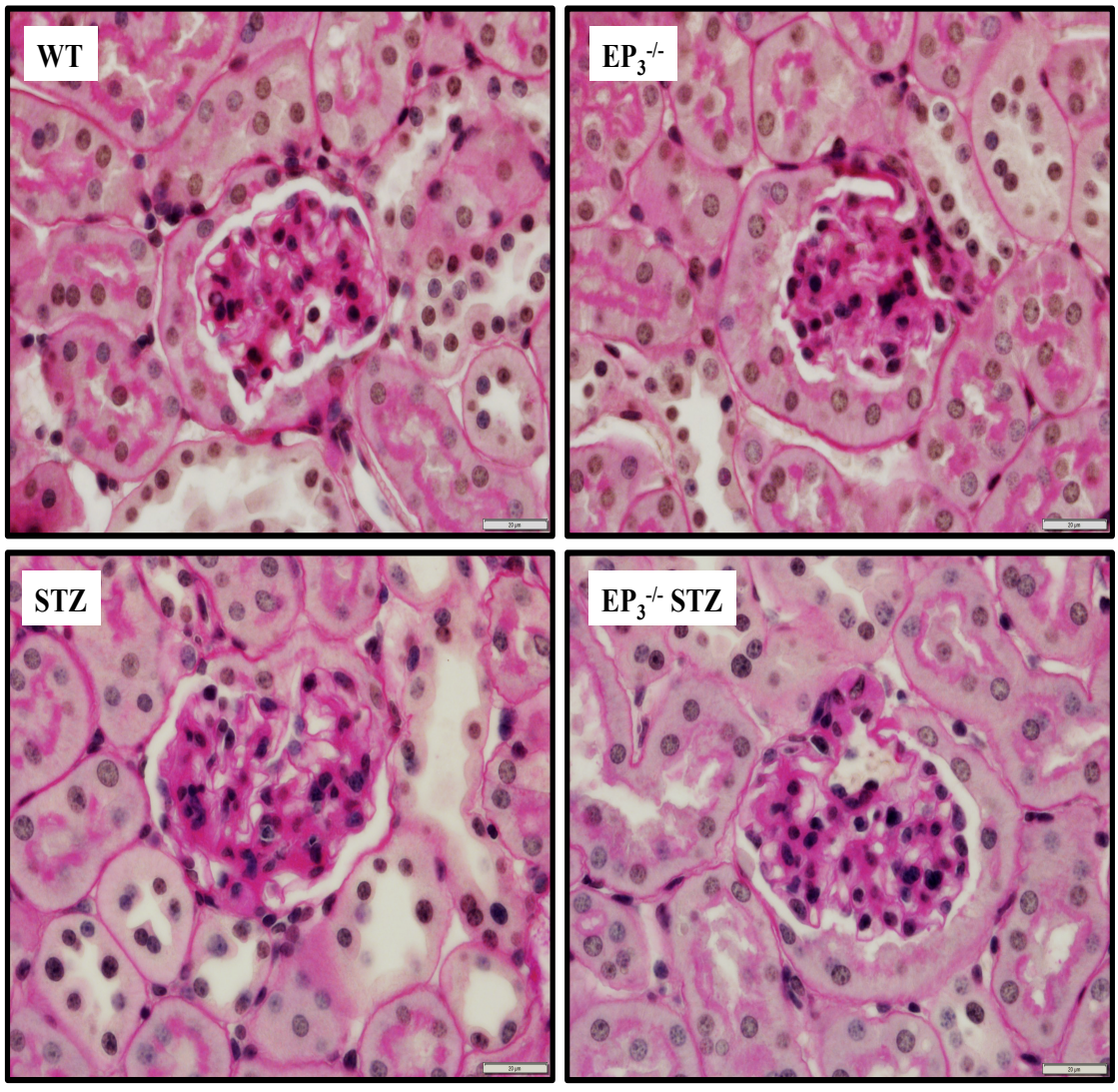

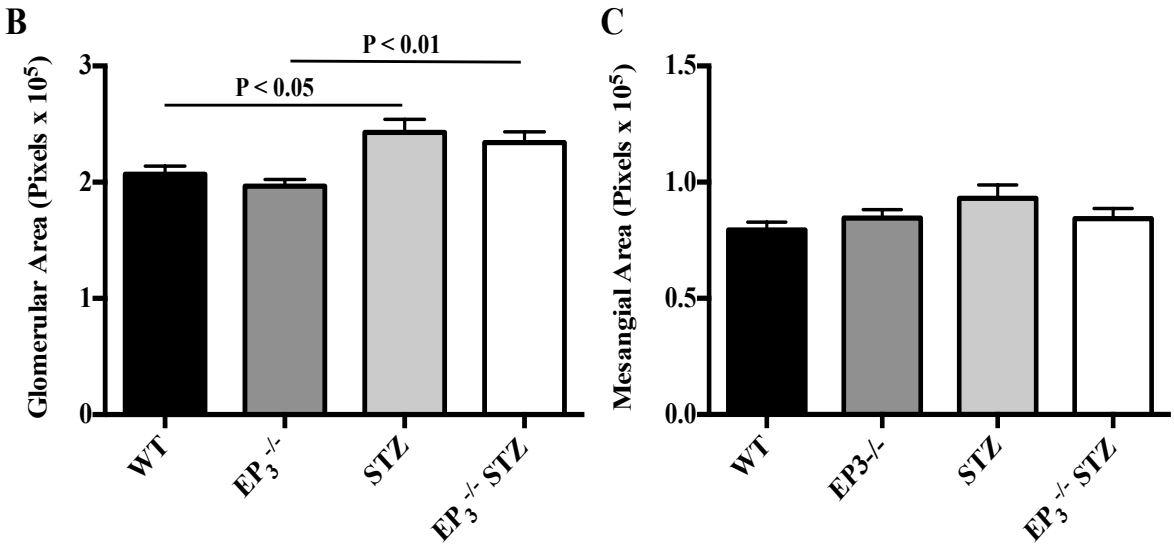

Figure 6. Enlarged glomerular and mesangial area in diabetic mice. (A) Representative images of periodic acid-Schiff stained paraffin-embedded kidney (PAS) sections, (B) quantification of glomerular area, and (C) quantification of PAS positive mesangial area. Images are shown at 20X magnification. Approximately 25 images showing a cluster of glomeruli were taken per group. Data presented as means ± SEM. P-values were calculated using a one-way ANOVA and a Tukey post-test.

3.6 Attenuated Hyperfiltration and Albuminuria in $EP_3^{-/-}$ STZ Mice

Increased GFR or hyperfiltration is a key feature of early diabetic kidney disease followed by urinary albumin excretion (6, 7). STZ mice show a 50% increase in GFR indicative of hyperfiltration accompanied by a doubling in urinary albumin excretion (Figures 7A, 7B). In contrast, $EP_3^{-/-}$ STZ mice show a GFR and a urinary albumin excretion rate comparable to controls (Figures 7A, 7B).

As kidney function declines with the progression of diabetic kidney disease, certain metabolites build up in the plasma (6, 7). Plasma creatinine and urea were found to be generally comparable across all four groups confirming that these mice are still in the early stage of diabetic kidney disease (Figure 5C). However, STZ mice showed an upward trend in plasma urea compared to WT and $EP_3^{-/-}$ STZ mice (Figure 5C).

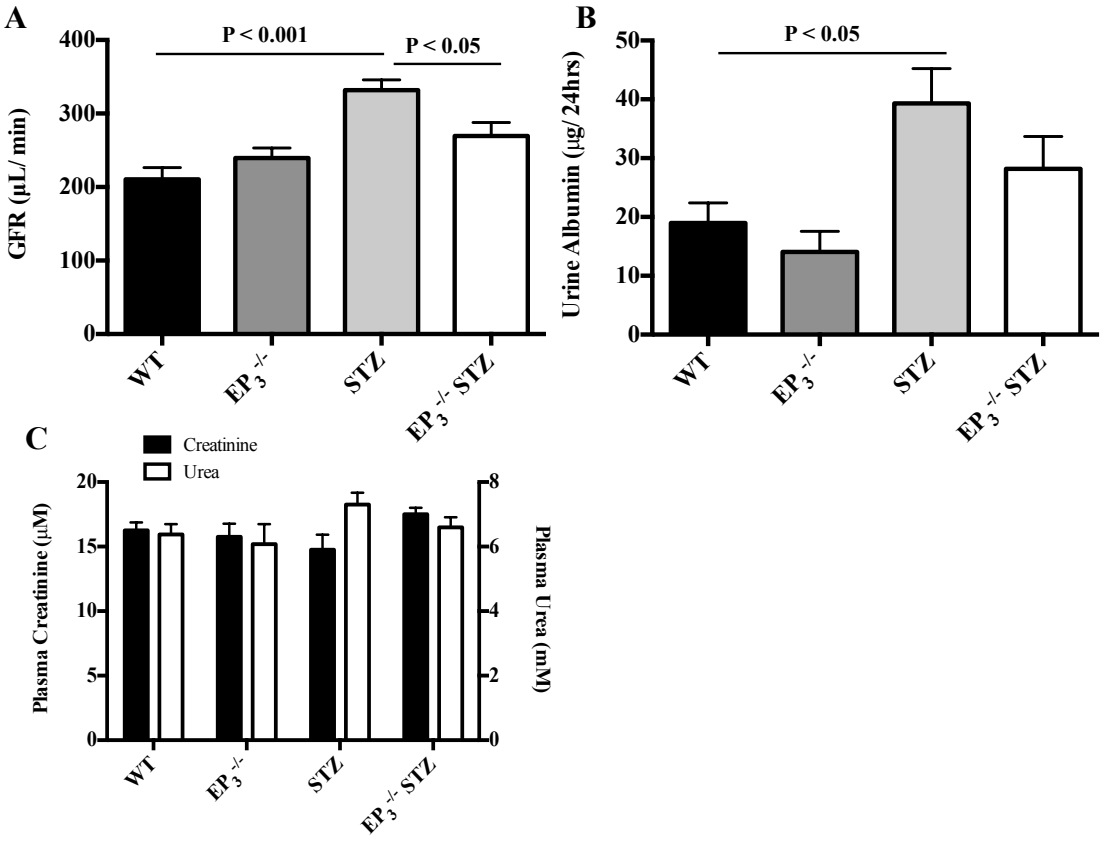

Figure 7. Diabetic hyperfiltration and albuminuria attenuated in $EP_3^{-/-}$ STZ mice. (A) GFR estimated by inulin plasma clearance, (B) daily urine albumin excretion, and (C) plasma creatinine (black bar) and urea (white bar). N = 5 - 10 per group. P values calculated using a one-way ANOVA and Tukey post-test.

3.7 COX-1 Unchanged in $EP_3^{-/-}$ STZ Mice.

Although renal COX-1 is involved in house-keeping functions and is not typically induced under pathological stress, we have reported it to increase in more than one diabetic mouse model (32). By Western immunoblotting, neither STZ or $EP_3^{-/-}$ STZ mice showed any change in cortical or medullary COX-1 protein expression (Figures 8A-8D).

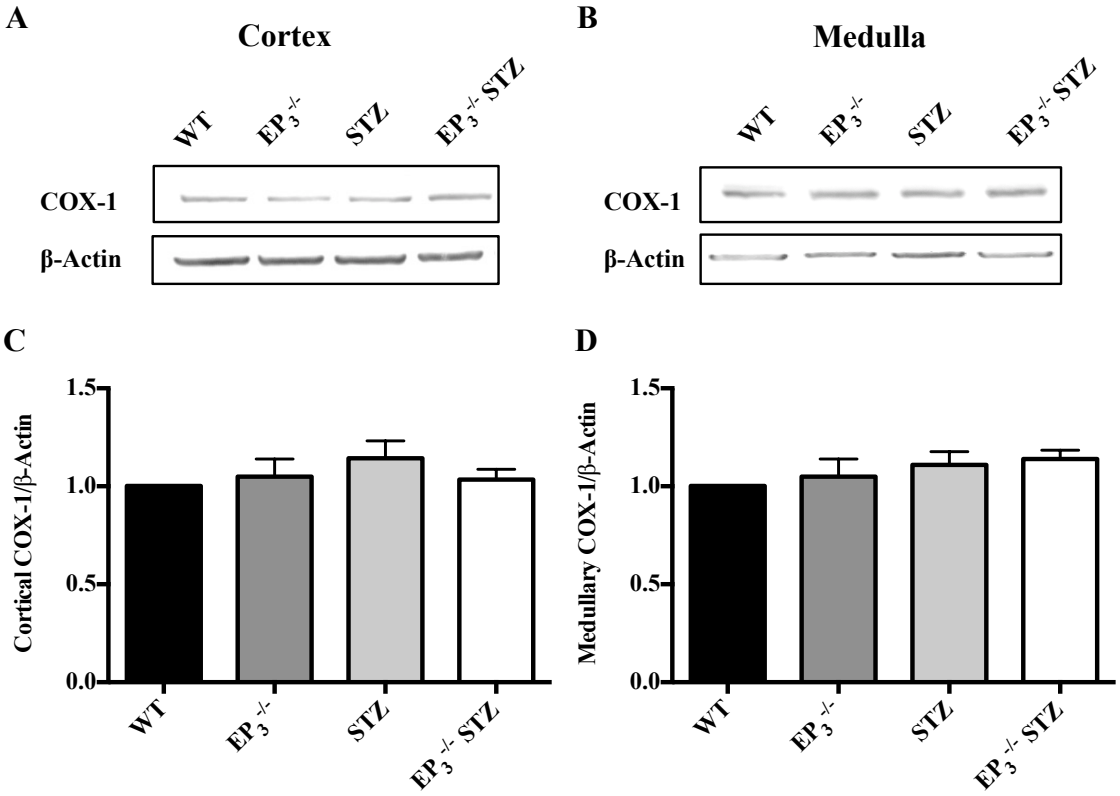

Figure 8. Cortical and medullary COX-1 expression are unchanged in $EP_3^{-/-}$ STZ mice. (A-B) Representative Western blots showing cortical and medullary COX-1 and β-Actin protein bands and (C-D) densitometric analysis. Densitometric data presented as fold wild-type (WT) and as means ± SEM. N = 5 per group. P-values calculated using a one-way ANOVA and a Tukey post-test.

3.8 Diabetic Induction of COX-2 Blunted in $EP_3^{-/-}$ STZ Mice

Renal cyclooxygenase-2 (COX-2) has been consistently reported to increase in diabetes and has been implicated in renal functional and structural changes (20-24). By Western immunoblotting, STZ mice showed a 50% increase in cortical COX-2 and a 100% increase in medullary COX-2 protein expression (Figures 9A-9D). On the other hand, $EP_3^{-/-}$ STZ mice showed no change in cortical or medullary COX-2 protein expression (Figures 9A-9D).

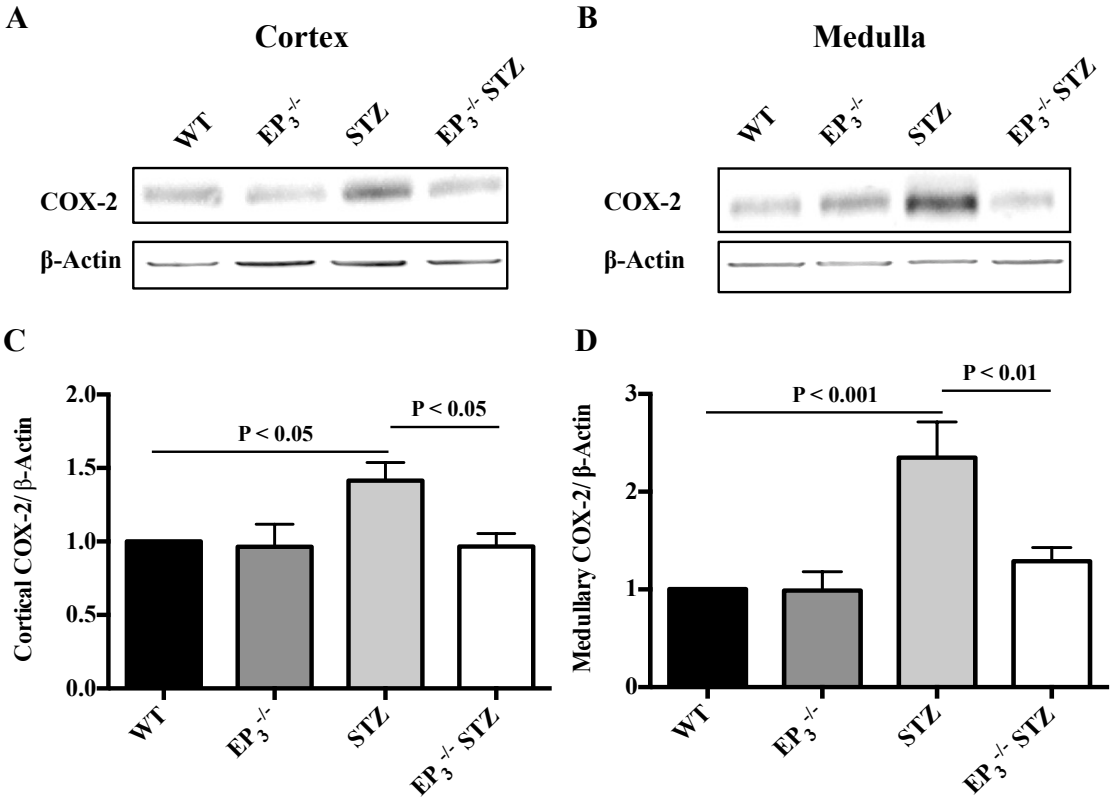

Figure 9. STZ mice but not $EP_3^{-/-}$ STZ mice express increased cortical and medullary COX-2 protein expression. (A-B) Representative Western blots showing cortical and medullary COX-2 and β-Actin protein bands and (C-D) densitometric analysis. Densitometric data presented as fold wild-type (WT) and as means ± SEM. N = 5 per group. P-values calculated using a one-way ANOVA and a Tukey post-test.

3.9 Altered EP mRNA Profile in $EP_3^{-/-}$ STZ Mice

We have previously shown that the EP profile is considerably altered during STZ diabetes (32). Given this fact and the absence of COX-2 induction in $EP_3^{-/-}$ STZ mice, we quantified the cortical and medullary EP profile in all the mouse groups at 12-weeks post injection of STZ or vehicle. Using SYBR Green detection, we found that STZ mice show a 2-fold increase in medullary EP_1 and this is reversed back to baseline in $EP_3^{-/-}$ STZ mice (Figure 10A). On the other hand, cortical EP_1 mRNA was unchanged across all groups (Figure 10B). Cortical and medullary EP_2 mRNA was found to be unchanged in STZ and $EP_3^{-/-}$ STZ mice (Figures 10C, 10D). Medullary EP_3 mRNA was increased by approximately two-fold while cortical EP_3 mRNA was increased by 50% in STZ mice (Figures 10E, 10F). EP_3 mRNA was absent in $EP_3^{-/-}$ and $EP_3^{-/-}$ STZ mice as determined by genotyping in Figure 3. Medullary EP_4 mRNA was increased by 50% in STZ mice and this effect was reversed in $EP_3^{-/-}$ STZ mice (Figure 10G). Cortical EP_4 mRNA was found to be unchanged across all groups (Figure 10H).

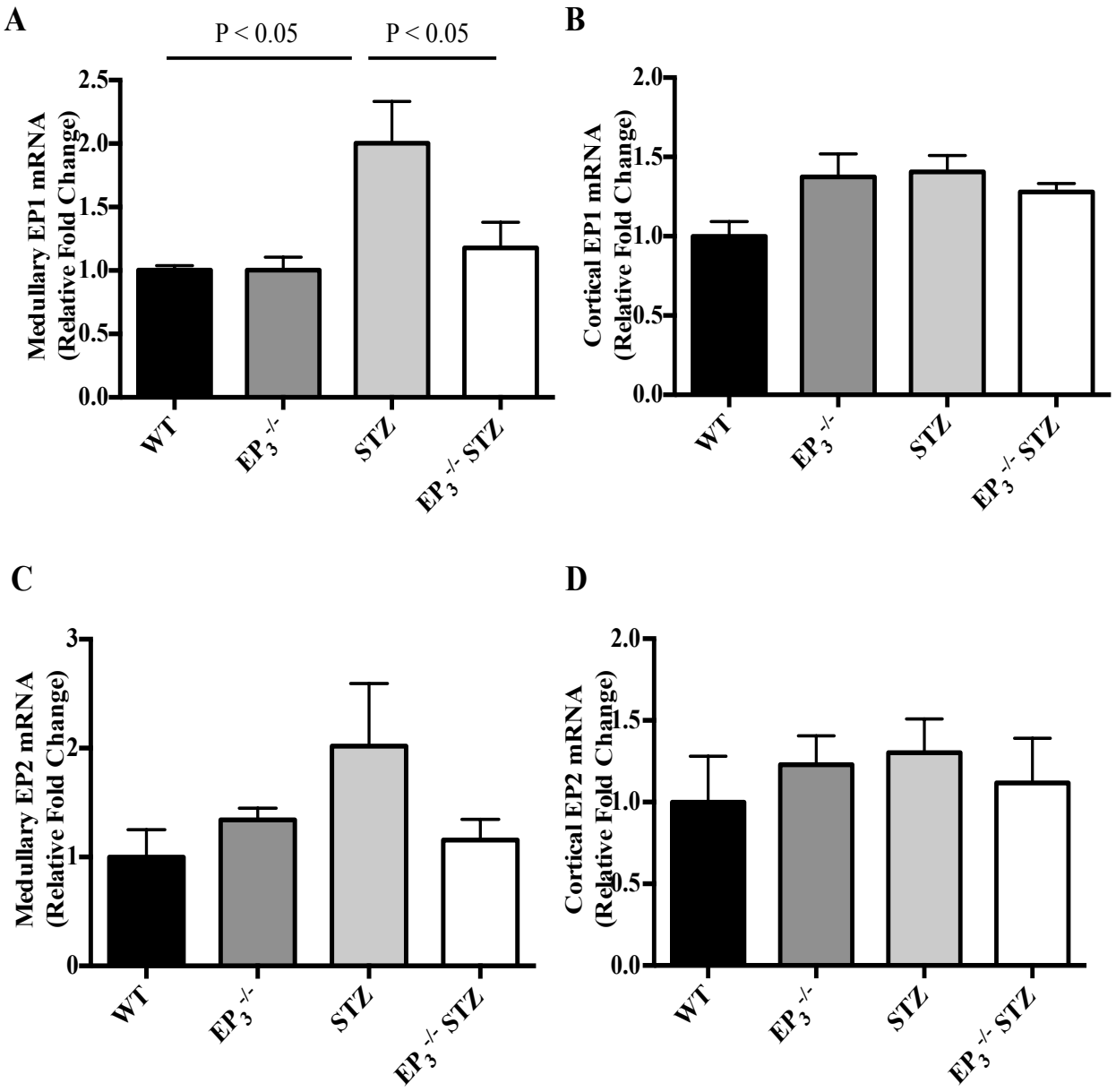
A
P < 0.05
P < 0.05
Medullary EP1 mRNA (Relative Fold Change)
2.5
2.0
1.5
1.0
0.5
0.0
WT
EP3 -/-
STZ
EP3 -/- STZ
B
Cortical EP1 mRNA (Relative Fold Change)
2.0
1.5
1.0
0.5
0.0
WT
EP3 -/-
STZ
EP3 -/- STZ
C
Medullary EP2 mRNA (Relative Fold Change)
3
2
1
0
WT
EP3 -/-
STZ
EP3 -/- STZ
D
Cortical EP2 mRNA (Relative Fold Change)
2.0
1.5
1.0
0.5
0.0
WT
EP3 -/-
STZ
EP3 -/- STZ

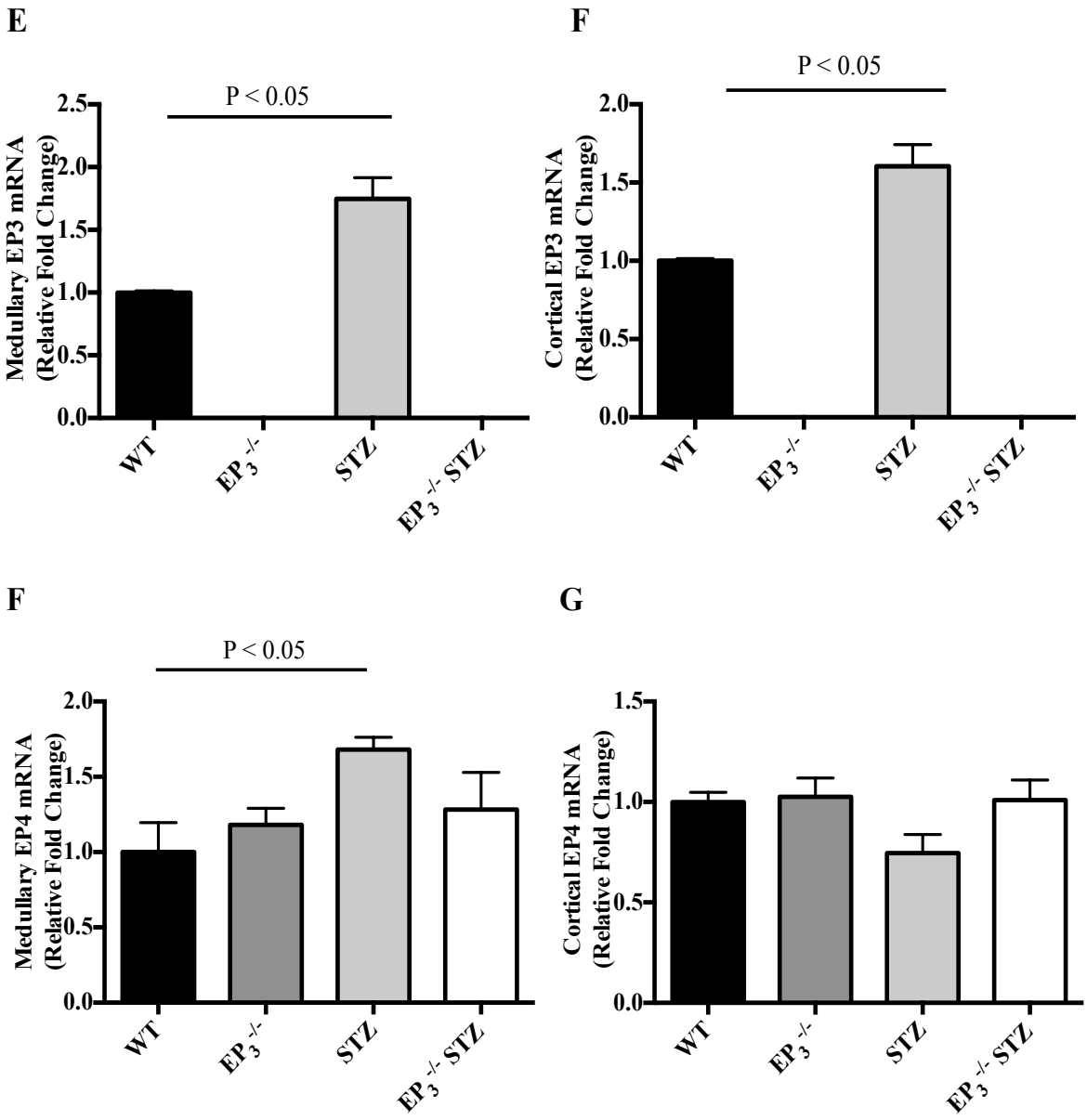

Figure 10. Renal medulla and cortex (A-B) EP_1, (C-D) EP_2, (E-F) EP_3, and (G-H) EP_4 mRNA expression 12-weeks post STZ or vehicle injection. mRNA expression was determined using the SYBR Green detection system. Data presented as means ± SEM. N = 5-7. P values calculated using one-way ANOVA and a Tukey post-test.

3.10 Induction of Salt Transporters Unchanged in $EP_3^{-/-}$ STZ Mice

Salt handling is dysfunctional during diabetes, therefore we employed Western immunoblotting to quantify cortical and medullary Na^+-K^+-Cl^- co-transporter 2 (NKCC2), epithelial Na channel alpha subunit (αENaC), and Na^+-K^+-ATPase-α1 subunit (NKA-α1) protein expression (87). STZ injected mice show a numerical increase in cortical expression of NKCC2, however, this did not reach statistical significance (Figures 11A-11D). In contrast, diabetic mice showed a 2-fold increase in medullary NKCC2 (Figures 11A-11D). Additionally, αENaC protein expression was significantly increased in both diabetic mice showing about a 3-fold increase in the cortex and about a 5-fold increase in the medulla (Figures 12A-12D). Similarly, NKA-α1 protein expression was significantly increased in both diabetic mice in the cortex and medulla (Figures 13A-13D). Interestingly, a greater increase in NKA-α1 protein expression was seen in the cortex (2.5-fold increase) as opposed to the medulla (1.5-fold increase) as was observed with the other salt transporters (Figures 13A-13D).

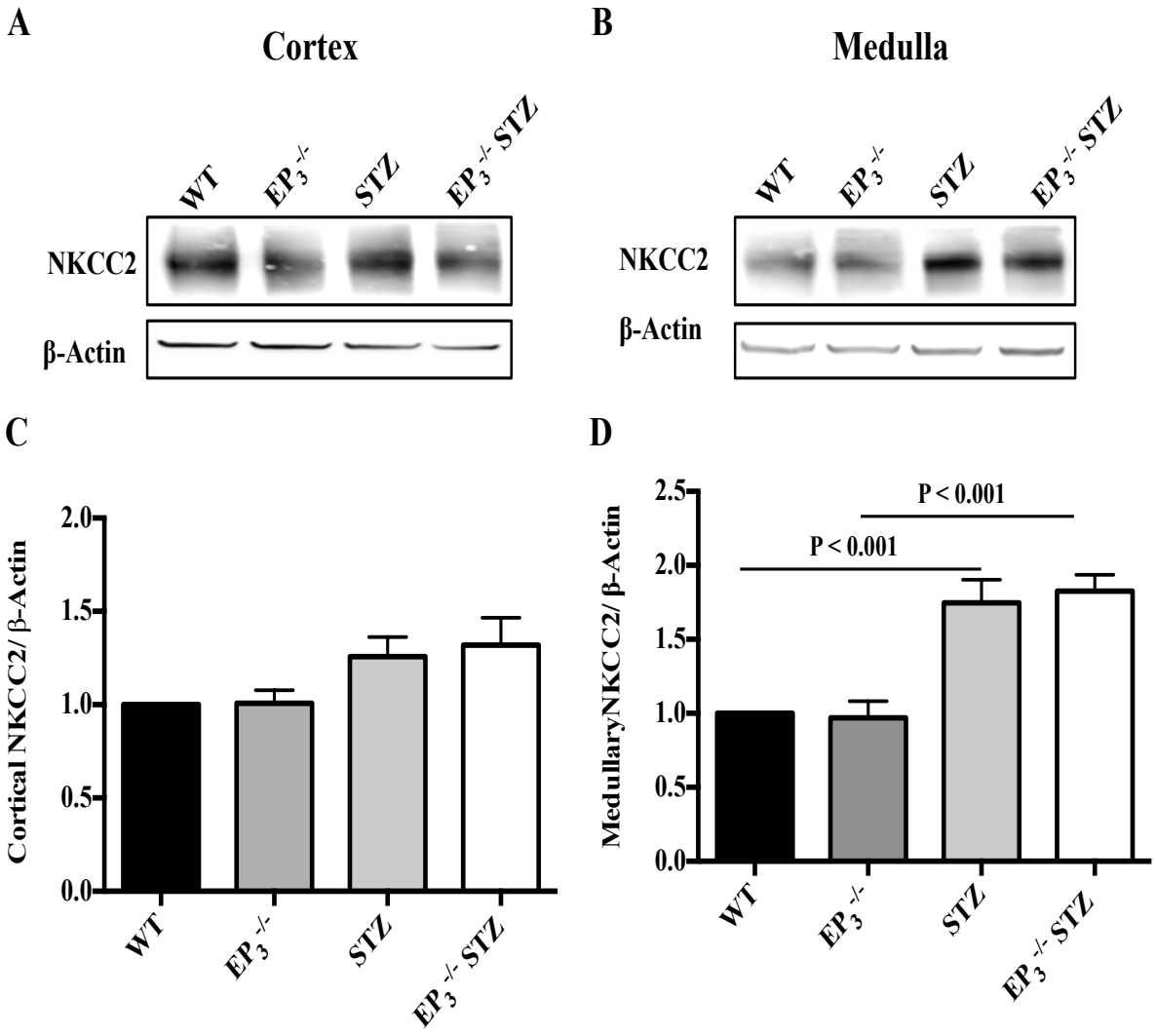

Figure 11. Medullary NKCC2 increased in diabetic mice. (A-B) Representative Western blots showing cortical and medullary NKCC2 and β-Actin protein bands and (C-D) densitometric analysis. Densitometric data presented as fold wild-type (WT) and as means ± SEM. N = 5 per group. P-values calculated using a one-way ANOVA and a Tukey post-test.

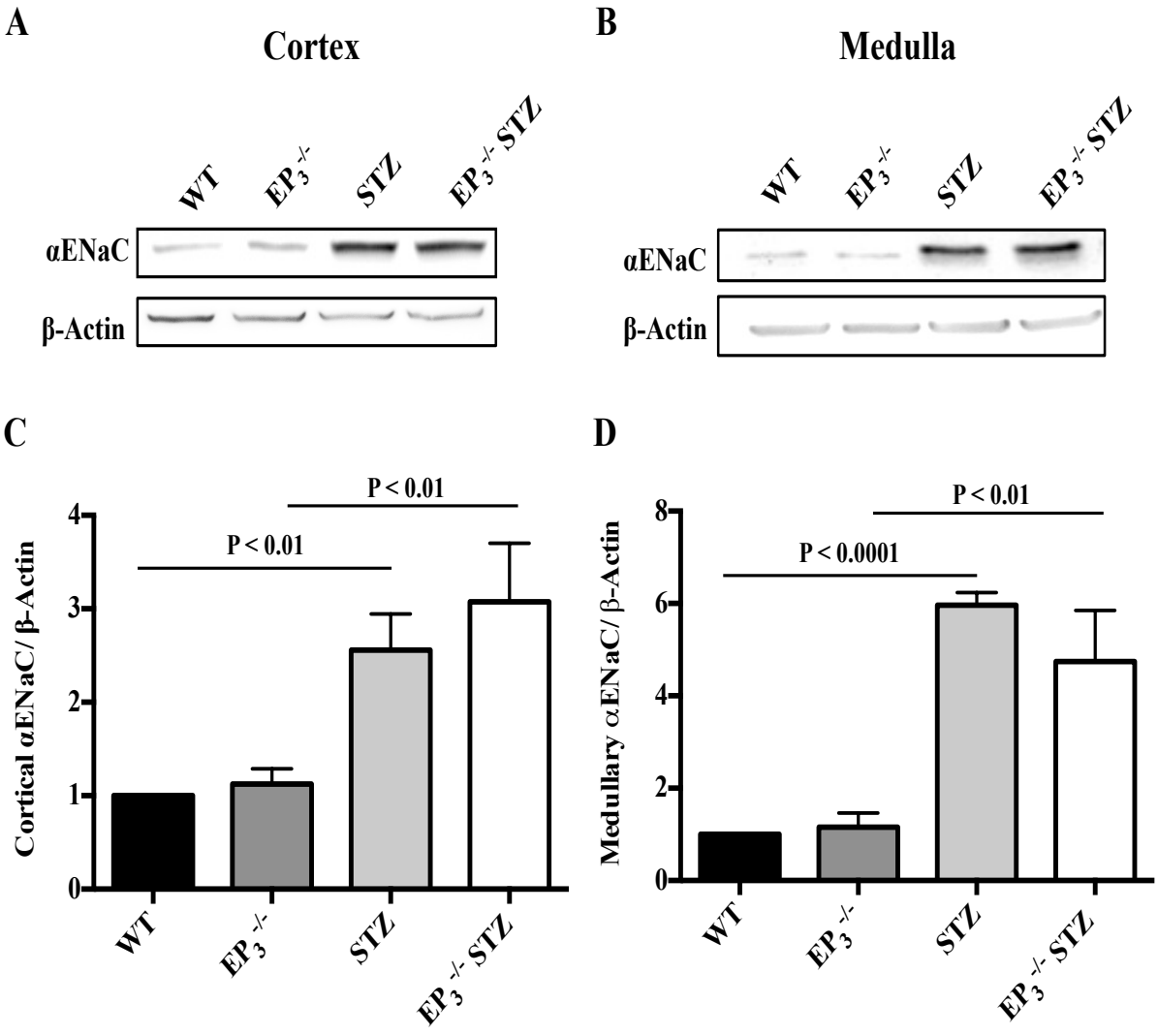

Figure 12. Increased medullary and cortical αENaC in diabetic mice. (A-B) Representative Western blots showing cortical and medullary αENaC and β-Actin protein bands and (C-D) densitometric analysis. Densitometric data presented as fold wild-type (WT) and as means ± SEM. N = 5 per group. P-values calculated using a one-way ANOVA and a Tukey post-test.

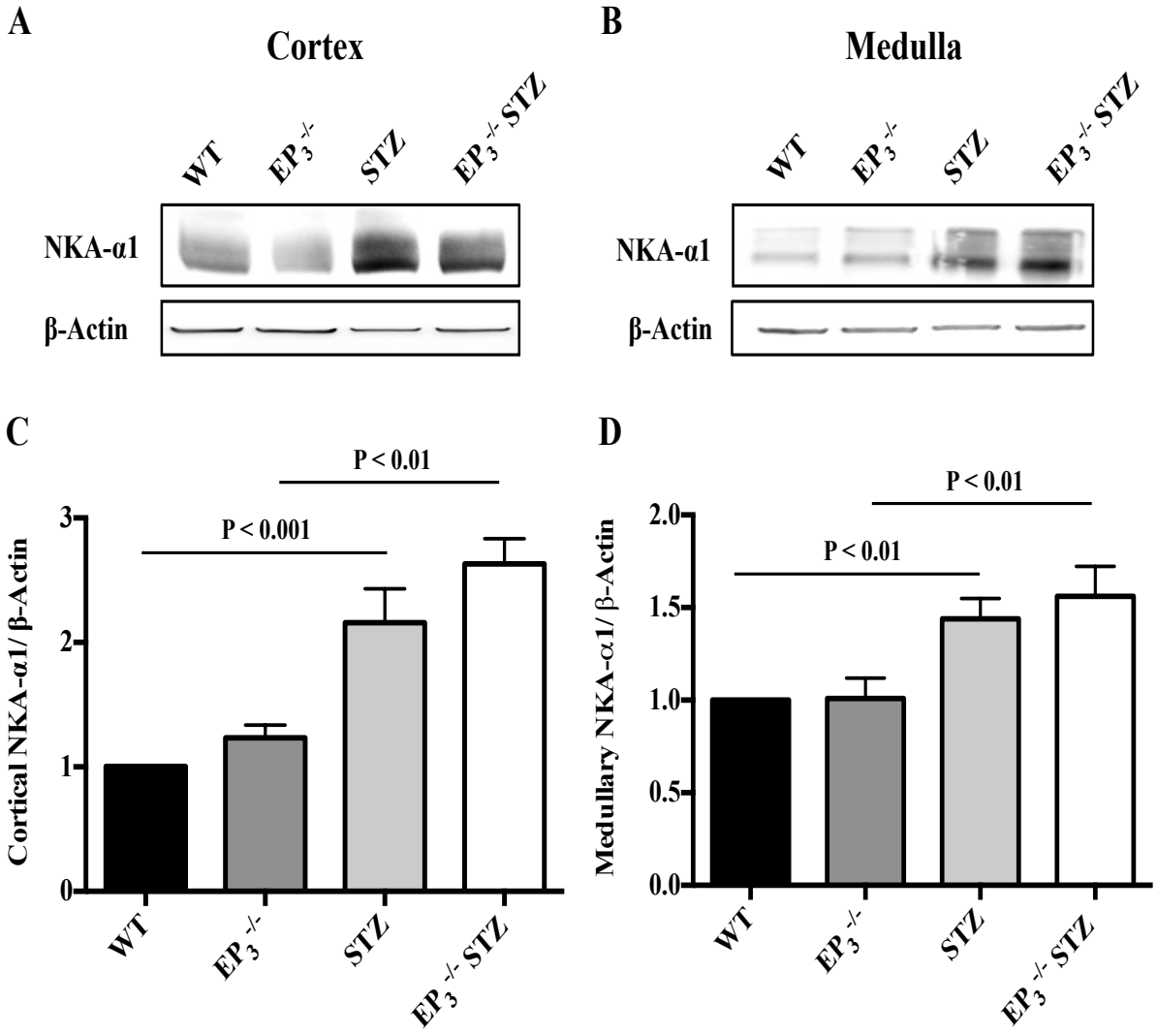

Figure 13. Increased medullary and cortical NKA-α1 in diabetic mice. (A-B) Representative Western blots showing cortical and medullary NKA-α1and β-Actin protein bands and (C-D) densitometric analysis. Densitometric data presented as fold wild-type (WT) and as means ± SEM. N = 5 per group. P-values calculated using a one-way ANOVA and a Tukey post-test.

3.11 Plasma Parameters in Mice

Due to the altered salt and water transporters in the kidney as well as the metabolic changes due to diabetes, we assessed plasma biochemistry to determine if these changes translated to changes in its composition. We observed no difference in the major electrolytes between all four groups (Table 5). However, we observed a numerical downward trend in plasma sodium, potassium, and chloride (Table 5). Intriguingly, STZ mice show significantly increased triglycerides compared to WT (Table 5).

Table 5. Plasma biochemistry of non-diabetic and diabetic WT and $EP_3^{-/-}$ mice. N = 5 for WT and $EP_3^{-/-}$. N = 2 for STZ and $EP_3^{-/-}$ STZ. $^{*}P < 0.05$ vs. WT using a one-way ANOVA and a Tukey post-test.

Plasma Biochemistry (mmol/ L)	**WT**	**$EP_3^{-/-}$**	**STZ**	**$EP_3^{-/-}$ STZ**
Sodium	149 ± 0.8	147 ± 1	141	142 ± 5
Potassium	7.68 ± 0.5	7.60 ± 0.3	7.15 ± 0.3	7.15 ±0.8
Chloride	107 ± 0.8	107 ± 1	102	103 ± 4
Phosphorus	2.05 ± 0.2	2.05 ± 0.2	1.95 ± 0.3	2.70 ± 0.7
Calcium	2.18 ± 0.05	2.15 ± 0.03	1.95 ± 0.05	2.20 ± 0.3
Magnesium	0.755 ± 0.03	0.798 ± 0.03	0.720 ± 0.03	0.965 ± 0.3
Bicarbonate	30.8 ± 0.8	27 ± 3	27	26.0 ± 8
Cholesterol	3.00 ± 0.1	3.35 ± 0.3	2.35 ± 0.8	3.00 ± 0.5
Triglycerides	0.898 ± 0.1	1.02 ± 0.2	1.71 ± 0.1	1.23 ± 0.1

3.12 Attenuated Polyuria and Polydipsia in $EP_3^{-/-}$ STZ Mice

Polyuria was observed in both diabetic groups; however, the extent of polyuria was significantly attenuated by about 35% in the $EP_3^{-/-}$ STZ group (Figure 14A). Polydipsia was concomitantly observed with polyuria in the diabetic groups (Figure 14B). A significant 20% attenuation in polydipsia was also observed in the $EP_3^{-/-}$ STZ group (Figure 14B). A large reduction in urine osmolality was observed in the diabetic groups as a consequence of the polyuria (Figure 14C), however urine osmolality in the STZ and $EP_3^{-/-}$ STZ groups did not numerically match (STZ: 458 ± 7 mOsm/kg vs. $EP_3^{-/-}$: 536 ± 30 mOsm/kg) (Figure 14C). A 20% increase in urine osmolality is observed in the $EP_3^{-/-}$ STZ group suggesting increased water reabsorption (Figure 14C). Diabetic mice also exhibited an increase in daily food intake correlative to the increase in water intake (Figure 14D). Additionally, due to the polyuria, daily urinary excretion of electrolytes was greatly elevated in the diabetic groups and was comparable between STZ and $EP_3^{-/-}$ STZ mice (Table 6).

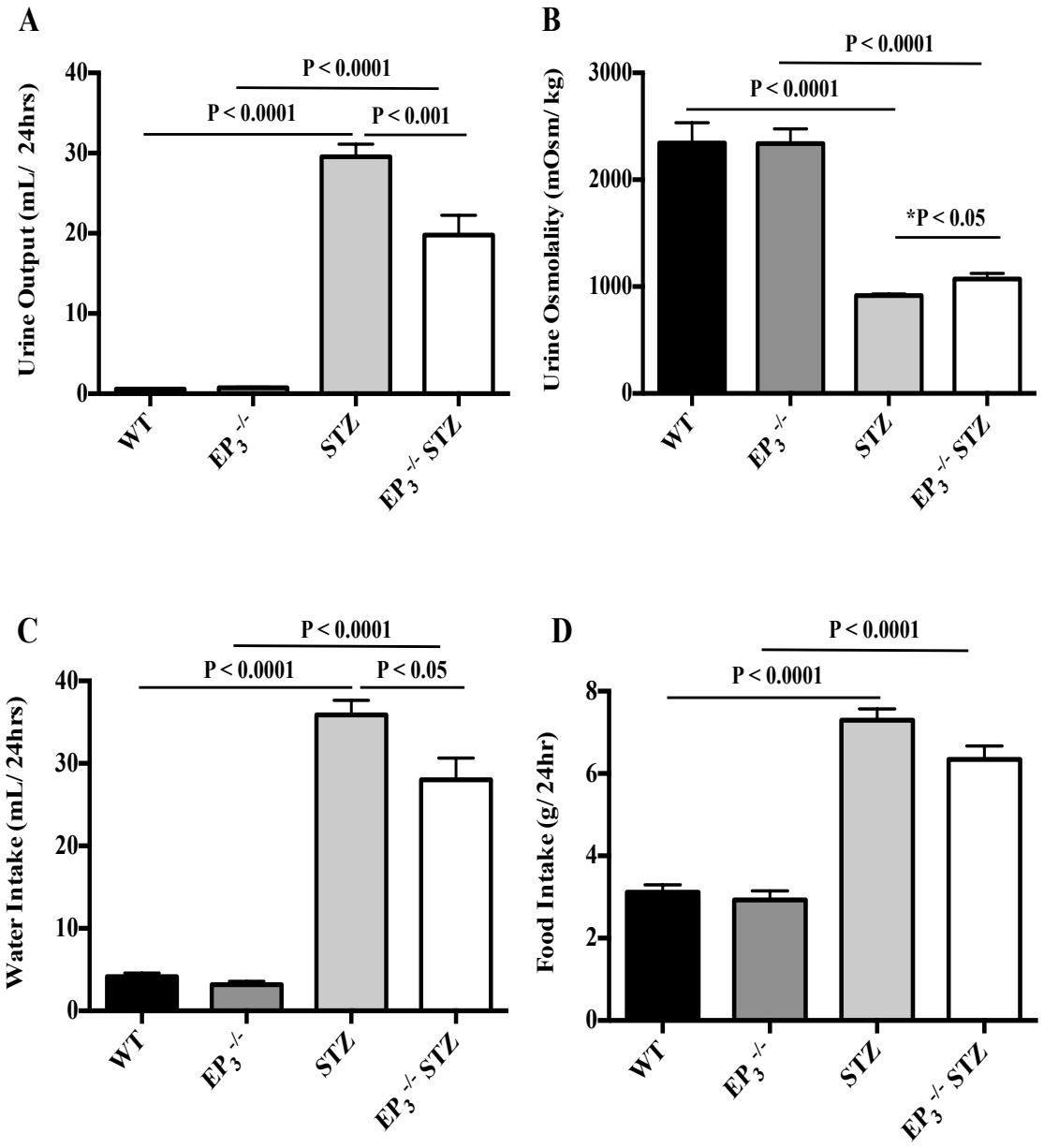

Figure 14. Decreased daily urine output and water intake in $EP_3^{-/-}$ STZ Mice. (A) Daily urine output, (B) urine osmolality, (C) daily water intake, and (D) daily food intake in diabetic and non-diabetic WT and $EP_3^{-/-}$ mice. N = 10 per group. P values calculated using a one-way ANOVA and a Tukey post-test. *P value calculated using an unpaired t-test.

Table 6. Daily urinary excretion of electrolytes in non-diabetic and diabetic WT and $EP_3^{-/-}$ mice. N = 5 per group. $^{*}P < 0.0001$ vs. WT and $^{\dagger}P < 0.0001$ vs. $EP_3^{-/-}$ using a one-way ANOVA and Tukey's post-test.

Urine Biochemistry (µmol/ 24hrs)	WT	$EP_3^{-/-}$	STZ	$EP_3^{-/-}$ STZ
Sodium	82.8 ± 10	89.9 ± 7	683 ± 50*	622 ± 70†
Potassium	141 ± 30	136 ± 30	1040 ± 30*	925 ± 70†
Chloride	141 ± 20	154 ± 10	1050 ± 70*	894 ± 90†
Phosphorus	44.4 ± 6	41.3 ± 5	173 ± 10*	179 ± 10†
Calcium	1.35 ± 0.2	0.947 ± 0.1	10.1 ± 2*	9.97 ± 3†
Magnesium	6.07 ± 1	7.26 ± 0.7	89.9 ± 7*	86.8 ± 7†
Creatinine	3.06 ± 0.3	2.45 ± 0.3	10.2 ± 0.5*	10.9 ± 1†
Glucose	2.40 ± 0.5	1.38 ± 0.2	4020 ± 300*	3540 ± 400†

3.13 Decreased Collecting Duct Luminal Area and Nuclear Cysts in $EP_3^{-/-}$ STZ Mice

PAS staining of paraffin-embedded kidney sections revealed several signs of polyuria-mediated injury of the distal nephron particularly the collecting ducts (Figure 15A). Markedly dilated collecting ducts were observed in STZ mice showing an approximate 2-fold increase in luminal area compared to the non-diabetic groups (Figures 15A, 15B). $EP_3^{-/-}$ STZ mice still show an increase in collecting duct luminal area compared to $EP_3^{-/-}$ however it is attenuated by about 20% compared to STZ mice (Figures 15A, 15B). Nuclear cysts were present in large numbers in the lining of collecting ducts in both diabetic groups (Figures 15A, 15C). Similar findings have been reported in other water-wasting diseases such as lithium-induced polyuria and diabetes insipidus (9, 88-91). Interestingly, the incidence of nuclear cysts was reduced in $EP_3^{-/-}$ STZ mice possibly

correlative to their reduced polyuria and polydipsia (STZ: 7.97 ± 1 vs. 5.26 ± 1 nuclear cysts/image) (Figures 15A-15C).

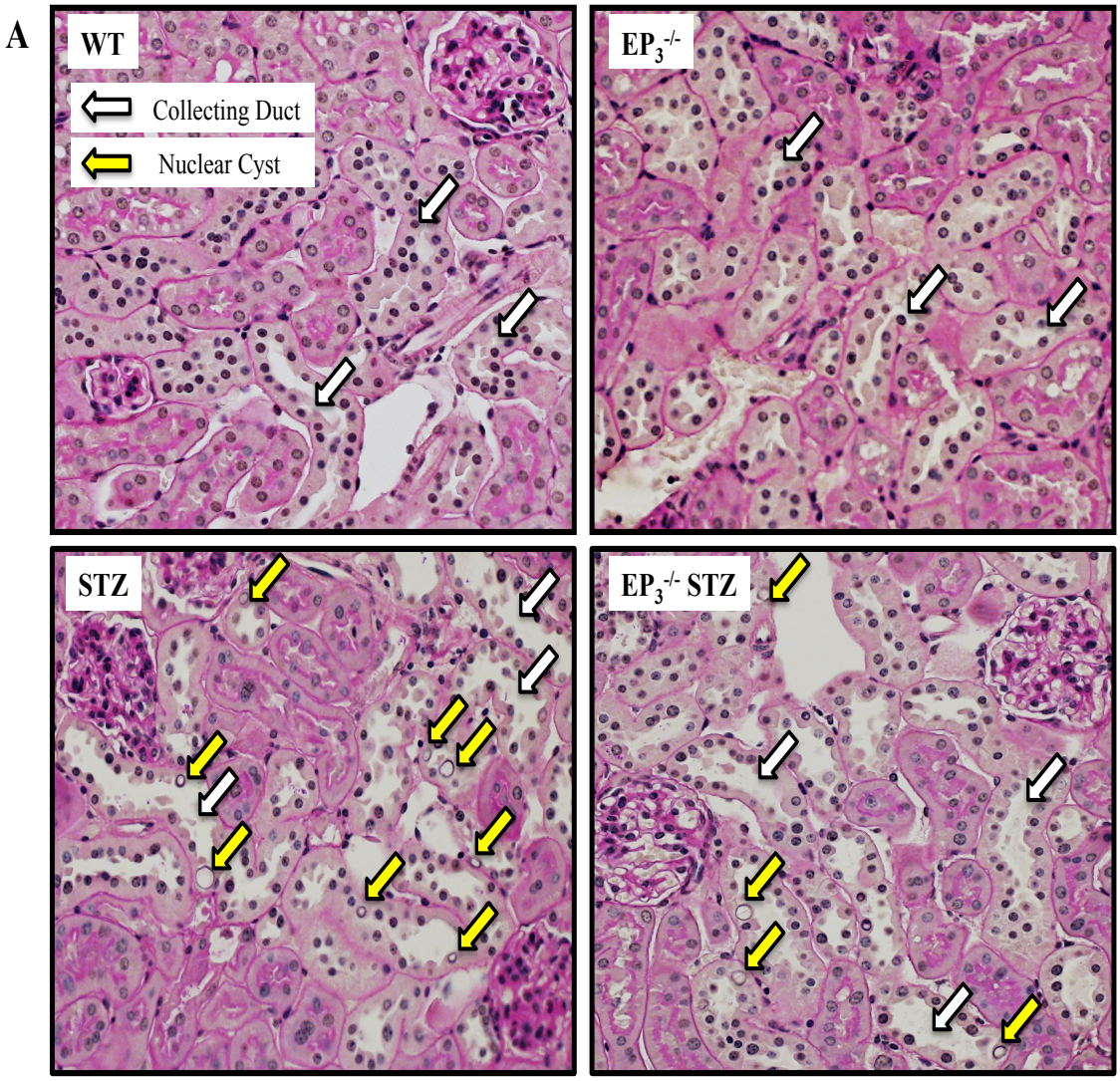

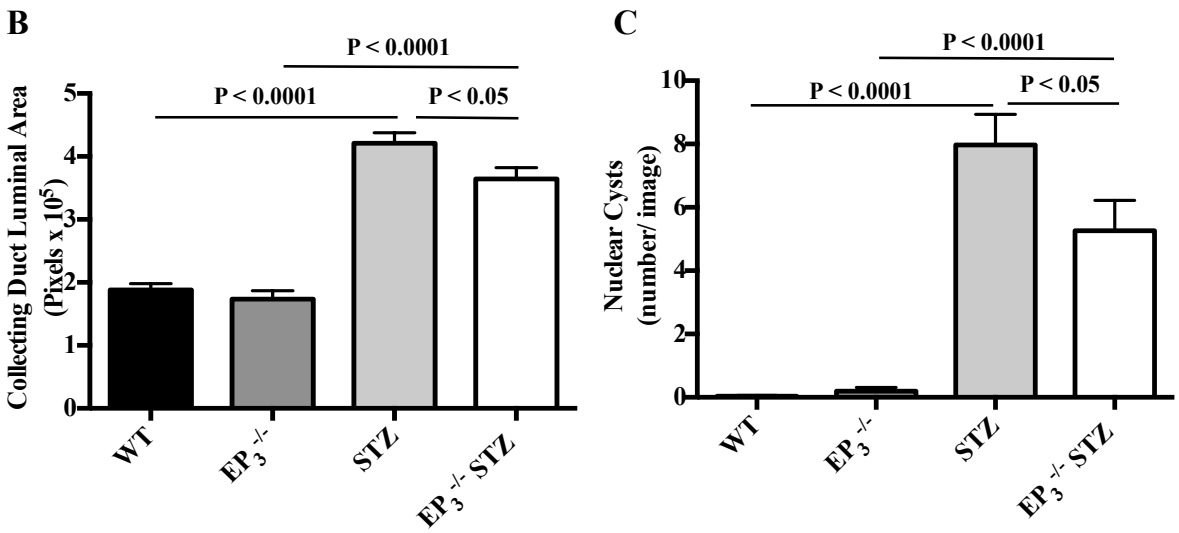

Figure 15. Attenuated collecting ducts luminal area dilation and nuclear cysts in $EP_3^{-/-}$ STZ mice. (A) Representative images of periodic acid-Schiff stained paraffin-embedded kidney sections, (B) quantification of collecting duct area, and (C) quantification of nuclear cysts. Images shown at 20X magnification. Approximately 25 images showing a cluster of collecting ducts were taken per group. Total collecting duct area including lumen and tubular lining was determined in pixels. Number of nuclear cysts were counted per field. Data presented as means ± SEM. P-values calculated using a one-way ANOVA and Tukey's post-test.

3.14 Increased AQP2 and AQP1 in $EP_3^{-/-}$ STZ Mice

Urine output and concentration depends, in part, on the expression of AQP2 water channels in the collecting duct (1, 2). Therefore the protein expression of AQP2 was assessed by Western immunoblotting. STZ mice showed a 50% reduction in cortical and medullary AQP2 protein expression (Figure 16A-16D). On the other hand, $EP_3^{-/-}$ STZ mice show comparable protein expression of cortical AQP2 to that of the control groups

(Figures 16A-16D). Additionally, medullary AQP2 protein was increased 50% beyond control levels in $EP_3^{-/-}$ STZ mice (Figures 16A-16D).

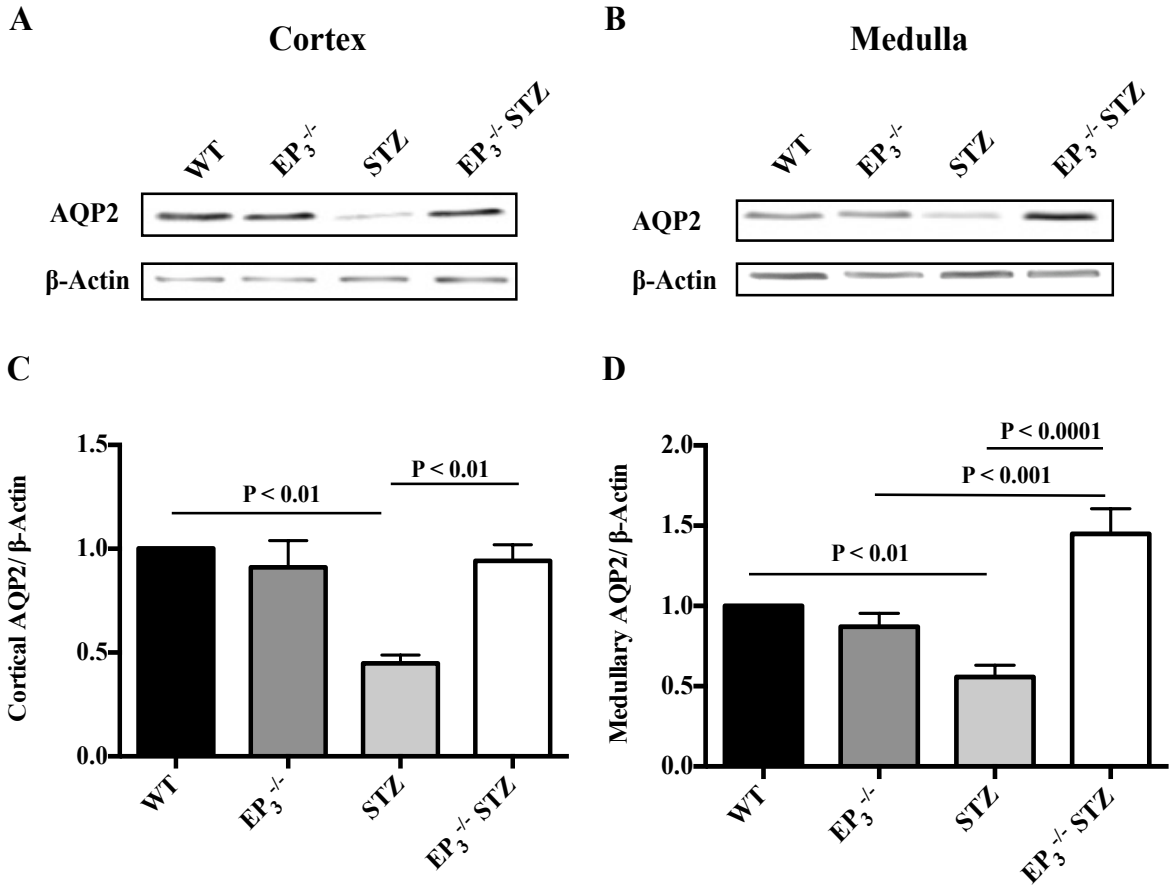

Figure 16. Increased cortical and medullary AQP2 protein expression in $EP_3^{-/-}$ STZ mice. (A-B) Representative Western blots showing cortical and medullary AQP2 and β-Actin protein bands and (C-D) densitometric analysis. Densitometric data presented as fold wild-type (WT) and as means ± SEM. N = 5 per group. P-values calculated using a one-way ANOVA and Tukey's post-test.

Furthermore, urine concentrating mechanisms also rely on the maintenance of an osmolar gradient across the tubular lumen and into the medullary interstitium and this is dependent, in part, on the expression of AQP1 water channels in the medullary thin descending limbs and vasa recta. On the other hand, AQP1 in the cortical proximal tubule is responsible for reabsorbing the bulk of filtered water. Therefore the protein expression of AQP1 was assessed by Western immunoblotting. Both diabetic groups show an approximate 50% reduction in cortical AQP1 protein expression corresponding to reduced AQP1 expression in the proximal tubules (Figures 17A, 17C). However, medullary AQP1 protein was decreased by 50% in only the STZ mice while $EP_3^{-/-}$ STZ mice show comparable levels to control mice (Figures 17B, 17D). AQP1 immunofluorescence analysis of kidney sections illustrates this difference whereby we observe a reduction in medullary AQP1 in STZ mice but not in $EP_3^{-/-}$ STZ mice (Figure 18).

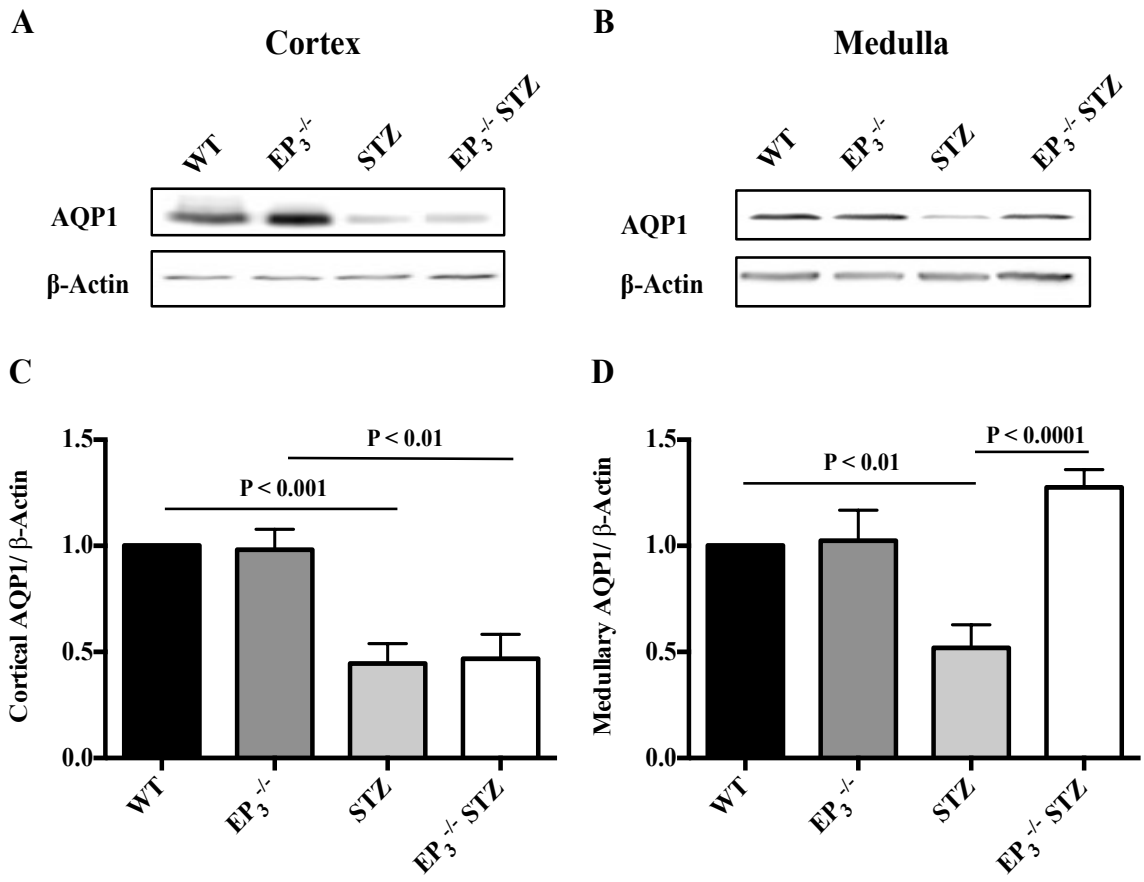

Figure 17. Increased medullary AQP1 protein expression in $EP_3^{-/-}$ STZ mice. (A-B) Representative Western blots showing cortical and medullary AQP1 and β-Actin protein bands and (C-D) densitometric analysis. Densitometric data presented as fold wild-type (WT) and as means ± SEM. N = 5 per group. P-values calculated using a one-way ANOVA and Tukey's post-test.

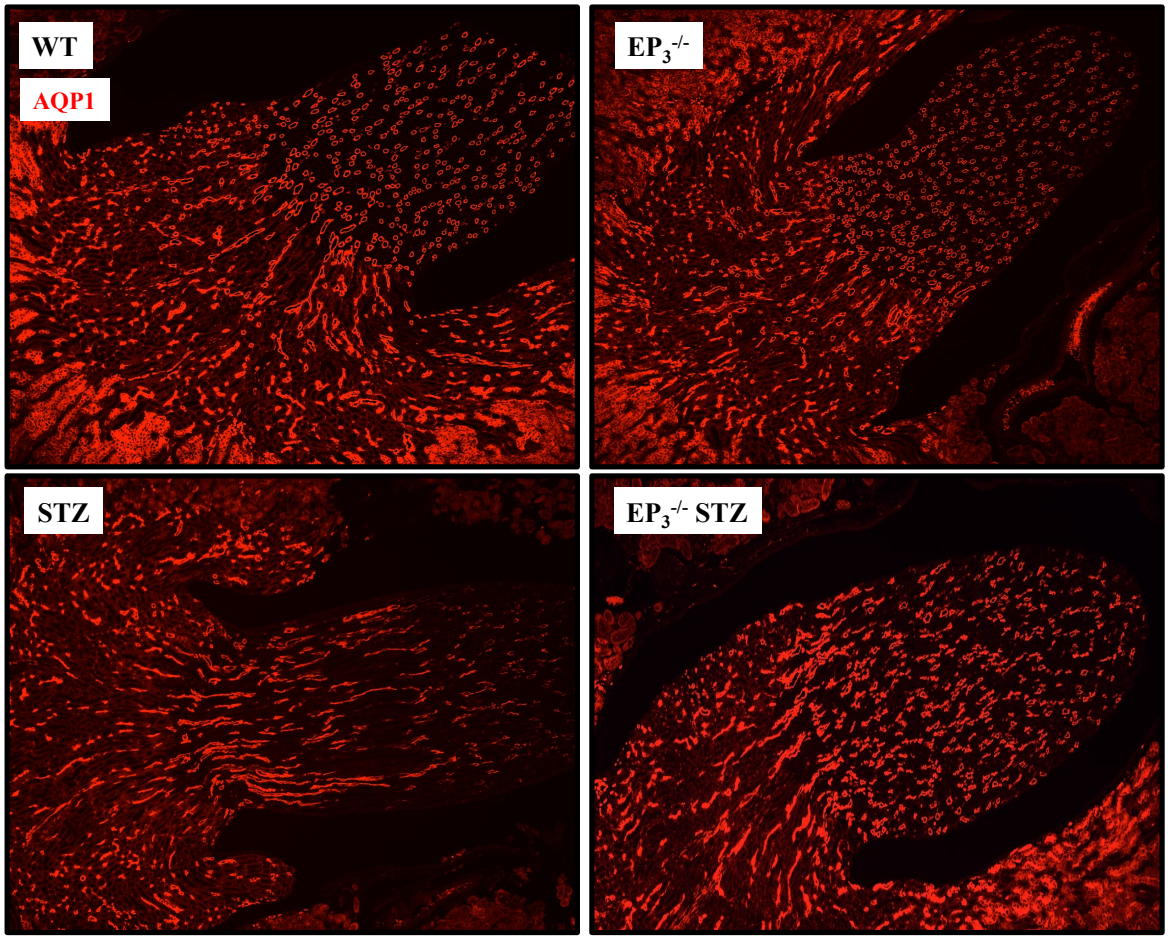

Figure 18. Increased medullary AQP1 protein expression in $EP_3^{-/-}$ STZ mice. Representative fluorescent images of paraffin-embedded kidney sections probed with AQP1 antibody. Images shown at 10X magnification.

3.15 Urinary AVP Excretion Rate is Blunted in $EP_3^{-/-}$ STZ Mice

AVP levels are consistently reported to be elevated in diabetes despite the presence of polyuria and inability to adequately concentrate urine (50-52). Given that we observed changes in AQP2, which is physiologically regulated by AVP, we measured urinary excretion of AVP. WT and $EP_3^{-/-}$ showed similar levels of urinary AVP excretion rates (Figure 19). We found that 24 hour urinary AVP excretion rate was elevated by 15-fold in STZ mice compared to WT mice (Figure 19). $EP_3^{-/-}$ STZ mice showed an attenuated elevation in urinary AVP excretion of approximately 10-fold compared to $EP_3^{-/-}$ mice (Figure 19). This represents a reduction of about 35% compared to STZ mice (Figure 19).

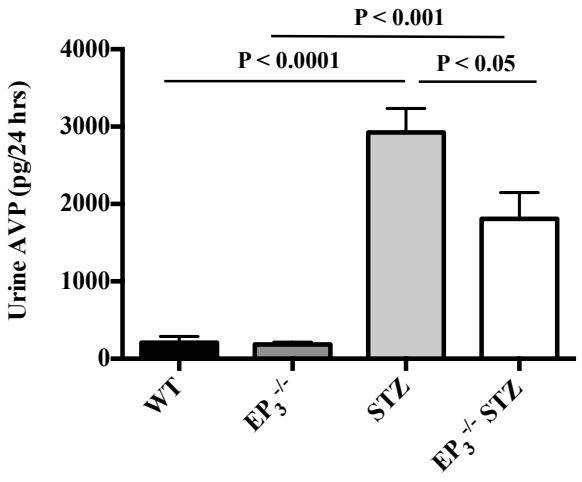

Figure 19. 24 hour urinary arginine-vasopressin (AVP) excretion in WT and $EP_3^{-/-}$ 3-month post vehicle or STZ injection. N = 6 per group. P values calculated using one-way ANOVA and Tukey's post-test.

3.16 AQP2 Unchanged with AVP, SLP, or High Salt in M-1 Cells

In order to understand the mechanistic link between EP_3 and AVP, we used M-1 cortical collecting duct cells and stimulated them with the EP_3/EP_1 agonist SLP under several conditions. Although, high glucose would be the best environment to recapitulate the diabetic mileu in vitro, we have previously shown that this cell line is unresponsive to high glucose concentrations (unpublished data). Therefore, we stimulated M-1 cells for 24 hours with 10^{-8} M AVP or high salt (HS; 240 mM NaCl) in the presence or absence of SLP. By Western immunoblotting, AQP2 protein expression was found to be unchanged after 24 hours stimulation with AVP, HS, and/or SLP (Figure 20).

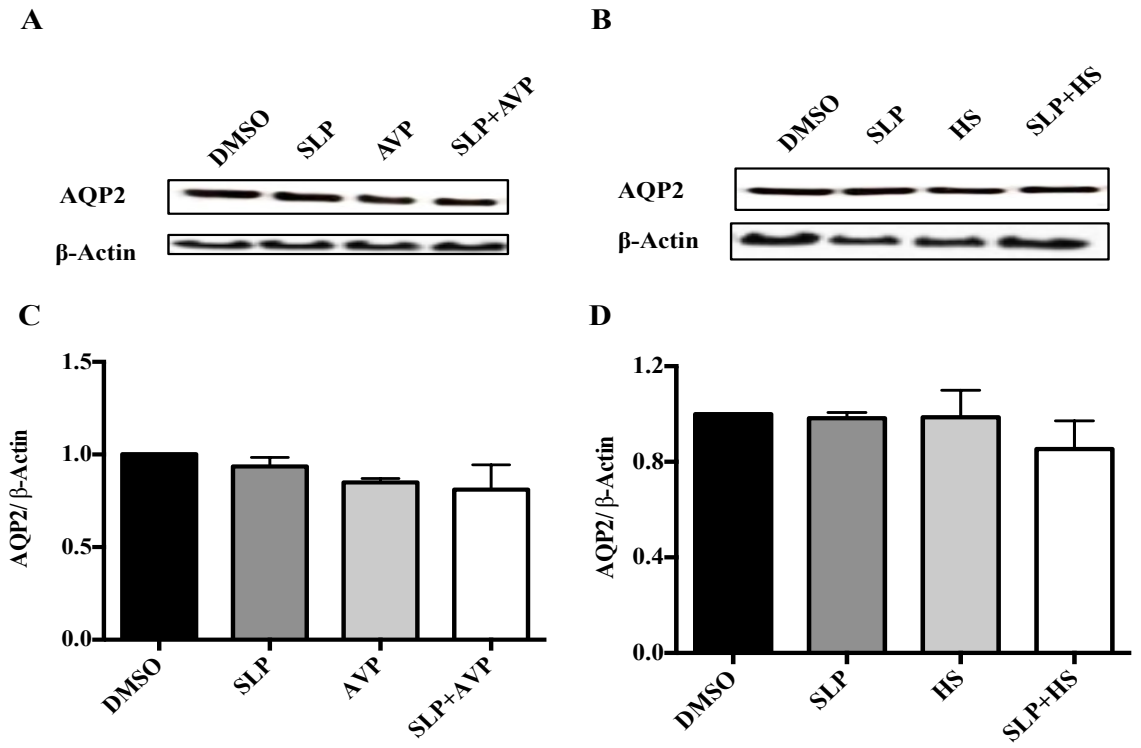

Figure 20. AQP2 protein expression was unchanged in M-1 cells following AVP, high salt (HS), and/or sulprostone (SLP) stimulation. (A-B) Representative Western blots showing cortical and medullary AQP2 and β-Actin protein bands and (C-D) densitometric analysis. Densitometric data presented as fold wild-type (WT) and as means ± SEM. N = 5 per group. P-values calculated using a one-way ANOVA and Tukey's post-test.

3.17 NKA α-1 Increased with HS but αENaC Unchanged in M-1 Cells

Several studies have demonstrated that PGE_2 may regulate NKA α-1 and αENaC expression in the collecting duct, therefore we explored if this occurs via EP_3. We used M-1 cortical collecting duct cells and stimulated them for 24 hours with the EP_3/EP_1 agonist SLP, with 10^{-8} M AVP, or high salt (HS; 240 mM NaCl). By Western immunoblotting, αENaC protein expression was found to be unchanged after 24 hours stimulation with AVP, HS, and/or SLP (Figure 21). NKA α-1 protein expression was found to be increased after 24 hours stimulation with HS and this effect was unchanged with SLP co-stimulation (Figure 22). NKA α-1 protein expression was unchanged with AVP or SLP alone (Figure 22).

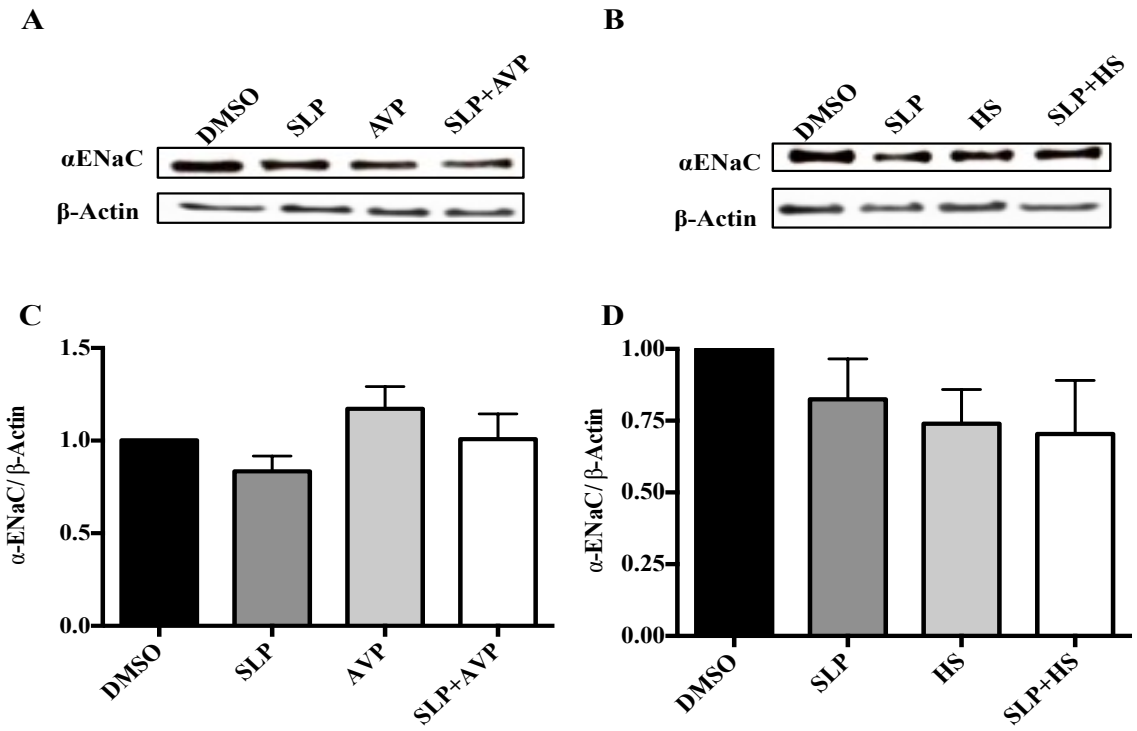

Figure 21. αENaC protein expression was unchanged in M-1 cells following AVP, HS, and/or SLP stimulation. (A-B) Representative Western blots showing cortical and medullary αENaC and β-Actin protein bands and (C-D) densitometric analysis. Densitometric data presented as fold wild-type (WT) and as means ± SEM. N = 5 per group. P-values calculated using a one-way ANOVA and Tukey's post-test.

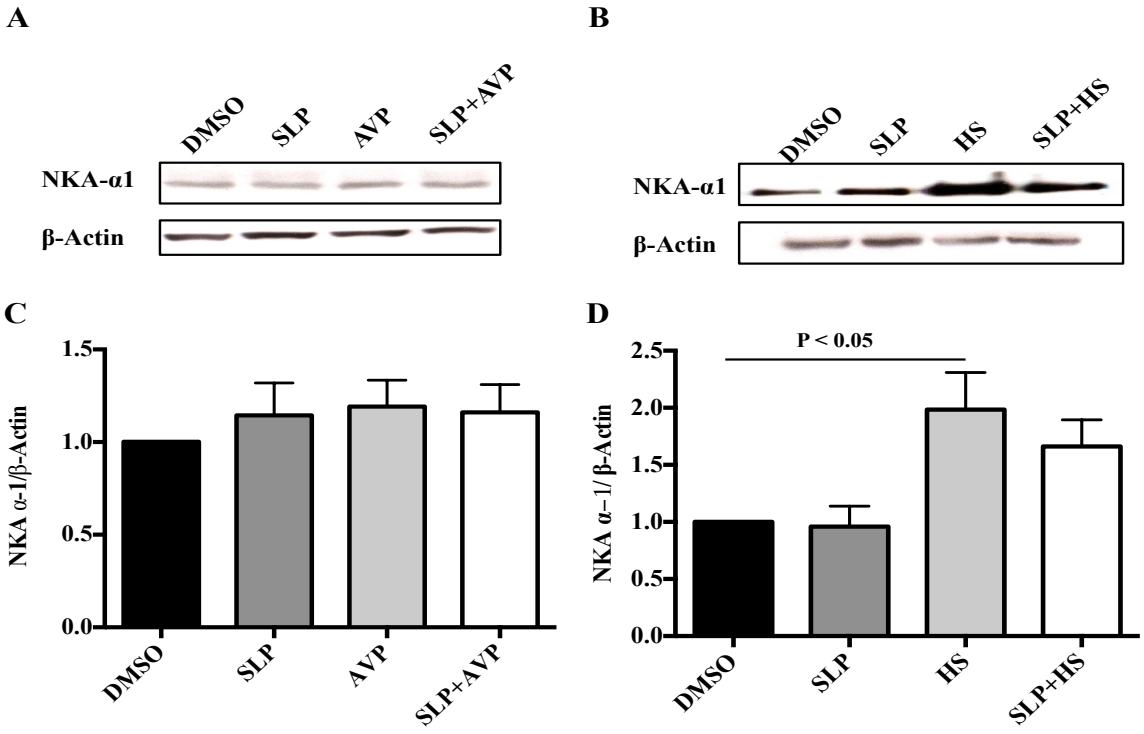

Figure 22. NKA α-1 protein expression increased with HS in M-1 cells but was unchanged with AVP or SLP. (A-B) Representative Western blots showing cortical and medullary NKA α-1 and β-Actin protein bands and (C-D) densitometric analysis. Densitometric data presented as fold wild-type (WT) and as means ± SEM. N = 5 per group. P-values calculated using a one-way ANOVA and Tukey's post-test.

3.16 In Vitro Microperfusion

We performed in vitro microperfusion experiments using isolated CCDs to confirm the role of EP_3 in water handling in the non-diabetic and diabetic state. Since baseline water reabsorption is absent or low in isolated CCD (61, 62), AVP was used to induce water reabsorption and sulprostone (SLP; $EP_{1/3}$ agonist) was used to agonize EP_3. AVP induced a 2-fold increase net water reabsorption (Jv) in both WT and $EP_3^{-/-}$ mice (Figure 23A). SLP partially reversed the AVP-induced increase in Jv in WT mice. In $EP_3^{-/-}$, mice SLP did not inhibit Jv in the presence of AVP and Jv remained elevated to the same extent as it was with AVP stimulation (Figure 23B). In STZ mice, AVP induced a 2-fold increase in Jv, while SLP completely reversed Jv back to baseline (Figure 23C). AVP induced an approximate 50 % increase in Jv in $EP_3^{-/-}$ STZ mice while SLP did not inhibit Jv in the presence of AVP (Figure 23D).

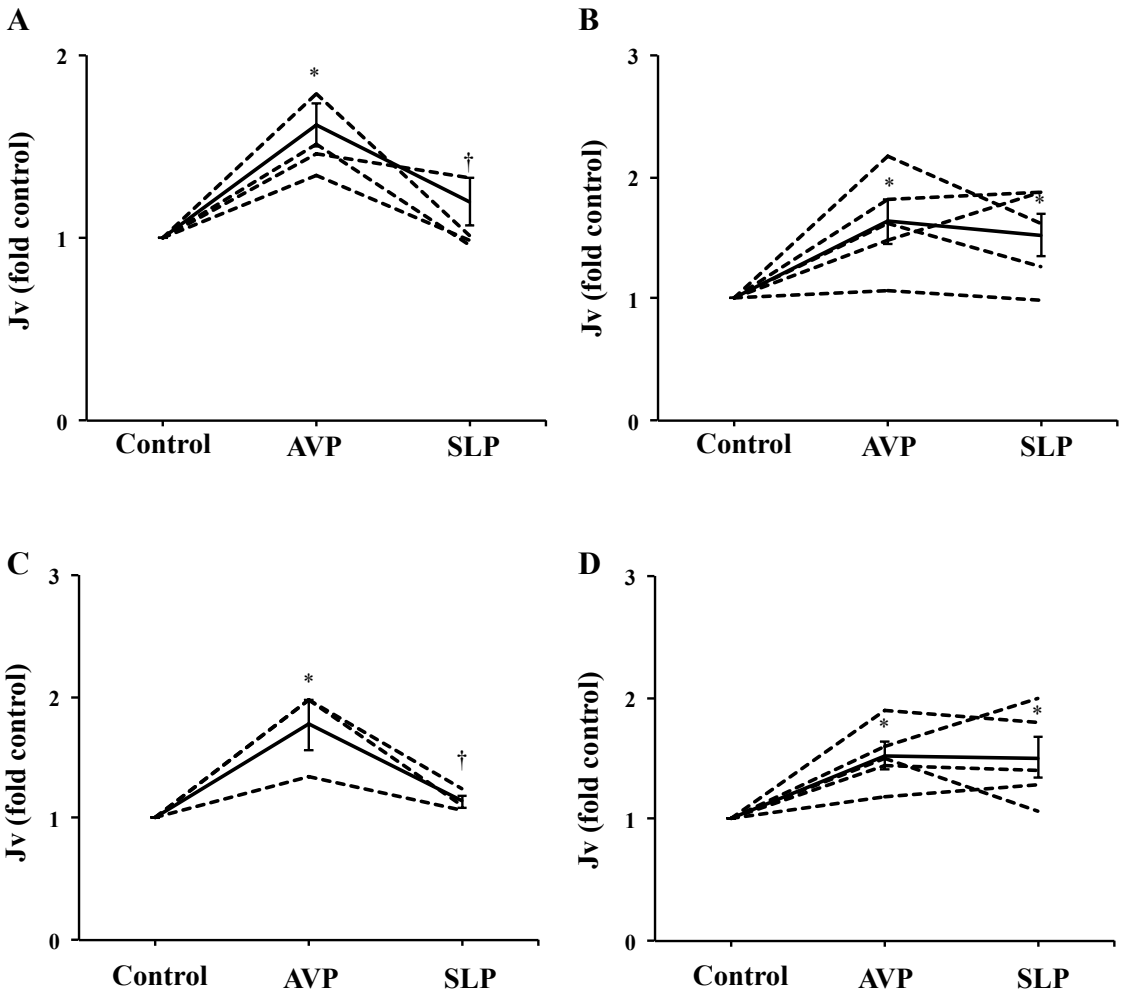

Figure 21. SLP inhibits AVP mediated fluid reabsorption via EP_3. Net fluid reabsorption (Jv) of cortical collecting ducts isolated from (A) WT, (B) $EP_3^{-/-}$, (C) STZ, and (D) $EP_3^{-/-}$ STZ mice 3-month post STZ or vehicle injection stimulated with AVP (10^{-8} M) and SLP (10^{-7} M) presented as fold change compared to control. Dashed lines represent individual experiments and solid line represents the mean ± SEM. N = 3-5. $^{*}P < 0.05$ versus control and $^{\dagger}P < 0.05$ versus AVP. P values calculated using one-way ANOVA with Tukey's post-test.

4. **DISCUSSION**

4.1 Major Findings

This study is the first to examine the in vivo role of the PGE_2/EP_3 receptor system in diabetes. The data clearly demonstrate a major role for EP_3 in the process of polyuria during diabetes. Whether EP_3 promotes polyuria and as a result promotes polydipsia or vice-versa is unknown. However, increased urine osmolality in $EP_3^{-/-}$ STZ mice alongside increased AQP2 and AQP1 protein expression suggest that EP_3 mediates polyuria at the renal level and this may drive changes in the thirst response. This is further emphasized in the in vitro microperfusion experiments, whereby SLP reduces AVP-mediated water reabsorption. Additionally, EP_3 seems to contribute to renal COX-2 induction during diabetes. The lack of an increase in renal COX-2 protein levels in $EP_3^{-/-}$ STZ mice may be protective by preventing renal hypertrophy, glomerular hyperfiltration, and urinary albumin excretion.

4.2 Phenotype of Global EP_3 Deletion in C57BL/6 Mice

Baseline $EP_3^{-/-}$ mice at 8-weeks of age exhibit a significant increase in body weight compared to WT when fed a standard chow diet *ad libitum*. Although increased body weight in these mice has been reported previously by Sanchez-Alavez et al, the magnitude of the increase was much greater (78). This is likely due to the difference in fat content in the chow given to the mice (78). When fed a high fat breeder diet, $EP_3^{-/-}$

mice are described as developing an obese phenotype as early as three months of age with increased abdominal and subcutaneous fat (78). The increased body weight is partly attributed to increased night-eating (78, 92, 93). This may suggest a role for EP_3 in the regulation of sleep architecture, as PGE_2 acting through hypothalamic EP_3 may act as a sleep-producing agent therefore explaining increased light cycle eating (94, 95). A role of PGE_2 in sleeping is supported by the fact that wakefulness was induced in rats administered an EP_4 agonist into the posterior hypothalamus (96). EP_3 may buffer these responses induced by EP_4 as it typically inhibits cAMP through Gi while EP_4 stimulates cAMP through Gs. Thus, in the absence of EP_3, mice may experience abnormal sleep patterns leading to increased night eating.

We demonstrate that baseline 8-week-old $EP_3^{-/-}$ mice show impaired glucose tolerance. Studies have reported that $EP_3^{-/-}$ mice show significantly increased plasma levels of insulin (78). This is likely due to the lack of EP_3 mediated inhibition of cAMP in pancreatic islets, which physiologically opposes and buffers the action of the glucagon-like-peptide-1 (GLP-1) receptor and inhibits glucose-stimulated insulin secretion (33). Continuous exposure to high levels of insulin is associated with the development of insulin resistance (97). Increasing doses of intermediate-acting insulin in rats was shown to decrease the number of insulin receptors on target tissues with a corresponding decrease in cell sensitivity to insulin (97). The fact that the mice exhibit impaired glucose tolerance, demonstrated by continued elevated blood glucose levels post glucose challenge compared to WT mice, suggests that these mice have impaired beta cell function and possibly insulin resistance. Surprisingly, the insulin tolerance test suggests that $EP_3^{-/-}$ mice respond equivalently to WT when challenged with insulin. However, the

insulin tolerance test is inherently less accurate than the glucose tolerance test due to the lack of a consistent baseline glucose level (98). Fasting prior to insulin injection is unfeasible due to the high risk of insulin shock and/or hypoglycemia (98). To circumvent this problem, data is presented as a percentage of basal glucose, however, basal glucose levels varied among the groups, which may lead to an erroneous interpretation (98). For the same absolute decrease in blood glucose following an insulin injection, a mouse with higher fasting glucose will exhibit a smaller percentage fall in glucose (98). Therefore, when expressing blood glucose as a percentage of basal, the conclusion would be that the mouse with higher fasting glucose is insulin resistant (98). This limitation likely impacted the results of the insulin tolerance test. Regardless, $EP_3^{-/-}$ mice clearly exhibit impaired glucose tolerance presumably due to impaired insulin secretion in pancreatic islets.

Baseline 8-week-old $EP_3^{-/-}$ mice exhibit increased systolic blood pressure compared to WT mice. This finding is contradictory to the published literature that suggests that EP_3 acts as a systemic vasoconstrictor (47). Chen et al showed that $EP_3^{-/-}$ mice exhibited reduced baseline mean arterial pressure monitored by both tail-cuff and carotid arterial catheterization (81). Additionally, the vasopressor effect of acute or chronic infusion of angiotensin II was attenuated in $EP_3^{-/-}$ mice (81). This diminished vasopressor effect in $EP_3^{-/-}$ mice is attributed to reduced Ca^{2+} sensitivity and reduced intracellular calcium concentration in vascular smooth muscle cells therefore decreasing arterial contractility (81). The $EP_3^{-/-}$ mice with these blood pressure changes have some key differences to the ones used in our experiments (81). Chen et al used only male $EP_3^{-/-}$ mice aged 12 to 16 weeks and with 20 to 25 g of body weight (81). We report that $EP_3^{-/-}$ mice aged 16 weeks are considerably heavier than 25 g when fed a standard chow diet.

At 12 weeks, the majority of $EP_3^{-/-}$ mice were heavier than 25 g. Excluding mice with increased body weight may select out mice with the metabolic abnormalities we and others have reported (i.e. impaired glucose tolerance and hyperinsulinemia). Hyperinsulinemia is closely linked to hypertension as insulin can cause sodium retention (99, 100, 105, 106); it enhances proximal tubule sodium-proton exchanger type 3 (NHE3), Na^+-K^+-ATPase (101-103), and epithelial sodium channel (ENaC) in the mouse collecting duct (104). We also characterized EP receptor expression in $EP_3^{-/-}$ mice in different nephron segments, which may account for the elevation in blood pressure. $EP_3^{-/-}$ mice showed the greatest alterations in EP expression in the thick ascending limb (TAL) with an increase in EP_4 mRNA. EP_4 is recognized to play a major role in regulation of renin (39, 44). EP_4 in the TAL is shown to stimulate renin secretion from the juxtamedullary apparatus/macula densa (39, 44). Stimulation of the RAAS markedly increases blood pressure through several mechanisms including vasoconstriction of systemic blood vessels and salt retention (1, 2). In contributing to salt retention and fluid retention, these mechanisms may in part account for the increased body weight in the $EP_3^{-/-}$ mice, however fluid content in these mice was not measured. Overall, the altered profile of EP receptors in $EP_3^{-/-}$ mice may also account for increased blood pressure.

4.3 Phenotype of Global EP_3 Deletion in STZ Diabetic C57BL/6 Mice

COX-2 and PGE_2 are consistently elevated in both rodent and human diabetes, and renal $EP_{1\text{-}4}$ receptor subtypes are altered (27-32). Although slight differences were observed in the magnitude of change of EP receptor mRNA depending on the diabetic animal model,

overall regional alterations were similar (32). In the renal cortex, EP_1, EP_2, and EP_3 are increased while EP_4 is decreased. In the renal medulla, EP_1 and EP_3 are increased (32). The roles of EP_1, EP_2, and EP_4 are well understood in the diabetic context however, the role of EP_3 in this disease model is yet to be studied. Given that EP_3 is elevated during early DN and that COX-2 inhibition is protective at this stage of the disease, it is likely that EP_3 plays a role in mediating renal injury. Therefore we studied the role of the EP_3 receptor on the progression of DN in C57BL/6 WT and $EP_3^{-/-}$ mice 12-weeks post STZ or vehicle injection.

To assess the COX signaling pathway, we analyzed cortical and medullary expression of the COX enzymes. The constitutively expressed COX isoform, COX-1, was found to be unchanged across all groups in both the cortex and medulla. This finding is in accordance with other reports showing that COX-1 is relatively unchanged during diabetes (108). On the other hand, cortical and medullary COX-2 protein was increased in STZ mice, with a larger increase in the medulla. The regional differences most likely reflect the higher abundance of inducible COX-2 in the renal medulla, particularly in the medullary interstitial cells, compared to the cortex (23-25). Contrastingly, COX-2 induction was blunted in $EP_3^{-/-}$ STZ mice in both renal cortex and medulla. We also assessed the EP mRNA profile in our mouse groups. Medullary EP_1 mRNA was increased in STZ mice while $EP_3^{-/-}$ STZ mice showed EP_1 mRNA levels similar to non-diabetic mice. Medullary EP_2 mRNA was numerically increased in STZ mice while $EP_3^{-/-}$ STZ mice showed EP_2 mRNA levels similar to non-diabetic mice. Both cortical and medullary EP_3 mRNA was elevated in STZ mice. Finally, medullary EP_4 was increased in STZ mice while $EP_3^{-/-}$ STZ mice showed EP_4 mRNA levels similar to non-diabetic

mice.

The reduction in COX-2 protein expression in $EP_3^{-/-}$ STZ mice is contrary to findings in recent studies showing that EP_3 downregulates COX-2 expression in the physiological and hypertonic medullary thick ascending limb (46, 109). Celecoxib treatment in mice resulted in an increase in COX-2 protein expression and sulprostone acting on EP_3 reversed this effect (46) suggesting that EP_3 deletion would result in greater levels of COX-2 especially in diabetes. However our lab as well as others have shown that during diabetes renal COX-2 and EP_3 both increase (32, 110), but the interaction has not been studied. Since EP_3 exists in several splice variants and can signal not only through G_i but also through G_q/PLC/Ca^{2+} (115), targeting different splice variants of EP_3 may account for these conflicting reports. Furthermore, COX-2 expression is also regulated by calcium-sensing receptors, bradykinin, and angiotensin II (112-114); and EP_3 has been impicated in PGE_2-induced enhancement of the bradykinin response of mouse and rat neurons (116, 117). We observe an increase in medullary EP_4 mRNA exclusively in STZ mice and given that EP_4 in the juxtamedullary apparatus stimulates renin secretion (thus making angiotensin II), it is possible that increased EP_4 leads indirectly to increases in COX-2 protein expression by activating angiotensin II (39, 44). Furthermore, the EP_2 receptor was shown to be part of a positive feedback loop to induce COX-2 via cAMP-PKA in Madin-Darby canine kidney cells (118). We show a numerical but non-significant increase in medullary EP_2 in STZ mice but the exact mechanisms contributing to increased COX-2 further exploration.

Twelve weeks post injection of STZ, both $EP_3^{+/+}$ and $EP_3^{-/-}$ mice exhibited hyperglycemia and glucosuria. This is to be expected as low-dose STZ treatment leads to

hyperglycemia as early as two weeks post injection (20, 21). Although $EP_3^{-/-}$ mice exhibited glucose metabolism abnormalities at baseline, namely impaired glucose tolerance, no difference in blood or urine glucose was observed between STZ and $EP_3^{-/-}$ STZ mice. We expected that $EP_3^{-/-}$ STZ mice may respond differently to STZ since EP_3 was implicated in insulin secretion, however, this was not the case (33). STZ increases blood glucose by destroying insulin-producing pancreatic β cells, therefore, it is possible that the mechanistic link between EP_3 and insulin secretion in β cells is severely defective or abolished together (20, 21).

As expected, STZ injected mice lost body weight relative to non-diabetic controls, despite an increase of food intake, presumably from the combined effects of persistent polyuria leading to severe volume contraction and the inability to store calories as fat induced by severe insulin deficiency (119). Furthermore, insulin deprivation in diabetes causes a profound increase in protein catabolism, especially in skeletal muscle (4). Catabolism of protein in skeletal muscle could also contribute to the reduction in body weight in STZ injected mice. Although the body weights of STZ and $EP_3^{-/-}$ STZ mice did not numerically match, when compared to their non-injected cohorts, the percent reduction in body weight was comparable. Therefore, the different starting body weights prior to injection most likely account for the different body weights post injection.

Both STZ and $EP_3^{-/-}$ STZ mice showed increased kidney weight when corrected for body weight, but STZ mice alone showed increased kidney weight (i.e. uncorrected) and increased kidney weight corrected for tibia length. Since STZ mice show significant reductions in body weight, correcting kidney weight to body weight might be unsuitable in this particular diabetic mouse model. A significantly reduced body weight would

artificially increase the kidney to body weight ratio when in fact kidney weight is unchanged when compared to the non-diabetic group. A more reliable reference for kidney weight in STZ diabetes is tibia length, which remains constant with STZ-induced hyperglycemia (120, 121). Using this correction method, $EP_3^{-/-}$ STZ show attenuated renal enlargement compared to STZ mice.

The early diabetic kidney typically undergoes significant enlargement predominantly via hypertrophy (cell enlargement) and to a lesser extent, via hyperplasia (cellular proliferation) (6-8). In vitro and in vivo studies have shown that exposing renal cells to high ambient glucose concentrations leads to the arrest of the cell cycle in the G1 phase followed by complementary signals increasing RNA and protein synthesis (122, 123). This G1-phase arrest is mediated by p27 and p21, which are inhibitors of cyclin-dependent kinases (122, 123). This involves the downregulation of the cyclin E/cdk2 complex which is required for the transition from G1 to S phase of the cell cycle (122, 123). COX-2 has been shown to be an important mediator of p21 as well as its upstream regulators: TGF-β and tumor necrosis factor α (TNF-α). COX-2 selective inhibition was shown to downregulate STZ induced increases in TGF-β, TNF-α, and p21 (30, 31). Additionally, COX-2 selective inhibition was shown to prevent STZ induced renal hypertrophy (124). The lack of COX-2 induction in $EP_3^{-/-}$ STZ mice might protect these mice against renal hypertrophy, presented as a reduced kidney weight to tibia length ratio compared to STZ mice. The altered EP mRNA profile may also account for this effect. STZ mice showed a significant increase in medullary EP_1 and EP_4 while this effect was attenuated in $EP_3^{-/-}$ STZ mice. Several lines of evidence suggest that EP_1 and EP_4 contribute to diabetic renal hypertrophy. STZ rats treated with an EP_1 selective antagonist

showed a significant attenuation in STZ induced kidney hypertrophy while STZ mice treated with an EP_4 agonist exhibited increases in regulators of renal hypertrophy, namely inflammatory chemokines (TNFα, TGF-β, IL-6, MCP-1, and IP-10) (125, 126). However, mice injected with an EP_4 agonist showed no change in STZ induced renal hypertrophy (126). Still, the role of EP_4 in contributing to injurious processes remains controversial as a number of studies suggest a potential protective role for EP_4 (127). Additionally, we recently demonstrated that EP_1 and EP_4 increase p27 while decreasing the cyclin E/cdk2 complex in proximal tubule cells (128). Although this suggests a role for EP_1 and EP_4 in cortical growth, it is very likely that these receptors mediate these same effects in the medulla. Taken altogether, it is likely that the $EP_3^{-/-}$ STZ mice are protected against renal hypertrophy due to blunted COX-2 and medullary EP_1/EP_4 induction.

We assessed glomerular and mesangial size in all groups using a routine PAS stain. We observed similar glomerular enlargement in both STZ and $EP_3^{-/-}$ STZ mice with no change in mesangial area. EP_3 is not located in the glomerulus and is only localized to the afferent arteriole, thick ascending limb, and collecting duct (129). Therefore, it is unlikely that EP_3 mediates glomerular growth responses. Although COX-2 is increased in the cortex in STZ mice, the cortical EP receptor profile is relatively unchanged suggesting that this glomerular hypertrophy is occurring independently of PGE_2. Furthermore, $EP_3^{-/-}$ STZ mice show no increase in cortical COX-2 expression yet still exhibit glomerular hypertrophy further emphasizing that this process is independent of COX-2. Whether COX-2 inhibitors (coxibs) are protective or detrimental in glomerular hypertrophy is controversial, most studies agree that COX-2 plays an important role in this process (30, 31, 124). However, all these studies report mesangial expansion, which

is absent in our mice suggesting that we are observing an early stage (30, 31, 124). Early glomerular growth may occur through other mediators including TGF-β and angiotensin II (6, 7).

The fact that $EP_3^{-/-}$ STZ can show attenuated diabetic renal hypertrophy yet glomerular hypertrophy reflects a primary attenuation of tubular hypertrophy. In addition to tubular cell hypertrophy, dilation and increased fluid content of tubules, mainly collecting ducts, contribute substantially to the maintenance of kidney size in DN with advanced chronic renal failure in animal models and humans (9). As will be discussed later in greater detail, $EP_3^{-/-}$ STZ mice exhibit attenuated polyuria, attenuated polydipsia, and attenuated hyperfiltration compared to STZ mice. The lowered fluid content in the kidneys as a result of these reduced parameters in $EP_3^{-/-}$ STZ mice may in part explain the attenuation in kidney size compared to STZ mice.

Glomerular hyperfiltration is a hallmark change in early DN (6-8). We detected an increase in GFR 12-weeks post injection in STZ mice however this increase was attenuated in $EP_3^{-/-}$ STZ mice. Hyperfiltration is hypothesized to be a precursor of intraglomerular hypertension leading to albuminuria (6-8). Therefore, it is no surprise that the hyperfiltering STZ mice show increased urinary albumin excretion while this is absent from the normofiltering $EP_3^{-/-}$ STZ mice. The reason for these changes is suspected to be due to alterations in COX-2 expression, whereby we observe an increase in STZ mice only, while no increase is observed in $EP_3^{-/-}$ STZ mice. This is consistent with other reports showing that coxibs decrease diabetic glomerular hyperfiltration (30, 124). Additionally, we observe an increase in medullary EP_4 in STZ mice while this is attenuated in $EP_3^{-/-}$ STZ mice suggesting that this pathway might be responsible for the

observed increase in GFR. Several studies show that EP_4 in the TAL stimulates renin production, which would constrict the efferent arteriole through the activity of angiotensin II (130, 131). This results in an increase in glomerular hypertension and consequently GFR. These findings initially seem confounding since Tang et al show that EP_3 acts as a vasoconstrictor on the afferent arteriole (34). Therefore in its absence one would expect that GFR would further increase during early DN. However, the predominant PGE_2 effect on the afferent arteriole appears to be vasodilatory as evidenced by the GFR lowering effect of coxibs and NSAIDs in STZ animals (30, 124). However, the vasoconstrictive effect of PGE_2 on the afferent arteriole is achieved only at supraphysiological concentrations (34). Furthermore, recent studies have shown that EP_3 is more abundant in the interlobular arteries rather than in the afferent arteriole (40).

EP_3 has been shown to modulate AVP responses in the kidney, particularly V2 receptor mediated water-reabsorption in the collecting duct (62). AVP can also modulate other processes in the kidney by binding to its V1 receptor, mainly located on renal vasculature, which may also be regulated by EP_3 (1, 2). Therefore, we measured urinary AVP excretion rates. WT and $EP_3^{-/-}$ mice show similar levels of urinary AVP excretion. On the other hand, STZ mice exhibit markedly elevated urinary AVP excretion. $EP_3^{-/-}$ STZ mice show elevated urinary AVP excretion compared to $EP_3^{-/-}$ mice; however, urine AVP was significantly attenuated compared to STZ mice. COX-2 and PGE_2 have repeatedly been shown to regulate the secretion of vasopressin in the hypothalamus (132, 133). Furthermore, PGE_2 was shown to modulate urine concentration by acting at EP_1 receptors, not in the collecting duct, but within the hypothalamus to promote AVP synthesis in response to acute water deprivation (134). EP_3 is readily expressed in the

hypothalamus, therefore it is conceivable that EP_3 regulates hypothalamic AVP secretion especially since splice variants of EP_3 can signal through the same Gq/PLC/Ca^{2+} pathway as EP_1 (94, 115). A reduction in urinary AVP in $EP_3^{-/-}$ mice can prove effective in protecting against diabetic nephropathy as AVP-deficient Brattleboro rats have been shown to be resistant to diabetic hyperfiltration, albuminuria, and renal hypertrophy (135).

Several human studies have demonstrated a link between vasopressin and increases in GFR. After an initial water diuresis, Andersen et al infused healthy subjects with AVP for 2 hours to raise AVP concentrations to levels within the physiological range (136). Creatinine clearance, a surrogate marker for GFR, increased significantly along with a marked increase in urine osmolality and a decrease in the fractional excretion of urea (136). Furthermore, in two independent studies, renal function was analyzed twice in healthy subjects at a 2-week interval, once during diminished hydration and once during increased hydration (137, 138). In both studies, AVP was increased alongside GFR (137, 138). Finally, infusion of the selective V2 receptor antagonist, tolvaptan, to patients with autosomal dominant polycystic kidney disease led to a significant reduction in GFR (139). It is thought that AVP, acting via renal V2 receptors indirectly reduces the efficiency of urea excretion and increases GFR (140). This leads to an increased energetic demand on the kidney and contributes to hypertrophy (140-143). Physiologically, AVP stimulation leads to a reduction in the fractional excretion of urea (140-143). AVP acting on urea transporters in the terminal inner medullary collecting duct promotes urea diffusion into the inner medullary interstitium (140-143). In the meantime plasma urea increases, therefore to filter more urea the kidney responds by

increasing GFR (140-143). The immediate benefit is to limit the rise in plasma urea and reduce the risk of toxicity (140-143). However, this comes with a metabolic cost due to the increased load of solutes to reabsorb requiring a greater energy demand (140-143). This physiological response is similar to what is observed in animal models fed a high protein diet, which causes a similar increase in both plasma urea concentration and GFR (144, 145). If this adaptation is maintained over a long period, it can lead to kidney and glomerular hypertrophy and increased risk of glomerulosclerosis (140-144). A sustained increase in GFR can also lead to albuminuria (140-144). We show that STZ mice have increased plasma urea concentration and increased urinary AVP excretion while these changes are attenuated in $EP_3^{-/-}$ STZ mice. Attenuation of urinary AVP excretion may serve a protective purpose by preventing glomerular hyperfiltration, renal hypertrophy, and albuminuria.

4.4 Role of EP_3 in altering water and salt transport in STZ diabetic C57BL/6 mice, M1 cortical collecting duct cells, and in vitro microperfused tubules

DN is commonly associated with dysregulated salt and water transport, where in the early stages the kidney enters a hyperfunctioning stage due to the large amounts of salt and water being filtered requiring reabsorption (56, 87, 146). However, even though the kidney attempts to reabsorb all the contents of the filtrate, loss of electrolytes and fluid ensues (56, 86, 146). PGE_2 is involved in the regulation of sodium and water reabsorption and is thought to act as a counter-regulatory mechanism under conditions of increased sodium and water reabsorption acting as a diuretic or natriuretic (44, 72). Therefore we

analyzed the expression of several salt and water transporters in STZ diabetic mice with or without EP_3. The three salt transporters analyzed: NKCC2, αENaC, and NKA α-1, were increased in diabetes and they remained increased in mice lacking the EP_3 receptor. We expected that EP_3 plays a role in NKCC2 expression in diabetes since EP_3, through coupling to Gi, was found to modulate AVP-induced increases in cAMP and thereby prevents recycling of NKCC2 in isolated single mouse medullary thick ascending limbs of Henle (147). Furthermore, Nusing et al showed that $EP_3^{-/-}$ mice exhibited blunted natriuresis in response to the NKCC2 inhibitor, furosemide (44). Nevertheless, an induction of medullary NKCC2 was observed in both STZ and $EP_3^{-/-}$ STZ mice, while cortical levels were unchanged. This can be attributed to the counter-current mechanism in the ascending limb whereby the vast majority of salt reabsorption occurs in the medulla, the location of the largest concentration gradients, which drive this transport function (1, 2). On the other hand, NKA α-1 and αENaC were increased in both cortical and medullary regions. AVP is also capable of activating ENaC through cAMP induction (148). PGE_2 has been shown to regulate ENaC activity in cultured mouse cortical collecting duct (149). Therefore we expected EP_3 to modulate αENaC by inhibiting AVP mediated increases in cAMP, however, no difference in αENaC was observed between STZ and $EP_3^{-/-}$ STZ mice. Although AVP may modulate the β and γ subunits of ENaC, studies suggest that aldosterone not AVP primarily regulates the limiting subunit in the assembly of the ENaC complex, αENaC (150). A larger increase in αENaC was observed in the medulla and this likely reflects the larger proportion of ENaC containing principal cells compared to intercalated cells in the medullary collecting duct (1, 2). NKA α-1 was found to be equivalently increased in both STZ and $EP_3^{-/-}$ STZ mice. As opposed to

NKCC2 and αENaC, the largest increase was observed to occur in the cortex. NKA α-1 is located throughout the nephron rather than localized to one segment and it facilitates salt reabsorption back into the blood on the basolateral side of tubular epithelial cells (1, 2). The largest proportion of salt reabsorption occurs in the cortical proximal tubule and this may explain the larger increase in cortical NKA α-1 versus medullary NKA α-1 (1, 2). Although we demonstrated that several major solute transporters are upregulated, STZ injected mice exhibit severe diuresis and natriuresis. This is evidenced by the large daily urinary excretion of salts and downward trend in plasma concentration of salts in both STZ and $EP_3^{-/-}$ STZ mice.

We further characterized the increased urine output in these mice and found that $EP_3^{-/-}$ STZ mice exhibited attenuated polyuria compared to STZ mice. Additionally, $EP_3^{-/-}$ STZ mice also showed attenuated polydipsia correlating with the reduction in urine output. If decreased input were the only cause of the attenuated polyuria, one would expect equivalent urine osmolality in both STZ mice. However, urine osmolality did not match in both groups, with the $EP_3^{-/-}$ STZ mice showing an increase. This highly suggests that not only are these mice drinking less, but they are also reabsorbing more water through their aquaporins. Which effect drives the other is unknown at the moment and warrants further investigation.

To characterize the changes in water reabsorption occurring at the level of the kidney, we assessed the protein levels of the two major water transporters AQP1 and AQP2. PGE_2 is heavily implicated in regulating the collecting duct water transporter, AQP2, where EP_3 is suspected to have a diuretic role by inhibiting AVP-mediated water reabsorption. (59-62). We found that AQP2 is markedly downregulated in the cortex in

STZ mice while AQP2 protein levels return to baseline in $EP_3^{-/-}$ STZ mice. Additionally, we found that AQP2 is markedly downregulated in the medulla in STZ mice while AQP2 protein levels were increased in $EP_3^{-/-}$ STZ mice. Since AQP2 is only present in the collecting duct, these expression levels represent the cortical and medullary collecting ducts.

On the other hand, cortical AQP1 protein levels are equally reduced in both STZ and $EP_3^{-/-}$ STZ mice. However, medullary AQP1 levels were also found to be reduced in STZ mice but their expression was restored to baseline in $EP_3^{-/-}$ STZ mice. There are controversial findings about AQP1/2 expression in STZ-induced diabetes (53-57). Some studies have shown an increase in both expression and translocation of AQP1/2, whereas others have shown either a decrease or no change in the expression of the proteins (52-57). The results seem highly dependent on the stage of development of diabetes as well as the strain of rodent being studied as discussed below (53-57).

AVP is the hormonal regulator of AQP2 in the collecting duct (1, 2). EP_3 has been shown to modulate AVP responses in the kidney, particularly V2 receptor mediated water-reabsorption in the collecting duct (62). Therefore, we measured urinary AVP excretion rates. We found similar levels of urinary AVP excretion in WT and $EP_3^{-/-}$ mice. However, STZ mice exhibit markedly elevated urinary AVP excretion. While $EP_3^{-/-}$ STZ mice also show elevated urinary AVP excretion compared to $EP_3^{-/-}$ mice, it is significantly attenuated compared to STZ mice. As discussed previously, EP_3 may affect hypothalamic AVP secretion similar to EP_1 as demonstrated in $EP_1^{-/-}$ mice (134). However, the data suggests that $EP_3^{-/-}$ STZ mice have enhanced water reabsorption compared to STZ suggesting a role for EP_3 at the renal level. This is evident by the

attenuated polyuria and increased urine osmolality in $EP_3^{-/-}$ STZ. The fact that the $EP_3^{-/-}$ mice have lower urinary AVP excretion yet enhanced water reabsorption suggests the cells are more sensitive to AVP stimulation. On the other hand, STZ mice seem to be resistance to AVP stimulation due to enhanced water contraction and polyuria. It has been suggested that diabetes mellitus may cause a form of partial nephrogenic diabetes insipidus, a disease characterized by excessive thirst and excretion of large amounts of severely dilute urine due to a deficiency in AVP production or insensitivity of the kidneys to AVP (151). Secretion of AVP in response to osmotic stimuli is regularly reported to be increased in type 1 diabetes (152-154). However, when diabetic patients were infused with hypertonic saline, their urine osmolality remained lower than in non-diabetic controls despite comparable plasma AVP concentrations (153). This suggests the presence of renal resistance to the antidiuretic actions of AVP in type 1 diabetes (153). Furthermore, urine osmolality in diabetic patients infused intravenously with AVP failed to match that of non-diabetic patients and was severely reduced (155). Additionally, urinary AQP2 concentrations after infusion of AVP were significantly higher in non-diabetic patients compared to diabetic patients (155). This further emphasizes that individuals with DM do develop some sort of resistance to AVP similar to what is observed in diabetes insipidus. We postulate that EP_3 is in part responsible for resistance of the kidneys to AVP in DM. We show that EP_3 is upregulated in the cortex and medulla of STZ mice. Persistent upregulation of EP_3 may inhibit AQP2 expression and translocation in STZ mice, while $EP_3^{-/-}$ STZ mice can freely express AQP2 unopposed.

On the other hand, cortical AQP1 is not hormonally regulated and is constitutively active in the proximal tubule (1, 2). The fact that both STZ and $EP_3^{-/-}$ STZ

mice show reductions in cortical AQP1 suggest that reductions in this transporter contributes the most to diabetic polyuria. This is in accordance to what occurs physiologically where the bulk of filtered water is reabsorbed by AQP1 in the proximal tubule. This is supported by the finding that selective proximal tubule AQP1 deletion in mice prevents the ability to concentrate urine and renders them constitutively polyuric (156). Medullary AQP1 is expressed in the descending loop of Henle and vasa recta and is regulated by the medullary osmolar gradient (1, 2). The hypertonicity of the medullary interstitium is created by the reabsorption of urea in the inner-medullary collecting duct (IMCD) (1, 2). IMCDs have been shown to display decreased AVP-induced urea permeability in response to PGE_2 (66). Given that STZ mice alone exhibit increased medullary COX-2, it is likely that the medullary hypertonicity is not maintained. Furthermore, PGE_2 possibly via EP_2 has been shown to increase hyaluronan production by papillary interstitial cells, which decreases the interstitial gradient (69-71). We show that STZ mice alone show an increase in medullary EP_2 mRNA while it is unchanged in $EP_3^{-/-}$ STZ mice. Upregulation of EP_2 may affect the papillary interstitial gradient and contribute to decreased medullary AQP1, and consequently reduced water reabsorption.

To demonstrate a mechanistic link between EP_3 and AQP2 expression, we used the M-1 cortical collecting duct cell line and stimulated the cells with AVP, high salt, and/or sulprostone (SLP; EP_3/EP_1 agonist). Unfortunately, M1 cells were unresponsive to AVP and SLP stimulation. No change in AQP2, αENaC, or NKA α-1 protein expression was observed. This is in accordance with a study published by Huang et al claiming that M-1 cells are not responsive to AVP (157). High salt did not produce a change in AQP2 or αENaC protein expression. However, high salt was found to induce an upregulation of

NKA α-1 expression. This same finding was reported by Nasrallah et al in M-1 cells as well (158).

Since M-1 cells could not demonstrate a mechanistic link between EP_3 and AQP2, we used in vitro microperfusion to assess the water transport function of microdissected cortical collecting ducts (CCD) in response to AVP followed by SLP. We found that fluid reabsorption was increased in WT CCDs in response to AVP and this effect was attenuated but not completely abolished with SLP treatment. This is similar to what was reported by Hebert et al in rabbit cortical collecting ducts (61, 62). CCDs derived from $EP_3^{-/-}$ mice showed a similar increase in fluid reabsorption in response to AVP but were unresponsive to SLP suggesting that EP_3 alone is mediating the SLP effect seen in WT mice. Also, fluid reabsorption was similarly increased in STZ CCDs in response to AVP but this effect was completely abolished with SLP treatment. CCDs derived from $EP_3^{-/-}$ STZ mice showed a similar increase in fluid reabsorption with AVP but were unresponsive to SLP. This again suggests that EP_3 alone mediates inhibition of AVP-induced water reabsorption post the V2 receptor. This follows logically as PGE_2 binding to EP_3 signals through Gi downregulating cAMP while AVP binding to the V2 receptor signals through Gs upregulating cAMP making these two molecules opposed in their mechanism of action. The fact that SLP was capable of completely abolishing the AVP effect in the STZ CCDs alone suggests that these tubules are more sensitive to inhibition of water reabsorption. This could be due to the increased expression of cortical EP_3 mRNA leading to more EP_3 receptors, thus increasing the target sites for SLP. The fact that CCDs derived from STZ mice show a similar response to AVP would suggest that these tubules are not resistant to AVP contrary to what was presented earlier. Firstly, STZ

tubules seem to be more susceptible to inhibition of AVP-mediated water reabsorption with SLP. PGE_2 has a very short half-life and it is likely that by the time the tubule is mounted for perfusion, the concentration of active PGE_2 is low (1, 2). Therefore, if the resistance to AVP is mediated by PGE_2 binding to EP_3 as we proposed, then when the tubule is placed in this artificial environment, this signaling pathway is suppressed. Secondly, one cannot discount the role of the medullary collecting duct. The medullary collecting duct consists of a larger proportion of AQP2-expressing principal cells (1, 2). The rat IMCD shows larger increases in water reabsorption compared to mouse CCD in response to AVP, however, this also might be due to differences in species (63, 66). Furthermore, we show that medullary AQP2 is reversed beyond baseline in $EP_3^{-/-}$ STZ mice, suggesting that the inhibition of AQP2 by EP_3 is more pronounced in the medullary collecting duct. Therefore, a resistance of medullary collecting ducts to AVP responses may occur in DM and this may contribute to polyuria and the inability to concentrate urine.

Persistent polyuria can be damaging to the distal tubules, particularly the collecting ducts which physiologically do not encounter such high flow rates (10). We demonstrate that STZ mice have severely dilated collecting duct lumens in accordance with their extreme polyuria while $EP_3^{-/-}$ STZ mice still show this dilation, but it is reduced correlative to their attenuated polyuria. In addition to luminal dilations, STZ mice exhibited a large number of nuclear cysts in the lining of these dilated collecting ducts while the number of these cysts was attenuated in the $EP_3^{-/-}$ STZ mice. These nuclei appear to be emptied of their contents and appear atrophic. Similar structural changes are reported in STZ-diabetic rats as well as other polyuric diseases including lithium-induced

polyuria (88, 89, 91, 159). The nature of this damage is thought to be driven by both polyuria and by the expression of paracrine mediators including PGE_2 and COX-2 (163). PGE_2 activity can lead to PI3 kinase-PKB/Akt-mediated phosphorylation and inactivation of GSK-3β enzyme activity by phosphorylation at the serine 9 residue, and pGSK-3β is associated with microcyst epithelium (160-162). As COX-2 is upregulated in conditions with negative salt balance and polyuria, as shown here in diabetes, the epithelium is exposed to elevated concentrations of PGE_2, which is free to exert its effects and produce cysts. In contrast, a new report suggests that the microcyst formation in lithium-induced polyuria occurs independent of COX-2 in rats (91). Use of a coxib did alleviate some symptoms of this disease including urine concentrating ability (91). It is clear that COX-2 does play a role in the damage in polyuric conditions, however its role in cyst formation is yet to be fully understood.

AVP is also known to inhibit cystogenesis in animal models orthologous to human autosomal recessive polycystic kidney disease and in mice with medullary cystic kidney disease by downregulating cAMP signalling, cell proliferation, and fluid secretion (164-166). The direct role of AVP in cyst growth was demonstrated by crossing polycystic kidney disease (PKD) rats with Brattleboro rats (i.e. $AVP^{-/-}$). PKD $AVP^{-/-}$ rats had lower cAMP and almost complete inhibition of cystogenesis compared with PKD $AVP^{+/+}$ rats. Attenuated urinary AVP excretion in $EP_3^{-/-}$ STZ mice may account for the reduction in nuclear cysts compared to STZ mice.

4.5 Summary

PGE_2 and COX-2 are known to regulate urine output in pathologic polyuric states including lithium-induced polyuria, diabetes insipidus, and postobstructive polyuria. This is the first study to demonstrate a role for PGE_2/COX2 and particularly EP_3 in urine output during diabetes mellitus. During diabetes, EP_3 appears to be upregulated and thus actively opposes water reabsorption contributing to polyuria. Although renal AVP levels are increased in STZ mice, these mice are polyuric and cannot concentrate their urine. Resistance of diabetic mice to renal AVP might be mediated by EP_3. Since polyuria is the first renal manifestation in DM, it presents a lucrative therapeutic target to prevent progression into DN. Furthermore, we show that EP_3 plays a role in the early stages of DN. EP_3 appears to regulate renal AVP levels as well as renal COX-2. These two molecules have many implications on the early renal injurious processes including renal enlargement, glomerular hyperfiltration, and albuminuria. Deletion of EP_3 recapitulates many features of coxib treatment as well as AVP-V2 inhibition in early DN. This highlights the potential benefit of antagonizing EP_3 during early DN without the unwanted side effects of inhibiting all prostaglandin production.

5. REFERENCES

1. Taal M, Chertow G, Marsden P, et al. 2012. Brenner & Rector's the kidney (9th edition). Philadelphia, PA: Elsevier Saunders.
2. Alpern R, Caplan M, Moe O. 2013. Seldin and Giebisch's the kidney physiological and pathophysiology (5th edition). Waltham, MA: Academic Press.
3. Wild S, Roglic G, Green A, et al. 2004. Global prevalence of diabetes: estimates for the year 2000 and projections for 2030. Diabetes Care. 27: 1047-1053.
4. Forbes JM, Cooper ME. 2013. Mechanisms of diabetic complications. Physiol Rev. 93: 137-188.
5. United States Renal Data System. 2014. Annual Data Report: Epidemiology of Kidney Disease in the United States. Bethesda, MD: National Institute of Health, National Institute of Diabetes and Digestive and Kidney Diseases.
6. Dronavalli S, Duka I, Bakris GL. 2008. The pathogenesis of diabetic nephropathy. Nat Clin Pract Endocrinol Metab. 4: 444-452.
7. Kanwar YS, Sun L, Xie P, et al. A glimpse of various pathogenic mechanisms of diabetic nephropathy. Annu Rev Pathol. 6: 395-423.
8. Vallon V, Thomas SC. 2012. Renal function in diabetic disease models: the tubular system in the pathophysiology of the diabetic kidney. Annu Rev Physiol. 74: 351-375.
9. Wang S, Mitu GM, Hirschenberg R. 2008. Osmotic polyuria: an overlooked mechanism in diabetic nephropathy. Nephrol Dial Transplant. 23(7): 2167-72.

10. Marsh DJ, Martin CM. 1975. Effects of diuretic states on collecting duct fluid flow resistance in the hamster kidney. Am J Physiol. 229: 13-17.
11. Simeoni M, Boyde A, Shirley DG, et al. 2004. Application of red laser video-rate scanning confocal microscopy to in vivo assessment of tubular function in the rat: selective action of diuretics on tubular diameter. Exp Physiol. 89: 181-185.
12. Kobayashi T, Okada H, Inoue T, et al. 2006. Tubular expression of connective tissue growth factor correlates with interstitial fibrosis in type 2 diabetic nephropathy. Nephrol Dial Transplant. 21: 548-549.
13. Cheng HF, Wang CJ, Moeckel GW, et al. 2002. Cyclo-oxygenase-2 inhibitor blocks expression of mediators of renal injury in a model of diabetes and hypertension. Kidney Int. 62: 929-939.
14. Chow F, Ozols E, Nikolic-Paterson DJ, et al. 2004. Macrophages in mouse type 2 diabetic nephropathy: correlation with diabetic state and progressive renal injury. Kidney Int. 65: 116-128.
15. Misseri R, Meldrum KK. 2005. Mediators of fibrosis and apoptosis in obstructive uropathies. Curr Urol Rep. 6: 140-145.
16. Du Z, Duan Y, Yan Q, et al. 2004. Mechanosensory function of microvilli of the kidney proximal tubule. Proc Natl Acad Sci USA. 101: 13068-13073.
17. Essig M, Terzi F, Burtin M, et al. 2001. Mechanical strains induced by tubular flow affect the phenotype of proximal tubular cells. Am J Physiol Renal Physiol. 281: F751-F762.

18. Houston P, White BP, Campbell CJ, et al. 1999. Delivery and expression of fluid shear stress-inducible promoters to the vessel wall: applications for cardiovascular gene therapy. Hum Gene Ther. 10: 3031-3044.

19. Cai Z, Xin J, Pollock DM, et al. 2000. Shear stress-mediated NO production in inner medullary collecting duct cells. Am J Physiol Renal Physiol. 279: F270-F274.

20. Brosius FC, Alpers CE, Bottinger EP, et al. 2009. Mouse models of diabetic nephropathy. J Am Soc Nephrol. 20(12): 2503-12.

21. Alpers CE, Hudkins KL. 2011. Mouse models of diabetic nephropathy. Curr Opin Nephrol Hypertens. 20: 278-284.

22. Soler MJ, Riera M, Batlle D. 2012. New experimental models of diabetic nephropathy in mice models of type 2 diabetes: efforts to replicate human nephropathy. Exp Diabetes Res. 2012: 616313.

23. Hao CM and Breyer MD. 2008. Physiological regulation of prostaglandins in the kidney. Annu Rev Physiol. 70: 357-77.

24. Breyer MD and Breyer RM. 2001. G protein-coupled prostanoid receptors and the kidney. Annu Rev Physiol. 63: 579-605.

25. Breyer MD and Breyer RM. 2000. Prostaglandin receptors: their role in regulating renal function. Cuu Opin Nephrol Hyperten. 9: 23-29.

26. Norwood VG, Morham SG, and Smithies O. 2000. Postnatal development and progression of renal dysplasia in cyclooxygenase-2 null mice. Kidney Int. 58(6): 2291-300.

27. Cherney DZ, Miller J, Scholey JW, et al. 2008. The effect of cyclooxygenase 2 inhibition on renal hemodynamic function in humans with type 1 diabetes mellitus. Diabetes. 57: 688-695.

28. Cherney DZ, Reich HN, Jiang S, et al. 2012. Hyperfiltration and effect of nitric oxide inhibition on renal and endothelial function in humans with uncomplicated type 1 diabetes mellitus. Am J Physiol Regul Integr Compl Physiol. 303: R710-R718.

29. Cherney DZ, Scholey JW, Nasrallah R, et al. 2008. Renal hemodynamic effect of cyclooxygenase 2 inhibition in young men and women with uncomplicated type 1 diabetes mellitus. Am J Physiol Renal Physiol. 294: F1336-F1341.

30. Nasrallah R, Robertson SJ, Hébert RL. 2009. Chronic COX inhibition reduces diabetes-induced hyperfiltration, proteinuria, and renal pathological markers in 36-week B6-Ins2 (Akita) mice. Am J Nephrol. 30: 346-353.

31. Nasrallah R, Robertson SJ, Karsh J, et al. 2013. Celecoxib modifies glomerular basement membrane, mesangial area, and podocyte structure in OVE26 mice, but ibuprofen is more detrimental. Clin Sci. 124: 685-694.

32. Nasrallah R, Xiong H, Hébert RL. 2007. Renal prostaglandin E_2 receptor (EP) expression profile is altered in streptozotocin and B6-Ins2Akita type 1 diabetic mice. Am J Physiol Renal Physiol. 292: F278-F284,

33. Kimple ME, Keller MP, Rabaglia MR, et al. 2013. Prostaglandin E_2 receptor, EP_3, is induced in diabetic islets and negatively regulates glucose- and hormone-stimulated insulin secretion. Diabetes. 62(6): 1904-12.

34. Tang L, Loutzenhiser K, and Loutzenhiser R. 2000. Biphasic actions of prostaglandin E_2 on the renal afferent arteriole. Circ Res. 86: 663-670.

35. Purdy KE, Arendshorst WJ. 2000. EP_1 and EP_4 receptors mediate prostaglandin E_2 actions in the microcirculation of rat kidney. Am J Physiol Renal Physiol. 279: F755–F764.

36. Ren Y, D'Ambrosio MA, Garvin JL, et al. 2013. Prostaglandin E_2 mediates connecting tubule glomerular feedback. Hypertension. 62: 1123–1128.

37. Imig JD, Breyer MD, Breyer RD. 2002. Contribution of prostaglandin EP_2 receptors to renal microvascular reactivity in mice. Am J Physiol Renal Physiol. 283: F415–F422

38. Audoly LP, Ruan X, Wagner VA, et al. 2001. Role of EP_2 and EP_3 PGE_2 receptors in the control of murine renal hemodynamics. Am J Heart Circ Physiol. 280: H327–H333.

39. Schweda F, Klar J, Narumiya S, et al. 2004. Stimulation of renin release by prostaglandin E_2 is mediated by EP_2 and EP_4 receptors in mouse kidneys. Am J Physiol Renal Physiol. 287: F427–F433.

40. van Rodijnen WF, Korstjens IJ, Legerstee N, et al. 2007. Direct vasoconstrictor effect of prostaglandin E_2 on renal interlobular arteries: role of the EP_3 receptor. Am J Physiol Renal Physiol. 292: F1094–F1101.

41. Badzynska B, Sadowski J. 2008. Opposed effects of prostaglandin E_2 on perfusion of rat renal cortex and medulla: interactions with the renin-angiotensin system. Exp Physiol. 93: 1292–1302.

42. Pena-Silva RA, Heistad DD. 2010. EP1c times for angiotensin: EP_1 receptors facilitate angiotensin II- induced vascular dysfunction. Hypertension. 55: 846–848.

43. Thibodeau JF, Nasrallah R, He Y, et al. 2013. PTGER1 deletion attenuates renal injury in diabetic mice. Am J Pathol. 183: 1789–1802.

44. Nüsing RM, Treude A, Weissenberger C, et al. 2005. Dominant role of prostaglandin E_2 EP_4 receptor in furosemide-induced salt-losing tubulopathy: a model for hyperprostaglandin E syndrome/antenatal Bartter syndrome. J Am Soc Nephrol. 16: 2354–2362.

45. Harrison-Bernard LM, Monjure CJ, Bivona BJ. 2006. Efferent arterioles exclusively express the subtype 1A angiotensin receptor: functional insights from genetic mouse models. Am J Physiol Renal Physiol. 290: F1177–F1186.

46. Vio CP, Quiroz-Munoz M, Cuevas CA, et al. 2012. Prostaglandin E_2 EP_3 receptor regulates cyclooxygenase-2 expression in the kidney. Am J Physiol Renal Physiol. 303(3): F449-57.

47. Swan CE, Breyer RM. 2011. Prostaglandin E_2 modulation of blood pressure homeostasis: studies in rodent models. Prostaglandins Other Lipid Mediat. 96(1-4): 10-13.

48. Mori A, Saito M, Sakamoto K, et al. 2007. Stimulation of prostanoid IP and EP(2) receptors dilates retinal arterioles and increases retinal and choroidal blood flow in rats. Eur J Pharmacol. 570:135–141.

49. Ariumi H, Takano Y, Masumi A, et al. 2002. Roles of the central prostaglandin EP_3 receptors in cardiovascular regulation in rats. Neurosci Lett. 324:61–64.

50. Bankir L, Bardoux P, Ahloulay M. 2001. Vasopressin and diabetes mellitus. Nephron. 87(1): 8-18.

51. Ahloulay M, Schmitt F, Dechaux M, et al. 1999. Vasopressin and urinary concentrating activity in diabetes mellitus. Diabetes Metab. 25(3): 213-22.

52. Zerbe R, Vinicor F, Robertson G. 1979. Plasma vasopressin in uncontrolled diabetes mellitus. Diabetes. 28(5): 503-508.

53. Nejsum LN, Kwon TH, Marples D, et al. 2001. Compensatory increase in AQP2, p-AQP2, and AQP3 expression in rats with diabetes mellitus. Am J Physiol Renal Physiol. 280(4): F715-26.

54. Bardoux P, Ahloulay M, Le Maout S, et al. 2001. Aquaporin-2 and urea transporter-A1 are up-regulated in rats with type 1 diabetes mellitus. Diabetologica. 44(5): 637-45.

55. Leung JC, Chan LY, Tsang AW, et al. 2005. Differential expression of aquaporins in the kidneys of streptozotocin-induced diabetic mice. Nephrology (Carlton). 10(1): 63-72.

56. Ward DT, Yau SK, Mee AP, et al. 2000. Functional, molecular, and biochemical characterization of streptozotocin-induced diabetes. J Am Soc Nephrol. 12(4): 779-790.

57. Ortiz MC, Albertoni Borghese MF, Balonga SE, et al. 2014. Renal response to L-arginine in diabetic rats. A possible link between nitric oxide system and aquaporin-2. PLoS One. 9(8): e104923.

58. Anderson RJ, Berl T, McDonald KD, et al. 1975. Evidence for an in vivo antagonism between vasopressin and prostaglandin in the mammalian kidney. J Clin Invest 56: 420-426.

59. Chabardes D, Brick-Ghannam C, Montegut M, et al. 1988. Effect of PGE_2 and alpha-adrenergic agonists on AVP-dependent cAMP levels in rabbit and rat CCT. Am J Physiol. 255: F43–F48.

60. Noland TD, Carter CE, Jacobson HR, et al. 1992. PGE2 regulates cAMP production in cultured rabbit CCD cells: Evidence for dual inhibitory mechanisms. Am J Physiol. 263: C1208–C1215.

61. Hébert RL, Jacobson HR, Fredin D, et al. 1993. Evidence that separate PGE_2 receptors modulate water and sodium transport in rabbit cortical collecting duct. Am J Physiol. 265: F643–F650.

62. Hébert RL, Jacobson HR, Breyer MD. 1990. PGE_2 inhibits AVP-induced water flow in cortical collecting ducts by protein kinase C activation. Am J Physiol. 259: F318–F325.

63. Maeda Y, Terada Y, Nonoguchi H, et al. 1992 Hormone and autacoid regulation of cAMP production in rat IMCD subsegments. Am J Physiol. 263: F319–F327.

64. Nadler SP, Zimpelmann JA, Hébert RL. 1992. PGE_2 inhibits water permeability at a post-cAMP site in rat terminal inner medullary collecting duct. Am J Physiol. 262: F229–F235, 1992.

65. Tamma G, Wiesner B, Furkert J, et al. 2003. The prostaglandin E_2 analogue sulprostone antagonizes vasopressin-induced antidiuresis through activation of Rho. J Cell Sci. 116: 3285–3294.

66. Rouch AJ, Kudo LH. 2000. Role of PGE(2) in alpha(2)-induced inhibition of AVP- and cAMP-stimulated H(2)O, Na(+), and urea transport in rat IMCD. Am J Physiol Renal Physiol. 279: F294–F301.

67. Breyer MD, Davis L, Jacobson HR, et al. 1996. Differential localization of prostaglandin E receptor subtypes in human kidney. Am J Physiol. 270: F912-918.

68. Sugimoto Y, Namba T, Shiemoto R, et al. 1994. Distinct cellular localization of mRNAs for three subtypes of prostaglandin E receptor in kidney. Am J Physiol. 266: F823-828.

69. Rugheimer L, Johnsson C, Maric C. 2008. Hormonal regulation of renomedullary hyaluronan. Acta Physiol (Oxf). 193: 191-198.

70. Rugheimer L, Olerud J, Johnsson C, et al. 2009. Hyaluronan synthases and hyaluronidases in the kidney during changes in hydration status. Matrix Biol. 28: 390-395.

71. Zhang L, Bowen T, Grennan-Jones F, et al. 2009. Thyrotropin receptor activation increases hyaluronan production in pre-adipocyte fibroblasts: contributory role in hylauronan accumulation in thyroid dysfuntion. J Biol Chem. 284: 26447-26455.

72. Gonzalez AA, Cespedes C, Villanueva S, et al. 2009. E prostanoid-1 receptor regulates renal medullary alphaENaC in rats infused with angiotensin II. Biochem Biophys Res Commun. 389(2): 372-7.

73. Takeuchi K, Abe T, Takahashi N, et al. 1993. Molecular cloning and intrarenal localization of rat prostaglandin E_2 receptor EP_3 subtype. Biochem Biophys Res Commun 194: 885–891.

74. Torikai S, Kurokawa K. 1983. Effect of PGE_2 on vasopressin-dependent cell cAMP in isolated single nephron segments. Am J Physiol 245: F58–F66.

75. Culpepper RM, Andreoli TE. 1983. Interactions among prostaglandin E_2, antidiuretic hormone, and cyclic adenosine monophosphate in modulating Cl- absorption in single mouse medullary thick ascending limbs of Henle. J Clin Invest. 71: 1588–1601.

76. Tran POT, Gleason CE, Poitout V, et al. 1999. Prostaglandin E_2 mediates inhibition of insulin secretion by interleukin-1B. J Biol Chem. 274(44): 31245-21248.

77. Nishi S, Seino Y, Seino S, et al. 1984. Different effects of prostaglandin E_1, E_2, and D_2 on pancreatic somatostatin release. Horm Metab Res. 1: 114-8.

78. Sanchez-Alavez M, Klein I, Brownell S, et al. 2007. Night eating and obesity in the EP_{3R}-deficient mouse. Proc Natl Acad Sci USA. 104(8): 3009-14.

79. Fleming ED, Athirakul K, Oliverio MI, et al. 1998. Urinary concentrating function in mice lacking EP_3 receptors for prostaglandin E_2. Am J Physiol. 275(6 Pt 2): F955-61.

80. Zhang Y, Pop IL, Carlson NG, et al. 2012. Genetic deletion of the P2Y2 receptor offers significant resistance to development of lithium-induced polyuria accompanied by alterations in PGE_2 signaling. Am J Physiol Renal Physiol. 302(1): F70-7.

81. Chen L, Miao Y, Zhang Y, et al. 2012. Inactivation of the E-prostanoid 3 receptor attenuates the angiotensin II pressor response via decreasing arterial contractility. Arterioscler Thromb Vasc Biol. 32(12): 3024-32.

82. Qi Z, Whitt I, Mehta A, et al. Serial determination of glomerular filtration rate in conscious mice using FITC-inulin clearance. Am J Physiol Renal Physiol. 286(3): F590-6.

83. Qi Z, Fujita H, Jin J, et al. 2005. Characterization of susceptibility of inbred mouse strains to diabetic nephropathy. Diabetes. 54: 2628-37.

84. Rao X, Huang X, Zhou Z, et al. 2013. An improvement of the 2^(-delta delta CT) method for quantitative real-time polymerase chain reaction data analysis. Biostat Bioinforma Biomath. 3(3): 71-85.

85. Stroos BA, Naray-Fejes-Toth A, Carretero OA, et al. 1991. Characterization of a mouse cortical collecting duct cell line. Kidney Int. 39(6): 1168-75.

86. Haverty TP, Kelly CJ, Hines WH, et al. 1988. Characterization of a renal tubular epithelial cell line which secretes the autologous target antigen of autoimmune experimental interstitial nephritis. J Cell Biol. 107: 1359-1368.

87. Song J, Knepper MA, Verbalis JG, et al. 2003. Increased renal ENaC subunit and sodium transporter abundances in streptozotocin-induced type 1 diabetes. Am J Physiol Renal Physiol. 285(6): F1125-37.

88. Rasch R. 1984. Tubular lesions in streptozotocin-diabetic rats. Diabetologia. 27(1): 32-37.

89. Tuazon J, Casalino D, Syed E, et al. 2008. Lithium-associated kidney microcysts. ScientificWorldJournal. 8: 828-9.

90. Kolatsi-Joannou M, Bingham C, Ellard S, et al. 2001. Hepatocyte nuclear factor-1beta: a new kindred with renal cysts and diabetes and gene expression in normal human development. J Am Soc Nephrol. 12(10): 2175-80.

91. Kjaersgaard G, Madsen K, Marcussen N, et al. 2014. Lithium induces microcysts and polyuria in adolescent rat kidney independent of cyclooxygenase-2. Physiol Rep. 2(1): e00202.

92. Fonken LK, Workman JL, Walton Jc, et al. 2010. Light at night increases body mass by shifting the time of food intake. Proc Natl Acad Sci USA. 107(43):18664-9.

93. Stunkard A and Lu XY. 2010. Rapid changes in night eating: considering mechanisms. Eat Weight Disord. 15(1-2):e2-8.

94. Nakamura K, Kaneko T, Yamashita Y, et al. 1999. Immunocytochemical localization of prostaglandin EP3 receptor in the rat hypothalamus. Neurosci Lett. 260(2): 117-20.

95. Matsumura H, Honda K, Choi WS, et al. 1989. Evidence that brain prostaglandin E2 is involved in physiological sleep-wake regulation in rats. Proc Natl Acad Sci USA. 86(14): 5666-5669.

96. Huang Z, Sato Y, Mochizuki T, et al. 2003. Prostaglandin E_2 activates the histaminergic system via the EP_4 receptor to induce wakefulness in rats. J Neurosci. 23(14): 5975-83.

97. Shanik MH, Xu T, Skrha J, et al. 2008. Insulin resistance and hyperinsulinemia. Is hyperinsulinmeia the cart or the horse? Diabetes Care. 31(2): S262-S268.

98. Ayala JE, Samuel VT, Morton GJ, et al. 2010. Standard operating procedures for describing and performing metabolic tests of glucose homeostasis in mice. Dis Model Mech. 3(9-10): 525-534.

99. El-Atat FA, Stas SN, McFarlane SI, et al. 2004. The relationship between hyperinsulinemia, hypertension, and progressive renal disease. J Am Soc Nephrol. 15: 2816-2827.

100. Horita S, Seki G, Yamada H, et al. 2011. Insulin resistance, obesity, hypertension, and renal sodium transport. Int J of Hyperten. 2011: e391762.

101. Gesek FA, Schoolwerth AC. 1991. Insulin increases Na+-H+ exchange activity in proximal tubules from normotensive and hypertensive rats. Am J Physiol. 260(5): F695-F703.

102. Fuster DG, Bobulescu A, Zhang J, et al. 2007. Characterization of the regulation of renal Na+/H+ exchanger NHE3 by insulin. Am J Physiol. 292(2): F577-F585.

103. Talor Z, Emmanouel S, Katz AI. 1982. Insulin (INS) stimulates Na-K-ATPase activity in basolateral (BL) renal tubular membranes. Kid Int. 21(1): 266.

104. Blazer-Yost BL, Liu X, Helman SI. 1998. Hormonal regulation of eNaCs: insulin and aldosterone. Am J Physiol. 274(5): C1373-C1379.

105. Sohara E, Rai T, Ohta A, et al. 2009. Novel insulin-WNK4-NCC phosphorylation cascade in pathogenesis of PHA II caused by WNK4 R1185C mutation. Proc of the 42nd Ann Meet of Am Soc of Nephrol. San Diego, CA. p. F-FC279.

106. Ellison DH, Oyama TT, Yang CL, et al. 2009. Altered WNK4/NCC signaling in a rat model of insulin resistance. Proc of the 42nd Ann Meet of Am Soc of Nephrol. San Diego, CA. p. SA-FC432.

107. Libano-Soares JD, Landgraf SS, Gomes-Quintana E, et al. 2011. Prostaglandin E_2 modulates proximal tubule Na+-ATPase activity: cooperative effect between protein kinase A and protein kinase C. Arch of Biochem and Biophys. 507(2): 281-286.

108. Hao S, Hernandez A, Quiroz-Munoz M, et al. 2014. PGE_2 EP_3 receptor downregulates COX-2 expression in the medullary thick ascending limb induced by hypertonic NaCl. Am J Physiol Renal Physiol. 307(6): F736-F746.

109. Tang LQ, Liu S, Zhang ST, et al. 2014. Berberine regulates the expression of E-prostanoid receptors in diabetic rats with nephropathy. Mol Biol Rep. 41(5): 3339-47.

110. Steinert D, Kuper C, Bartels H, et al. 2009. PGE_2 potentiates tonicity-induced COX-2 expression in renal medullary cells in a positive feedback loop involving EP2-cAMP-PKA signaling. Am J Physiol Cell Physiol. 296: C75-C87.

111. Zhang MZ, Tao B, Cheng HF, et al. 2006. Renal cortical cyclooxygenase 2 expression is differentially regulated by angiotensin II AT1 and AT2 receptors. Proc Natl Acad Sci USA. 103: 16045-16050.

112. Abdullah HI, Pedraza PL, McGiff JC, et al. 2008. Calcium-sensing receptor signaling pathways in medullary thick ascending limb cells mediate COX-2 derived PGE_2 production: functional significance. Am J Physiol Renal Physiol. 295(4): F1082-9.

113. Rodriguez JA, Vio CP, Pedraza PL, et al. 2004. Bradykinin regulates cyclooxygenase-2 in rat renal thick ascending limb cells. Hypertension. 44: 230-235.

114. Zhang MZ, Tao B, Cheng HF, et al. 2006. Renal cortical cyclooxygenase 2 expression is differentially regulated by angiotensin II AT1 and AT2 receptors. Proc Natl Acad Sci USA. 103: 16045-16050.

115. Yamaoka K, Yano A, Kuroiwa K, et al. 2009. Prostaglandin EP_3 receptor superactivates adenylyl cyclase via the Gq/PLC/Ca^{2+} pathway in a lipid raft-dependent manner. Biochem Biophys Res Commun. 389(4): 678-82.

116. Kumazawa T, Mizumura K, Koda H. 1993. Involvement of EP_3 subtype of prostaglandin E receptors in PGE_2-induced enhancement of the bradykinin response of nociceptors. Brain Res. 632(1-2): 321-4.

117. Kozaki Y, Kambe F, Hayashi Y, et al. 2007. Molecular cloning of prostaglandin EP3 receptors from canine sensory ganglia and their facilitatory action on bradykinin-induced mobilization of intracellular calcium. J Neurochem. 100(6): 1636-47.

118. Steinert D, Kuper C, Bartels H, et al. 2009. PGE_2 potentiates tonicity-induced COX-2 expression in renal medullary cells in a positive feedback loop involving EP2-cAMP-PKA signaling. Am J Physiol Cell Physiol. 296: C75-C87.

119. Ventura-Sobrevilla J, Boone-Villa VD, Aguilar CN, et al. 2011. Effect of varying dose and administration of streptozotocin on blood sugar in male CD1 mice. Proc West Pharmacol Soc. 54:5-9.

120. Farrell PA, Fedele MJ, Hernandez J, et al. 1999. Hypertrophy of skeletal muscle in diabetic rats in response to chronic resistance exercise. J Appl Physiol. 87(3): 1075-82.

121. Thibodeau JF, Holterman CE, Burger D, et al. 2014. A novel mouse model of advanced diabetic kidney disease. PLoS One. 9(12): e113459.

122. Zhang Y, Shi Y, Liu Y, et al. 2007. Growth pattern switch of renal cells and expression of cell cycle related proteins at the early stage of diabetic nephropathy. Biochem Biophys Res Commun. 363(1): 159-64.

123. Wolf G, Shroeder R, Ziyadeh FN, et al. 1997. High glucose stimulates expression of p27Kip1 in cultured mouse mesangial cells: relationship to hypertrophy. Am J Physiol. 272(3 Pt 2): F348-56.

124. Quilley J, Santos M, Pedraza P. 2011. Renal protective effect of chronic inhibition of COX-2 with SC-58236 in streptozotocin-diabetic rats. Am J Physiol Heart Circ Physiol. 300(6): H2316-22.

125. Makino H, Tanaka I, Mukoyama M, et al. 2002. Prevention of diabetic nephropathy in rats by prostaglandin E receptor EP_1-selective antagonist. J Am Soc Nephrol. 13(7): 1757-1765.

126. Mohamed R, Jayakumar C, Ramesh G. 2013. Chronic administration of EP_4-selective agonist exacerbates albuminuria and fibrosis of the kidney in streptozotocin-induced diabetic mice through IL-6. Lab Invest. 93(8): 933-45.

127. Vukicevic S, Simic P, Borovecki F, et al. 2006. Role of EP_2 and EP_4 receptor-selective agonists of prostaglandin E_2 in acute and chronic kidney failure. Kidney Int. 70: 1099-1106.

128. Nasrallah R, Hassouneh R, Zimplemann J, et al. 2015. Prostaglandin E_2 increases proximal tubule fluid reabsorption, and modulates cultured proximal tubule cell responses via EP_1 and EP_4 receptors. Lab Invest. In press.

129. Breyer MD, Jacobson HR, Davis LS, et al. 1993. In situ hybridization and localization of mRNA of the rabbit prostaglandin EP_3 receptor. Kidney Int. 44(6): 1372-8.

130. Facemire CS, Nguyen M, Jania L, et al. 2011. A major role for the EP_4 receptor in regulation of renin. Am J Physiol Renal Physiol. 301(5): F1035-41.

131. Poschke A, Kern N, Maruyama T, et al. 2012. The PGE(2)-EP_4 receptor is necessary for stimulation of the renin-angiotensin-aldosterone system in response to low dietary salt intake in vivo. Am J Physiol Renal Physiol. 303(10): F1435-42.

132. Norregaard R, Madsen K, Hansen PBL, et al. 2011. COX-2 disruption leads to increased central vasopressin stores and impaired urine concentrating ability in mice. 301(6): F1301-F1313.

133. Knigge U, Kjaer A, Kristoffersen U, et al. 2003. Histamine and prostaglandin interaction in regulation of oxytocin and vasopressin secretion. J Neuroendocrinol. 15(10): 940-5.

134. Kennedy CR, Xiong H, Rahal S, et al. 2007. Urine concentrating defect in prostaglandin EP1-deficient mice. Am J Physiol Renal Physiol. 292(2): F868-75.

135. Bardoux P, Martin H, Ahloulay M, et al. 1999. Vasopressin contributes to hyperfiltration, albuminuria, and renal hypertrophy in diabetes mellitus: Study in vasopressin-deficient Brattleboro rats. Proc Natl Acad Sci USA. 96(18): 10397-10402.

136. Andersen LJ, Andersen JL, Schutten HJ, et al. 1990. Antidiuretic effects of subnormal levels of arginine vasopressin in normal humans. Am J Physiol. 259: R53-R60.

137. Bouby N, Ahloulay M, Nsegbe E, et al. 1996. Vasopressin increases glomerular filtration rate in conscious rats through its antidiuretic action. J. Am. Soc. Nephrol. 7: 842–851.

138. Yang B, Bankir L. 2005. Urea and urine concentrating ability: new insights from studies in mice. Am. J. Physiol. Renal Physiol. 288: F881–F896.

139. Fenton, RA. 2009. Essential role of vasopressin-regulated urea transport processes in the mammalian kidney. Pflugers Arch. 458: 169–177.

140. Bankir L, Ahloulay M, Bouby N, et al. 1993. Is the process of urinary urea concentration responsible for a high glomerular filtration rate? J. Am. Soc. Nephrol. 4: 1091–1103.

141. Bankir L, Bouby N, Trinh-Trang-Tan MM, et al. 1996. Direct and indirect cost of urea excretion. Kidney Int. 49: 1598–1607.

142. Bankir L, Kriz W. 1995. Adaptation of the kidney to protein intake and to urine concentrating activity: similar consequences in health and CRF. Kidney Int. 47: 7–24.

143. Bickel CA, Knepper MA, Verbalis JG, et al. 2002. Dysregulation of renal salt and water transport proteins in diabetic Zucker rats. Kidney Int. 61: 2099-2110.

144. Culpepper RM, Andreoli TE. 1983. Interactions among prostaglandin E_2, antidiuretic hormone, and cyclic adenosine monophosphate in modulating Cl- absorption in single mouse medullary thick ascending limbs of Henle. J Clin Invest. 71: 1588-1601.

145. Mironova E, Chen Y, Pao AC, et al. 2015. Activation of ENaC by AVP contributes to the urinary concentrating mechanism and dilution of plasma. Am J Phsyiol Renal Physiol. 308(3): F237-43.

146. Wang S, Meng F, Xu J, et al. 2009. Effects of lipids on ENaC activity in cultured mouse cortical collecting duct cells. J Membr Biol. 227(2): 77-85.

147. Stockand JD. 2012. The role of the epithelial Na(+) channel (ENaC) in high AVP but low aldosterone states. Front Physiol. 3:304.

148. Brodsky WA, Rapoport S, West CD. 1950. The mechanism of glycosuric diuresis in diabetic man. J Clin Invest. 29: 1021-1032.

149. Thompson CJ, Davis SN, Baylis PH. 1989. Effect of blood glucose concentration on osmoregulation in diabetes mellitus. Am J Physiol Regulatory Integrative Comp. 256: R597-R604.

150. Thompson CJ, Davis SN, Butler PC, et al. 1988. Osmoregulation of thirst and vasopressin secretion in insulin-dependent diabetes mellitus. Clin Sci (Colch). 74: 599-606.

151. Zerbe RL, Vinivor F, Robertson GL. 1985. Regulation of plasma vasopressin in insulin-dependent diabetes mellitus. Am J Physiol Endocrinol Metab. 249: E317-E325.

152. McKenna K, Morris AD, Ryan M, et al. 2000. Renal resistance to vasopressin in poorly controlled type 1 diabetes mellitus. 279(1): E155-160.

153. Vallon V, Verkman AS, Schnermann J. 2000. Luminal hypotonicity in proximal tubules of aquaporin-1-knockout mice. Am J Physiol Renal Physiol. 278(6): F1030-3.

154. Huang CN, Liu KL, Cheng CH, et al. 2005. PGE_2 enhances cytokine-elicited nitric oxide production in mouse cortical collecting duct cells. Nitric Oxide. 12(3): 150-8.

155. Nasrallah R, Paris G, Hebert RL. 2012. Hypertonicity increases sodium transporters in cortical collecting duct cells independently of PGE_2. Biochem Biophys Res Commun. 418(2): 372-7.

156. Hestbech J, Hansen HE, Amdisen A, et al. 1977. Chronic renal lesions following long-term treatment with lithium. Kidney Int. 12: 205-213.

157. Kjaersgaard G, Madsen K, Marcussen N, et al. 2012. Tissue injury after lithium treatment in human and rat postnatal kidney involves glycogen synthase kinase 3beta-positive epithelium. Am J Physiol Renal Physiol. 302: F455-465.

158. Fujino H, West KA, Regan JW. 2002. Phosphorylation of glycogen synthase kinase-3 and stimulation of T-cell factor signaling following activation of EP_2 and EP_4 prostanoid receptors by prostaglandin E_2. J Biol Chem. 277(4): 2614-9.

159. Belibi FA, Reif G, Wallace DP, et al. 2004. Cyclic AMP promotes growth and secretion in human polycystic kidney epithelial cells. Kidney Int. 66(3): 964-73.

160. Rao R, Zhang MZ, Zhao M, et al. 2005. Lithium treatment inhibits renal GSK-3 activity and promotes cyclooxygenase 2-dependent polyuria. Am J Physiol Renal Physiol. 288(4):F642-9.

161. Gattone VH, Wang X, Harris PC, et al. 2003. Inhibition of renal cystic disease development and progression by a vasopressin V2 receptor antagonist. Nat Med. 9:1323-1326.

162. Torres VE, Wang X, Qian Q, et al. 2004. Effective treatment of an orthologous model of autosomal dominant polycystic kidney disease. Nat Med. 10: 363-364.

163. Wang X, Gattone VH II, Harris PC, et al. Effectiveness of vasopressin V2 receptor antagonists OPC-31260 and OPC-41061 on polycystic kidney disease development in the PCK rat. J Am Soc Nephrol. 16: 846-851.

164. Wang X, Yanhong Wu, Ward CJ, et al. 2008. Vasopressin directly regulates cyst growth in polycystic kidney disease. J Am Soc Nephrol. 19(1): 102-108.